A HADRONIC TRANSPORT MODEL FOR RELATIVISTIC HEAVY ION COLLISIONS

By

Bao-An Li

A DISSERTATION

Submitted to
Michigan State University
in partial fulfillment of the requirements
for the degree of

DOCTOR OF PHILOSOPHY

Department of Physics and Astronomy

1991

ABSTRACT

A HADRONIC TRANSPORT MODEL FOR RELATIVISTIC HEAVY ION COLLISIONS

By

Bao-An Li

A hadronic transport model for relativistic heavy ion collisions is developed by deriving and solving numerically a coupled set of transport equations for the phase space distribution functions of nucleons, Delta resonances and pions. Starting from an effective hadronic Lagrangian density with minimal couplings between baryons and mesons, we first derive coupled equations of motion for the density matrices of nucleons, Delta resonances, and pi mesons as well as for the pion-baryon interaction vertex function. By truncating at the level of two-body correlations a closed set of equations of motion for the one body density matrix is obtained. A subsequent Wigner transformation then leads to a tractable set of relativistic transport equations for interacting nucleons, Delta resonances and pions. The transport equations are then solved numerically with the test particle method to study relativistic heavy ion collisions.

The validity of the model can be seen from its ability of reproducing available experimental data, explaining experimental and theoretical puzzles, as well as its predicting power for new phenomena. The experimentally observed concave shape of the pion spectra in relativistic heavy ion collisions is well reproduced. The mechanism that causes the concave shape of the pion spectra is found to be the different

contributions of the delta resonance produced during the early and the late stages of the heavy ion collision and due to the energy dependence of the pion and delta absorption cross sections. The dependence of the shape of the pion spectra on the beam energy, the target and projectile mass, and the impact parameter is also studied. An approximate scaling function for the shape parameter of the pion spectra is predicted. Another new phenomenon that the model is able to explain is the preferential emission of pions in asymmetric nucleus-nucleus collisions. It is found that the preferential emission of pions away from the interaction zone towards the projectile side in the transverse direction and longitudinal direction is due to the stronger pion absorption by the heavier target spectator.

This thesis is dedicated with love to my wife Wei Sun

ACKNOWLEDGEMENTS

First and foremost, I am deeply grateful to my thesis advisor, Dr. Wolfgang Bauer, for his invaluable tutelage and constant support. The freedom given to me by Wolfgang to study various topics as well as his insight, encouragement, patience and enthusiasm in trying to understand these different research topics have been critical for my being able to write this thesis and to broaden my knowledge in the vast field of nuclear physics.

I would like to thank Dr. George F. Bertsch for all of his help and enlightening advice during my graduate study at MSU. From him I learned details of the BUU transport model for heavy ion collisions. Collaborations with him in the study of pion collectivity and pion flow have resulted in two published papers and one part of this thesis. Dr. Pawel Danielewicz deserves a great deal of my appreciation for his many pertinent comments and suggestions during my thesis research and the friendship of his family. I would like to thank Dr. Walt Benenson for answering my questions regarding the experimental aspects of pion physics and his encouragement by telling me details of his planned experiments. I would like to express my gratitude to Shari Conroy for her invaluable assistance and friendship through out the course of this research. I am very grateful to Dr. Dan Stump and Dr. Philip Duxbury for serving on my thesis guidance committee. I would also like to acknowledge all other faculty and staff members of the Department of Physics and the National Superconducting Cyclotron Laboratory for their quality education and their support in many ways. I sincerely thank all of my fellow graduate students for their friendship.

I would like to take this space to express my gratitude to the nuclear theory group at Oak Ridge National Laboratory and the Department of Physics and Astronomy at the University of Tennessee for the hospitality and the intellectual stimulation I

received when I was visiting there from August, 1986 to July, 1987. Particularly, I am greatly indebted to Dr. Cheuk-Yin Wong for his friendship and guidance in research. From him I learned the Glauber-type multiple collision model for relativistic heavy ion collisions and much basic knowledge which has been very essential in doing research. His continuous encouragement and valuable advice have been very helpful during my graduate study.

A heartfelt "thank you" goes to Dr. Philip J. Siemens now at Oregon State University. His invaluable assistance in many ways enabled me to enter graduate school in the U.S. and be successful. More importantly, I benefited from his guidance and teaching when we were at Oak Ridge. From him I learned the basic idea of liquid-gas phase transition and nuclear multifragmentation. I have profited from knowing him as a teacher and take pleasure from knowing him as a friend.

I would like to express my gratitude to Dr. Jakob Bondorf at the Neils Bohr Institute and Dr. Christerfer J. Pethick at NORDITA for their warm hospitality during my visit of Copenhagen in the summer of 1987.

I greatly appreciate the essential contributions from all of my collaborators. Dr. Shun-Jin Wang at University of Lanzhou and Dr. Jørgen Randrup at Lawrence Berkeley Laboratory contributed a great deal to this thesis through the collaboration in the study of the relativistic transport theory for hadronic matter. I benefited from the collaboration with Dr. Scott Pratt now at the University of Wisconsin, Madison in the study of nuclear liquid-gas phase transition, the collaboration with Dr. Volker Koch at the State University of New York at Stony Brook in the study of pion collectivity in relativistic heavy ion collisions, and the collaboration with Dr. Mahir S. Hussein at the University of São Paulo in the study of pion production with radioactive nuclei. I give my special thanks to Dr. Jing-Ye Zhang at the Institute of Modern Physics, Chinese Academy of Science, who taught me the cranking model for

studying nuclear structure at high spin states. With him I published my first paper entitled "The shape coexistence of Krypton isotopes" when I was an undergraduate student. His influence has been essential to me in studying nuclear physics.

I owe a great deal to my family, my parents and my sisters for their encouragement and moral support throughout the years. Finally, I would like to deeply thank my wife, Wei Sun, for her love, understanding and encouragement and so I dedicate this thesis to her with love.

Contents

List of Tables

List of Figures

Chapter 1

Introduction

In relativistic heavy ion collisions at beam energies from a few hundred MeV up to about 2 GeV per nucleon, nuclear matter at high density and high temperature can be formed transiently. From a theoretical standpoint, this energy region provides interesting challenges. Since the beam energy is comparable to the mass of the nucleon, nonrelativistic approximations to the nuclear dynamics problem are no longer suitable. In addition, the energies are high enough to create baryonic excitations, and mesonic degrees of freedom become important as well. However, the achieved energy density is well below what is required to dissolve the hadrons into deconfined quarks and gluons.

Relativistic heavy ion collisions offer us a unique opportunity to study the behaviour of nuclear matter at extreme conditions as well as the reaction dynamics of finite-size hadronic systems. Aspects of particular interest are both of microscopic nature, such as the in-medium hadron-hadron interactions and the dispersion relation of mesons in hot and dense matter, and macroscopic, such as the nuclear equation of state, the transport properties (*e.g.* viscosity and heat conductivity), and the collective motion during the compression and decompression phase of the reaction.

A thorough understanding of these aspects has consequences which reach far be-

yond the scope of nuclear physics. The explosion mechanism of supernovae, the interior structure of neutron stars and the formation of matter during the early universe strongly depends on the properties of hadronic matter over a wide range of densities and temperatures. For example, in the gravitational collapse of massive stars the matter density can reach 2-4 times the normal nuclear matter density[Brow89a], and the stiffness of the nuclear equation of state then determines whether a prompt explosion of the supernova can take place.

The beam energy range considered here is below what is required to produce a quark-gluon plasma[Qmat87, Qmat90], a state of matter in which the building blocks of nucleons and mesons become deconfined and move in an extended volume. However, an understanding of the physics mentioned above is mandatory for any reliable analysis of the ongoing experimental search for this new state of matter. This is because the created quark-gluon plasma would be surrounded by and finally hadronize to the "colder" highly compressed hadronic matter. The properties of the hot and dense hadronic matter must therefore be well understood so that particles emitted from it will not be confused with those from the quark-gluon plasma[Kapu91] and therefore clear signals for the formation of the quark-gluon plasma can be detected.

As for the reaction dynamics, relativistic heavy ion collisions provide us the possibility to study the evolution of hadronic matter towards the equilibrium, the details of the reaction mechanisms, and how the nuclear force acts in the hot and dense hadronic environment. In particular, particles produced in relativistic heavy ion collisions are good probes of the reaction dynamics and the elementary particle production mechanism[Cass90a, Cass90b, Mose91].

However, the extraction of the properties of hot and dense nuclear matter from experimental data is complicated by the reaction dynamics. When we use the term hot and dense nuclear matter, about which we would like to gain information, we

refer to nuclear matter in equilibrium. However, the initial state of the reaction is far from equilibrium. In momentum space two Fermi spheres are separated by the beam momentum. The hot and dense nuclear matter is formed transiently, its properties can only be inferred from observables in the final state. Equilibrium situations can only be formed in very low energy and possibly very high energy nuclear reactions. At lower energies we find compound nuclear reactions where nucleon-nucleon collisions are severly suppressed due to the Pauli blocking, and the mean field keeps the nucleons together long enough to equilibrate. At high beam energies, on the contrary, frequent nucleon-nucleon collisions cause the thermalization whereas effects of the mean field are small. However, in the energy range considered here, the Pauli blocking of the collisions is neither strong enough to avoid particle emission during the mean field equilibration time, nor is it weak enough to allow a sufficient number of nucleon-nucleon collisions to happen before the system desintegrates. Therefore, the extraction of the properties of nuclear matter at high density and temperature strongly depends on our understanding of the reaction dynamics. It is the complexity involved in the reaction dynamics which makes the properties of nuclear matter under extreme conditions extracted up to now far from being accurate.

Considerable amounts of experimental data have been accumulated during the past decade by observing the products resulting from relativistic heavy-ion collisions, such as nucleons, light and heavy nuclear fragments, pions, dileptons, photons and kaons (see, for example, refs. [Harw87, Rand90]). Yet, many of the quantitative interpretations of these data remain rather uncertain, as the properties of the hot and dense matter extracted by comparing the experimental observations with theoretical calculations vary considerably with the specific model employed. Some properties extracted with different methods are even mutually conflicting. One example for this is the numerical value of the nuclear compressibility which varies greatly depending

on the model assumptions employed [Glen88].

The most successful models, in terms of reproducing a variety of the experimental observables in intermediate-energy nuclear collisions, are the Boltzmann-Uhling-Uehlingbeck model (*BUU*) [Bert88a, Stöc86] and its relativistic extensions[Koli87, Blät88], quantum molecular dynamics (QMD) [Aich91], and quantum-correlation dynamics [Cass90a, Cass90b]. These models are developed by numerically solving the BUU transport equation either in its quantum version or in its relativistic extensions. However, the BUU transport equation describes the time evolution of the phase space distribution function for only one kind of fermions. The collision integral in this equation was derived by assuming particles can make elastic collisions only. The dynamics in these models developed for heavy ion collisions at intermediate energies is therefore restricted to the baryonic level. Mesonic degrees of freedom enter via nuclear potentials only. In relativistic heavy ion collisions at beam energies around 1 GeV/nucleon, however, about one half of the nucleon-nucleon cross section is inelastic, mainly through pion production. Therefore, the energy range to which these models can be successfully applied is limited to beam energies below a few hundred MeV/nucleon, although meson production has been treated in a perturbative manner in the subthreshold regions [Cass90a, Mose91, Baue89]. Also within these models, one has studied pion production by assuming that Delta resonances have lifetimes longer than the nuclear reaction time; this is the so-called Frozen Delta Approximation. The number of Deltas at the end of the calculation then is equated to the total pion multiplicity[Bert84].

Another approach which has been successfully applied to high-energy nucleus-nucleus collisions is to treat all nucleons as essentially free particles interacting with each other with their free nucleon-nucleon cross sections. Intranuclear cascade models [Cugn81, Cugn82, Rand79, Cugn88] are based on this approach. Here, pion produc-

tion and reabsorption is included into the dynamical process through the formation and decay of Δ resonances. These models were able to calculate properly the overall features of nuclear equilibration [Rand79] and pion production [Cugn82, Kita86] in heavy-ion collisions with beam energies around 1 GeV per nucleon. Although they have some shortcomings when quantitatively compared to experimental data, the intranuclear cascade models have been remarkably successful.

However, in this energy range the long range nucleon-nucleon interactions are still sufficiently significant that the particles are not free but are moving in a varying mean field. Recent computer simulations of relativistic heavy-ion collisions[Wolf90, Xion90a, Liba91a] have extended the original *BUU* model to contain pion production and reabsorption in the dynamical process. They indicate that it is important to include the mesonic degrees of freedom explicitly, while keeping the mean field, in order to explain the dilepton production data [Roch88] and quantitative aspects of pion spectra such as the two-temperature shape observed at the BEVALAC [Odyn88, Chas90].

Nevertheless, a complete set of transport equations which govern the dynamical process in the hadronic matter was not available until recently. With this situation in mind, several groups have set out to provide a derivation of such transport equations [Siem89, Schö89, Davi91, Bote90]. These attempts, however, are still at an early stage, and a complete numerical realization is not available as of yet.

It is the purpose of this thesis to present a complete hadronic transport model for relativistic heavy ion collisions[Liba91a, Baue91a, Liba91b, Wlbr91a, Liba91c, Baue91b]. The framework for describing nuclear reactions is extended from the baryon dynamics level to the hadron dynamics level. The model provides a framework for the theoretical understanding of the nuclear physics phenomena observed, expected and unexpected, in the energy range from a few hundred MeV/nucleon to a few

GeV/nucleon.

The thesis is organized as follows.

By starting from a hadronic Lagrangian density we derive in Chapter 2 a coupled set of transport equations for the phase space distribution functions of nucleons, deltas, and pions, which are the main constituents of hadronic matter formed in relativistic nuclear collisions. These equations reflect the physics of relativistic nuclear collisions in an instructive manner. Moreover, an approximate solution of the equations is possible with present computers (Chapter 3). Our derivation is rather similar to the approach taken in ref. [Wang89, Cass90c], but we go beyond that work by including both Δ resonances and dynamical pions, which are expected to be significant at relativistic energies.

Chapter 3 is devoted to the numerical realization of the hadronic transport model. We discuss in detail how the transport equations are solved numerically and present inputs of the model.

In Chapter 4 we apply our model to study the dynamics of pion production.

In Chapter 5 we study the concave shape of the pion spectra in relativistic heavy ion collisions. The mechanism that causes the concave shape of the pion spectra is found to be the different contributions of the delta resonance produced during the early and the late stage of the heavy ion collisions and the energy dependence of the pion and delta reabsorption cross sections.

Chapter 6 is devoted to the study of the preferential emission of pions in asymmetric nucleus-nucleus collisions. The experimentally observed preferential emission of pions away from the interaction zone towards the projectile side in the transverse direction is found to be due to the stronger pion reabsorption by the heavier target spectator.

We will summarize in Chapter 7.

Chapter 2

Relativistic Transport Equations for Hadronic Matter

In this chapter, we derive a coupled set of transport equations for the phase space distribution functions of nucleons, baryon resonances and pions, and establish notations for succeeding chapters. The transport equations furnish a computationally manageable scheme for treating the dynamics of the interacting baryons and pions, reducing the many-body problem to a set of coupled one-body problems.

First, in section 1, we construct the Hamiltonian for the hadronic matter, starting from the effective Lagrangian density containing free fields of nucleons, deltas, σ-, ω- and π-mesons, as well as the minimum coupling between them. In section 2 we derive equations of motion for the one-body density matrix of nucleons, delta resonances and pions. Subsequently, in section 3, we make Wigner transformations of these equations, in order to obtain a set of transport equations for the phase-space distribution functions of baryons and pions. These equations contain a Vlasov term of the usual form and several collision terms, in analogy with the standard Boltzmann-Uehling-Uhlenbeck equation[Bert88a].

2.1 Model for hadronic matter

This section introduces the model description of hadronic matter in terms of interacting baryonic and mesonic fields. Throughout the developments, we employ units in which $\hbar$ and c are unity.

2.1.1 Model Lagrangian

For nuclear collisions at beam energies of up to around one GeV per nucleon, the main baryonic excitation is the $\Delta(1236)$ resonance. Higher resonances have negligible excitation functions. Therefore, a first step towards a complete description of hadronic matter should include nucleons and Δ resonances, in addition to π, σ and ω mesons. Accordingly, we adopt a model hadronic Lagrangian density involving the baryon fields $N(x)$ and $\Delta^{\nu}(x)$, the meson fields $\boldsymbol{\pi}(x)$, $\sigma(x)$, and $\omega^{\mu}(x)$, and their interactions in the minimal coupling scheme commonly used for relativistic hadronic systems [Wang89, Cass90c, Wlbr91a],

$$\mathcal{L}(x) = \mathcal{L}^{0}(x) + \mathcal{L}^{\rm int}(x) \; , \tag{2.1}$$

where $\mathcal{L}^{0}$ and $\mathcal{L}^{\rm int}$ are the free-field and interaction Lagrangian densities, respectively. We have used x to denote the Minkowski four-vector $(t, \mathbf{r})$. Moreover, the free Lagrangian density is

$$\begin{aligned} \mathcal{L}^{0}(x) &= \overline{N}(x)(i\gamma^{\mu}\partial_{\mu} - m_{N})N(x) + \overline{\Delta}_{\nu}(x)(i\gamma^{\mu}\partial_{\mu} - M_{\Delta})\Delta^{\nu}(x) \\ &+ \frac{1}{2}[\partial_{\mu}\boldsymbol{\pi}(x)\cdot\partial^{\mu}\boldsymbol{\pi}(x) - m_{\pi}^{2}\boldsymbol{\pi}(x)\cdot\boldsymbol{\pi}(x)] \\ &+ \frac{1}{2}[\partial_{\mu}\sigma(x)\partial^{\mu}\sigma(x) - m_{\sigma}^{2}\sigma^{2}(x)] \\ &- \frac{1}{4}F_{\mu\nu}(x)F^{\mu\nu}(x) + \frac{1}{2}m_{\omega}^{2}\omega_{\mu}(x)\omega^{\mu}(x) \; , \end{aligned} \tag{2.2}$$

and the interaction Lagrangian density is

$$\mathcal{L}^{\rm int}(x) = -ig_{\pi NN}\overline{N}(x)\gamma_{5}\boldsymbol{\tau}N(x)\cdot\boldsymbol{\pi}(x) + g_{\sigma NN}\overline{N}(x)N(x)\sigma(x)$$

$$
\begin{aligned}
&- \; g_{\omega NN}\overline{N}(x)\gamma^{\mu}N(x)\omega_{\mu}(x) \\
&+ \; g_{\pi N\Delta}[\overline{\Delta}_{\mu}(x)\boldsymbol{\mathcal{T}}N(x)\cdot\partial^{\mu}\boldsymbol{\pi}(x)+\overline{N}(x)\boldsymbol{\mathcal{T}}^{\dagger}\Delta^{\mu}(x)\cdot\partial_{\mu}\boldsymbol{\pi}(x)] \\
&- \; ig_{\pi\Delta\Delta}\overline{\Delta}_{\mu}(x)\gamma_5\boldsymbol{T}\Delta^{\mu}(x)\cdot\boldsymbol{\pi}(x)+g_{\sigma\Delta\Delta}\overline{\Delta}_{\mu}(x)\Delta^{\mu}(x)\sigma(x) \\
&- \; g_{\omega\Delta\Delta}\overline{\Delta}_{\mu}(x)\gamma^{\nu}\Delta^{\mu}\omega_{\nu}(x)\;, \qquad (2.3)
\end{aligned}
$$

with $F_{\mu\nu} = \partial_{\mu}\omega_{\nu} - \partial_{\nu}\omega_{\mu}$. The nucleon field $N(x)$ is an isospinor, the Δ field is described by the Rarita-Schwinger formalism[Rari41] as a four-vector with each component as an isospinor. The pion field $\boldsymbol{\pi}(x)$ is an isovector and a Minkowski pseudoscalar. Furthermore, the sigma field $\sigma(x)$ is a scalar in both Minkowski and isospin space, whereas the omega field $\omega_{\mu}(x)$ is a Minkowski vector and an isoscalar.

It is convenient to employ the isospin generators $\boldsymbol{\tau}$, $\boldsymbol{T}$ and $\boldsymbol{t}$ which act on the isospinor $N(x)$, the isospinor $\Delta(x)$, and the isovector $\boldsymbol{\pi}(x)$, respectively. They satisfy

$$\boldsymbol{T} = \boldsymbol{t} \oplus \frac{1}{2}\boldsymbol{\tau} \qquad (2.4)$$

and

$$\tau_3 \;=\; \begin{cases} 1 & \text{for } p \\ -1 & \text{for } n \end{cases}\;, \qquad (2.5)$$

$$t_3 \;=\; \begin{cases} 1 & \text{for } \pi^{+} \\ 0 & \text{for } \pi^{0} \\ -1 & \text{for } \pi^{-} \end{cases}\;, \qquad (2.6)$$

It is also convenient to employ the isospin transition operator $\boldsymbol{\mathcal{T}} = (\mathcal{T}_{+}, \mathcal{T}_{0}, \mathcal{T}_{-})$, as in refs. [Brow75, Oset82]. The matrix representation of $\mathcal{T}_{\mu}$, μ=1, 0, -1, can be obtained from the following equation,

$$(\mathcal{T})_{M_T m_\tau} = \sum_{k=-1}^{1} \langle \frac{3}{2} M_T | 1k \frac{1}{2} m_\tau \rangle (t^k)^{*}, \qquad (2.7)$$

where $t^{\pm 1} = (1, \pm i, 0)/\sqrt{2}$ and $t^0 = (0, 0.1)$, and only $k = M_T - m_\tau$ contributes. The above two expressions imply

$$\mathcal{T}_+ = \begin{pmatrix} \frac{1}{\sqrt{2}} & 0 \\ 0 & \frac{1}{\sqrt{6}} \\ 0 & 0 \\ 0 & 0 \end{pmatrix} , \quad \mathcal{T}_- = \begin{pmatrix} 0 & 0 \\ 0 & 0 \\ \frac{1}{\sqrt{6}} & 0 \\ 0 & \frac{1}{\sqrt{2}} \end{pmatrix} , \quad \mathcal{T}_0 = \begin{pmatrix} 0 & 0 \\ \sqrt{\frac{2}{3}} & 0 \\ 0 & \sqrt{\frac{2}{3}} \\ 0 & 0 \end{pmatrix} . \tag{2.8}$$

2.1.2 Equations of motion for the hadron fields

The equations of motion for the hadron fields can be obtained from the Lagrangian density given in equations (2.1-2.3) by means of the Euler-Lagrange equations. The result is

$$\begin{aligned} (i\gamma^\mu \partial_\mu - m_N) N(x) &= i g_{\pi NN} \boldsymbol{\pi}(x) \cdot \gamma_5 \boldsymbol{\tau} N(x) - g_{\sigma NN} \sigma(x) N(x) \\ &+ g_{\omega NN} \omega_\mu(x) \gamma^\mu N(x) - g_{\pi N\Delta} \boldsymbol{\mathcal{T}}^\dagger \Delta^\mu(x) \cdot \partial_\mu \boldsymbol{\pi}(x) , \end{aligned} \tag{2.9}$$

$$\begin{aligned} (i\gamma^\mu \partial_\mu - M_\Delta) \Delta^\mu(x) &= i g_{\pi\Delta\Delta} \boldsymbol{\pi}(x) \cdot \gamma_5 \boldsymbol{T} \Delta^\mu(x) - g_{\sigma\Delta\Delta} \sigma(x) \Delta^\mu(x) \\ &+ g_{\omega\Delta\Delta} \omega_\nu(x) \gamma^\nu \Delta^\mu(x) - g_{\pi N\Delta} \partial^\mu \boldsymbol{\pi}(x) \cdot \boldsymbol{\mathcal{T}} N(x) , \end{aligned} \tag{2.10}$$

$$(\partial^\mu \partial_\mu + m_\sigma^2) \sigma(x) = g_{\sigma NN} \overline{N}(x) N(x) + g_{\sigma\Delta\Delta} \overline{\Delta}_\mu(x) \Delta^\mu(x) , \tag{2.11}$$

$$\begin{aligned} (\partial_\mu \partial^\mu + m_\pi^2) \boldsymbol{\pi}(x) &= -i g_{\pi NN} \overline{N}(x) \gamma_5 \boldsymbol{\tau} N(x) - i g_{\pi\Delta\Delta} \overline{\Delta}_\mu(x) \gamma_5 \boldsymbol{T} \Delta^\mu(x) \\ &- g_{\pi N\Delta} [\partial^\mu (\overline{\Delta}_\mu(x) \boldsymbol{\mathcal{T}} N(x)) + \partial_\mu (\overline{N}(x) \boldsymbol{\mathcal{T}}^\dagger \Delta^\mu(x))] , \end{aligned} \tag{2.12}$$

$$\partial^\mu F^\omega_{\mu\nu} + m_\omega^2 \omega_\nu(x) = g_{\omega NN} \overline{N}(x) \gamma_\nu N(x) + g_{\omega\Delta\Delta} \overline{\Delta}_\mu(x) \gamma_\nu \Delta^\mu(x) . \tag{2.13}$$

The above set of equations form a complete closed set of equations for the evolution of the various hadronic fields considered. In principle, the solution of these equations can be used to describe nuclear reactions. However, due to computer limitations, their solution is presently not within reach. An alternative way is to solve transport equations for the hadron fields. For the purpose of deriving the transport equations within the framework of the density matrix formalism we construct the model Hamiltonian for hadronic matter in the next subsection.

2.1.3 Hamiltonian for hadronic matter

The main role of the meson fields in the Lagrangian (2.1) is to mediate the strong interaction between the baryons. This is strictly true for the fields $\sigma(x)$ and $\omega_\mu(x)$ which have no manifestations in terms of real physical particles. Therefore, these fields can be regarded as representing virtual mesons, and they can be eliminated in exchange for effective potentials acting among the baryons. However, the pion field plays a dual role; not only can the pion mediate interactions (and in this role it acts as a virtual meson, similar to σ and ω) but it can also be manifested as a real physical particle that can be observed. Thus, the pion field is somewhat akin to the electromagnetic field; the transverse component of the electromagnetic field represents real photons while the longitudinal component mediates the Coulomb interaction between charged particles.

In order to construct an effective Hamiltonian for hadronic matter, we eliminate all virtual meson fields, leaving only the real pion, in addition to the baryons, since real particles are amenable to numerical simulation. Of course, such a separation can not be made in an exact manner, because the pion has a finite mass, in contradistinction to the photon in *QED*. Nevertheless, a useful approximate treatment can be made, as we shall now describe.

The elimination of the virtual meson fields can be accomplished by means of the Green's function technique. However, the equation of motion for the baryon fields and pion field obtained in this way will be non-local in space and time. This is the price paid for the elimination of virtual meson fields. Since we wish to formulate a transport theory within the density-matrix framework, non-locality in time is inconvenient. Fortunately, meson retardation effects are not significant in the energy range considered here. Consequently, the instantaneous meson exchange approximation can be made to establish time locality and thus make the equations of motion amenable to the density-matrix treatment [Wang85, Cass90b, Wang89, Cass90c, Webe90]. For the σ and ω mesons this approximation seems to be well justified. The pion, however, has a smaller mass, our approximation has to be used with caution. In terms of the meson propogator the instantaneous meson exchange approximation can be expressed as

$$G(x-x') \approx G(\boldsymbol{r}-\boldsymbol{r}',t)\delta(t-t'). \tag{2.14}$$

We have to keep in mind, however, that by using the instantaneous meson exchange approximation, we give up relativistic covariance. With this approximation, an effective Hamiltonian for hadronic matter can be constructed as[Wlbr91a]

$$\hat{H}^h_{\rm eff} = \hat{H}^b_{\rm eff} + \hat{H}^\pi + \hat{V}^{b\pi} \ . \tag{2.15}$$

The effective baryon Hamiltonian $\hat{H}^b_{\rm eff}$, the Hamiltonian for the real pion $\hat{H}^\pi$, and the baryon-pion interaction $\hat{V}^{b\pi}$ are

$$\begin{aligned} \hat{H}^b_{\rm eff} &= \int \psi^\dagger(x)\hat{E}(x)\psi(x)d\boldsymbol{r} \\ &+ \frac{1}{2}\int \psi^\dagger(x_1)\psi^\dagger(x_2)\hat{V}(x_1-x_2)\psi(x_2)\psi(x_1)d\boldsymbol{r}_1 d\boldsymbol{r}_2 \ , \end{aligned} \tag{2.16}$$

$$\hat{H}^\pi = \frac{1}{2}\int [\dot{\boldsymbol{\pi}}(x)\cdot\dot{\boldsymbol{\pi}}(x) + \nabla\boldsymbol{\pi}(x)\cdot\nabla\boldsymbol{\pi}(x) + m_\pi^2\boldsymbol{\pi}(x)\cdot\boldsymbol{\pi}(x)]d\boldsymbol{r} \ , \tag{2.17}$$

and

$$\hat{V}^{b\pi} = \int \psi^{\dagger}(x)\hat{U}^{\pi}(x)\psi(x)d\boldsymbol{r} \ , \tag{2.18}$$

where

$$\psi(x) = \begin{pmatrix} \psi_N(x) \\ \psi_\Delta(x) \end{pmatrix} = \begin{pmatrix} N(x) \\ \Delta(x) \end{pmatrix} \tag{2.19}$$

and

$$\psi(x_2)\psi(x_1) = \begin{pmatrix} N(x_2)N(x_1) \\ N(x_2)\Delta(x_1) \\ \Delta(x_2)N(x_1) \\ \Delta(x_2)\Delta(x_1) \end{pmatrix} \tag{2.20}$$

The baryon energy operator $\hat{E}$ of eq. (2.16) can be written as

$$\hat{E}(x) = \begin{pmatrix} \hat{E}_N(x) & 0 \\ 0 & \hat{E}_\Delta(x) \end{pmatrix} , \tag{2.21}$$

where

$$\hat{E}_N(x) = \alpha_i(-i\partial^i) + \gamma_0 m_N \ , \tag{2.22}$$

$$\hat{E}_\Delta(x) = \alpha_i(-i\partial^i) + \gamma_0 M_\Delta \ , \tag{2.23}$$

and $\alpha_i = \gamma_0\gamma_i$ and $\alpha_o = \gamma_0\gamma_0 = 1$. Furthermore, $\hat{U}^{\pi}$ and $\hat{V}(x_1 - x_2)$ are defined as follows,

$$\hat{U}^{\pi}(x) = \hat{\boldsymbol{U}}_{\pi} \cdot \boldsymbol{\pi}(x) \ , \tag{2.24}$$

with

$$\hat{\boldsymbol{U}}_{\pi} = \begin{pmatrix} \hat{\boldsymbol{U}}_{NN} & \hat{\boldsymbol{U}}_{N\Delta} \\ \hat{\boldsymbol{U}}_{\Delta N} & \hat{\boldsymbol{U}}_{\Delta\Delta} \end{pmatrix} , \tag{2.25}$$

$$\hat{U}_{NN} = ig_{\pi NN}\gamma_0\gamma_5\boldsymbol{\tau}\ ,\ \hat{U}_{N\Delta} = -g_{\pi N\Delta}\gamma_0\boldsymbol{\mathcal{T}}^\dagger\partial_\nu\ , \tag{2.26}$$

$$\hat{U}_{\Delta N} = -g_{\pi N\Delta}\gamma_0\boldsymbol{\mathcal{T}}\partial^\nu\ ,\ \hat{U}_{\Delta\Delta} = ig_{\pi\Delta\Delta}\gamma_0\gamma_5\boldsymbol{T}\partial_{\mu\nu}\ , \tag{2.27}$$

and

$$\hat{V}(x_1 - x_2) = \hat{v}_{ij,kl}\ ,\ i,j,k,l = N,\Delta. \tag{2.28}$$

Keeping in mind that $\hat{\boldsymbol{U}}_\pi$ is a matrix of isovectors, we can omit the boldface in the following derivations without causing any confusion.

The equations of motion for the baryon fields and pion fields can be derived from the effective hadronic Hamiltonian under the instantaneous meson exchange approximation by virtue of the following Heisenberg equations,

$$i\frac{\partial N}{\partial t} = [\hat{H}^h_{\rm eff}, N]\ , \tag{2.29}$$

$$i\frac{\partial \Delta^\mu}{\partial t} = [\hat{H}^h_{\rm eff}, \Delta^\mu]\ , \tag{2.30}$$

$$i\frac{\partial \boldsymbol{\pi}}{\partial t} = [\hat{H}^h_{\rm eff}, \boldsymbol{\pi}]\ . \tag{2.31}$$

The salient features of the hadronic Hamiltanion (eq. (2.15)) and the above Heisenberg equations are 1) they have structure similar to those of non-relativistic quantum many-body theory, and, as we shall see below, 2) they can be cast into density-matrix form, which, when augmented with correlation dynamics, is suitable for a non-perturbative treatment of quantum many-body problems.

2.2 Density matrix treatment

In this section we shall reformulate the hadron dynamics in terms of the density matrix. Within the two-body correlation approximation, we obtain a set of coupled equations of motion for the one-body density matrix of baryons and pions.

2.2.1 Density operators

The n-body baryon density operator $\hat{\rho}_n$ is defined as

$$\hat{\rho}_n(1,2,\cdots n;1',2',\cdots n') = \psi^\dagger(1')\psi^\dagger(2')\cdots\psi^\dagger(n')\psi(n)\cdots\psi(1), \tag{2.32}$$

with

$$n = x_n = (t, \boldsymbol{r}_n, m_n)\ ,\ n' = x'_n = (t, \boldsymbol{r}'_n, m'_n)\ , \tag{2.33}$$

where m_n is the spin-isospin quantum number and we have used that $t' = t$ due to the instantaneous approximation (2.14). The n-body density matrix is defined as the expectation value of $\hat{\rho}_n$, namely

$$\rho_n(1,2,\cdots n;1',2',\cdots n') = \langle\hat{\rho}_n(1,2,\cdots n;1',2'\cdots n')\rangle\ . \tag{2.34}$$

The baryon number operator is defined as

$$\hat{N} = \mathrm{Tr}_1\psi^\dagger(1)\psi(1) = \mathrm{Tr}_1 N^\dagger(1)N(1) + \mathrm{Tr}_1\Delta^\dagger_\mu(1)\Delta^\mu(1)\ . \tag{2.35}$$

It is straightforward to show that[Wlbr91a]

$$[\hat{N},\psi(1)] = -\psi(1)\ ,\ [\hat{N},\psi^\dagger(1)] = \psi^\dagger(1)\ ,\ \hat{N}^\dagger = \hat{N}\ . \tag{2.36}$$

From eqs. (2.32,2.35,2.36) we obtain the following reduction relations

$$\hat{\rho}_n = \frac{1}{\hat{N}-n}\,\mathrm{Tr}_{(n+1)}\hat{\rho}_{n+1} = \mathrm{Tr}_{(n+1)}\hat{\rho}_{n+1}\,\frac{1}{\hat{N}-n}\ . \tag{2.37}$$

To obtain the correlation dynamics the key step is to separate out many-body correlations from the reduced density matrices. This can be realized by a non-linear

transformation [Wang85],

$$\begin{aligned} & \rho_n(1,2,\cdots,n;1',2',\cdots,n') \qquad (2.38) \\ = \; & AS_n \sum_{p=1}^{n-1} \rho_{n-p}(1,2,\cdots,n-p;1',2',\cdots,(n-p)') \\ & \times \rho_p(n-p+1,\cdots,n;(n-p+1)',\cdots,n') + C_n(1,2,\cdots,n;1',2',\cdots,n') \; , \end{aligned}$$

where the operation AS_n should be understood as follows. The operator A denotes the antisymmetrization operation among those of the variables $(1,2,\cdots,n)$ that refer to identical particles. (Thus, labels referring to nucleons are antisymmetrized separately from those referring to deltas.) Furthermore, the subsequent operation by S symmetrizes among variable pairs $(1,1'),\cdots,(n,n')$ of identical particles. The combined operation AS_n then acts among n particles, and the repeated terms should be omitted. Thus, for the one-particle density we have $\rho \equiv \rho_1 = C_1$, while the two-particle density ρ_2 is given by

$$\begin{aligned} \rho_2(1,2;1',2') &= AS_2\rho(1;1')\rho(2;2') + C_2(1,2;1',2') \qquad (2.39) \\ &= \rho(1;1')\rho(2;2') - \rho(1;2')\rho(2;1') + C_2(1,2;1',2'). \end{aligned}$$

The most common approximations in quantum many-body theory can be obtained by making the lowest order truncation. The simplest truncation approximation assumes that all the many-body correlations vanish and leads to the mean-field approximation. The next order truncation, namely, $C_2 \neq 0$ and $C_{n>2} = 0$ leads to the two-body correlation dynamics. In the following we restrict ourself to the two-body correlation dynamics.

2.2.2 Equation of motion for baryons

By using of the basic anticommutation relation among ψ and ψ^+ we obtain the equation of motion for the n-body density operator,

$$i\frac{\partial \hat{\rho}_n}{\partial t} = [\hat{H}^h(n), \hat{\rho}_n] + \mathrm{Tr}_{(n+1)}[\hat{V}(n+1), \hat{\rho}_{n+1}] \; . \qquad (2.40)$$

Here $\hat{H}^h(n)$ can be written as.

$$\hat{H}^h(n) = \sum_{i=1}^{n}[\hat{E}(i) + \hat{U}^\pi(i)] + \sum_{i<j}^{n} \hat{v}(i,j) = \hat{H}(n) + \sum_{i=1}^{n} \hat{U}^\pi(i) \ . \tag{2.41}$$

where H(n) is the single particle Hamiltonian

$$\hat{H}(n) = \sum_{i=1}^{n} \hat{E}(i) + \sum_{i<j}^{n} \hat{v}(i,j), \tag{2.42}$$

and the potential $\hat{U}^\pi(x)$ is given by eqs. (2.24-2.27). The operator $\hat{V}(n+1)$ appearing in eq. (2.40) is defined as

$$\hat{V}(n+1) = \sum_{i=1}^{n} \hat{v}(i,n+1). \tag{2.43}$$

The equation of motion for ρ_n can then be obtained by taking the expectation value of the operator $\hat{\rho}_n$,

$$i\frac{\partial \rho_n}{\partial t} = [\hat{H}(n), \rho_n] + \mathrm{Tr}_{(n+1)}[\hat{V}(n+1), \rho_{n+1}] + \langle [\sum_{i=1}^{n} \hat{U}^\pi(i), \hat{\rho}_n] \rangle \ . \tag{2.44}$$

Since $\hat{U}^\pi(x)$ contains the pion fields, the last term in the above equation depends on the quantity

$$\langle \hat{\rho}_n(x_1, x_2, \cdots x_n; x_1', x_2', \cdots x_n') \pi(y) \rangle \ , \tag{2.45}$$

which contain the irreducible vertices associated with the pion-baryon interactions. At present, we are not able to treat these in general. Nevertheless, we do find a way to include the lowest-order vertex, which suffices for our present purpose.

Truncating eq. (2.44) at the second order, *i.e.* assuming $C_{n>2} = 0$, we obtain

$$i\frac{\partial \rho}{\partial t} = [\hat{E}, \rho] + \mathrm{Tr}_2[\hat{v}(1,2), \rho_2] + [\hat{U}_\pi, \Gamma] \ , \tag{2.46}$$

$$i\frac{\partial \rho_2}{\partial t} = [\hat{E}(1) + \hat{E}(2) + \hat{v}(1,2), \rho_2] + \mathrm{Tr}_3[\hat{v}(1,3) + \hat{v}(2,3), \rho_3] + \langle [\hat{U}^\pi(1) + \hat{U}^\pi(2), \hat{\rho}_2] \rangle \ , \tag{2.47}$$

where the baryon-pion vertex function $\Gamma(x,y,x')$ is an isovector and it is defined as

$$\Gamma(x,y,x') = \langle\psi^\dagger(x')\pi(y)\psi(x)\rangle \ . \tag{2.48}$$

Noticing that in the two-body correlation approximation $C_3 \equiv 0$ and therefore

$$\rho_2 = AS_2(\rho\rho) + C_2 \ , \tag{2.49}$$

$$\rho_3 = AS_3(\rho\rho\rho + \rho C_2) \ , \tag{2.50}$$

the equations of motion, eqs. (2.46, 2.47), become a coupled set of equations of motion for ρ and C_2. Explicitly, C_2 satisfies

$$\begin{aligned} i\frac{\partial C_2}{\partial t} &= [\hat{E}(1) + \hat{E}(2) + \hat{v}(1,2), C_2] + [\hat{v}(1,2), AS_2\rho\rho] \\ &+ \mathrm{Tr}_3[\hat{v}(1,3) + \hat{v}(2,3), AS_3(\rho\rho\rho + \rho C_2)]_L \ , \end{aligned} \tag{2.51}$$

where $[\cdot]_L$ means linked terms in which any multi-variable functions can not be factorized according to particle variables[Wang85].

To further simplify the equation of motion for the one-body baryon density matrix eq. (2.46) we need to solve eq. (2.51) for C_2, this can be done by closely following the time-dependent G-matrix theory of ref.[Cass88, Wang89]. As we have shown in ref.[Wlbr91a] this leads to

$$\rho_2 = [1 + \hat{g}_{12}(E)\hat{\theta}_{12}\hat{G}(E)]AS_2(\rho(1)\rho(2))[1 + \hat{G}^\dagger(E)\hat{\theta}_{12}\hat{g}^\dagger_{12}(E)]. \tag{2.52}$$

Where

$$\hat{g}_{12}(E) = [E - \hat{h}(1) - \hat{h}(2) + i\varepsilon]^{-1} \ , \tag{2.53}$$

$$\hat{h}(i) = \hat{E}(i) + \hat{U}(i) \ , \tag{2.54}$$

$$\hat{U}(i) = \mathrm{Tr}_{3=3'}\hat{v}(i3)(1 - \hat{P}_{i3})\rho(33') \ , \tag{2.55}$$

$$\hat{\theta}_{12} = 1 - \mathrm{Tr}_{3=3'}(\hat{P}_{13} + \hat{P}_{23})\rho(33') \ . \tag{2.56}$$

Here the operator $\hat{P}_{ij}$ interchanges the coordinates of the identical particles i and j; for non-identical particles it is zero. The $\hat{G}$-matrix obeys the equation

$$\hat{G}(E) = \hat{v} + \hat{v}\hat{g}_{12}(E)\hat{\theta}_{12}\hat{G}(E). \tag{2.57}$$

From the above relations we can express the second term on the right hand side of eq. (2.46) as

$$Tr_2[\hat{v}, \rho_2] = [\hat{U}_{HF}(G), \rho] + I^b_{bb} \ , \tag{2.58}$$

where the mean field $\hat{U}_{HF}$ relates to the real part of the G-matrix and the baryon-baryon collision term I^b_{bb} relates to the imaginary part of the G-matrix

$$\hat{U}_{HF}\rho = \mathrm{Tr}_2\mathrm{Re}(\hat{G}\rho_{20}), \tag{2.59}$$

and

$$\begin{aligned} I^b_{bb} &= -i\mathrm{Tr}_2[i\hat{G}^\dagger\hat{\theta}_{12}\hat{G}\mathrm{Im}(\hat{g}_{12})\rho_{20} - i\rho_{20}\mathrm{Im}(\hat{g}^\dagger_{12})\hat{G}^\dagger\hat{\theta}_{12}\hat{G} \\ &+ \hat{G}\rho_{20}\hat{G}^\dagger\hat{\theta}_{12}\hat{g}^\dagger_{12} - \hat{g}_{12}\hat{\theta}_{12}\hat{G}\rho_{20}\hat{G}^\dagger] \ . \end{aligned} \tag{2.60}$$

The equation of motion for the one-body baryon density matrix then reduces to

$$i\frac{\partial\rho}{\partial t} = [\hat{U}_{HF}(G), \rho] + I^b_{bb} + I^b_{b\pi} \ , \tag{2.61}$$

where the baryon-pion collision term $I^b_{b\pi}$ is given by

$$I^b_{b\pi} = [\hat{U}_\pi, \Gamma] \ . \tag{2.62}$$

2.2.3 Equation of motion for pions

In order to close the equations of motion for baryons, it is necessary to determine the equations of motion for the pion density matrix and for the pion-baryon interaction vertex function Γ.

We start from the equation of motion for the pion field which can be written as

$$(\partial^\mu \partial_\mu + m_\pi^2)\pi(x) = -\hat{u}\hat{\rho}(xx) \ , \tag{2.63}$$

where

$$\hat{u} = \begin{pmatrix} \hat{u}_{NN} & \hat{u}_{N\Delta} \\ \hat{u}_{\Delta N} & \hat{u}_{\Delta\Delta} \end{pmatrix} = \begin{pmatrix} \hat{U}_{NN} & -\hat{U}_{N\Delta} \\ -\hat{U}_{\Delta N} & \hat{U}_{\Delta\Delta} \end{pmatrix} \ , \tag{2.64}$$

with

$$\hat{u}_{NN} = ig_{\pi NN}\gamma_0\gamma_5\boldsymbol{\tau} \ , \ \hat{u}_{N\Delta} = g_{\pi N\Delta}\gamma_0\boldsymbol{\mathcal{T}}^\dagger\partial_\mu \ , \tag{2.65}$$

$$\hat{u}_{\Delta N} = g_{\pi N\Delta}\gamma_0\boldsymbol{\mathcal{T}}\partial^\mu \ , \ \hat{u}_{\Delta\Delta} = ig_{\pi\Delta\Delta}\gamma_0\gamma_5\boldsymbol{T}\delta_{\mu\nu} \ . \tag{2.66}$$

Similarly to $\hat{U}$, $\hat{u}$ is a matrix of isovectors, and we omit the boldface in the following. Eq. (2.63) is the Klein-Gordon equation for the pion field, which contains the second-order time derivative. Therefore this equation is not a convenient starting point for the derivation of the equation of motion for the pion density matrix. In order to linearize the equation, we find the following identity useful,

$$\begin{aligned} \partial_\mu\partial^\mu + m_\pi^2 &= \frac{\partial^2}{\partial t^2} - \nabla^2 + m_\pi^2 \\ &= -\left(i\frac{\partial}{\partial t} + \sqrt{-\nabla^2 + m_\pi^2}\right)\left(i\frac{\partial}{\partial t} - \sqrt{-\nabla^2 + m_\pi^2}\right) \ . \end{aligned} \tag{2.67}$$

If this relation is combined with the free-particle approximation to the Klein-Gordon operator, namely

$$i\frac{\partial}{\partial t} \approx \sqrt{-\nabla^2 + m_\pi^2} = \hat{E}_\pi \ , \tag{2.68}$$

the Klein-Gordon equation for the pion can be approximated by the following two equations,

$$i\dot{\pi}(x) = \hat{E}_\pi\pi(x) + \frac{1}{2\hat{E}_\pi}\hat{u}\hat{\rho}(xx) \ , \tag{2.69}$$

$$\ddot{\pi} = -\hat{E}_\pi^2\pi(x) - \hat{u}\hat{\rho}(xx) \ . \tag{2.70}$$

The pion density operator is defined as

$$\hat{\rho}_\pi(x;x') = \boldsymbol{\pi}(x') \cdot \boldsymbol{\pi}(x) \ . \tag{2.71}$$

The Wigner function for the pions, $f_\pi(\boldsymbol{r},\boldsymbol{p},t)$, can be obtained from the density matrix $\rho_\pi(x;x')$ by means of a Fourier transformation (see eq. (2.76) in sect. 2.3.1),

$$\int \mathrm{Tr}\ \rho_\pi(\boldsymbol{r}+\frac{\boldsymbol{s}}{2};\boldsymbol{r}-\frac{\boldsymbol{s}}{2})\ \mathrm{e}^{-i\boldsymbol{p}\cdot\boldsymbol{s}} d\boldsymbol{s} = \frac{f_\pi(\boldsymbol{r},\boldsymbol{p},t)}{E_\pi(p)} \ . \tag{2.72}$$

The associated equation of motion for $\hat{\rho}_\pi$ is readily obtained from eqs. (2.69,2.70) and so is the expectation value of $\hat{\rho}_\pi$,

$$i\frac{\partial \rho_\pi}{\partial t} = [\hat{E}_\pi, \rho_\pi] + I^\pi_{b\pi} \tag{2.73}$$

where

$$I^\pi_{b\pi} = \frac{1}{2}[\frac{1}{\hat{E}_\pi}\hat{u}, \Gamma] \ . \tag{2.74}$$

The equation of motion for the pion-baryon interaction vertex operator $\hat{\Gamma}$ can be obtained by using of the Heisenberg equation. It is shown that an analytical solution for the baryon-pion interaction vertex can be obtained in the two-body approximation as[Wlbr91a]

$$\begin{aligned}\hat{\Gamma}(x,y,x') \ &= \ -i\pi\delta(\hat{h}(x)+\hat{E}_\pi(y)-\hat{h}(x'))[\frac{1}{\hat{E}_\pi(y)}+\frac{1}{2}(\hat{U}^\pi(x)-\hat{U}^\pi(x'))\frac{1}{\hat{E}_\pi(y)} \\ &+ \ \frac{1}{8}(\hat{U}^\pi(x)-\hat{U}^\pi(x'))^2\frac{1}{\hat{E}_\pi(y)^3}]\hat{\rho}(x;x')\hat{u}(y)\hat{\rho}(y;y) \ .\end{aligned} \tag{2.75}$$

2.3 Transport equations for hadronic matter

It should in principle be possible to solve equations (2.61 and 2.73) numerically by, for example, expansion on a basis of *TDHF* wave functions. This was done by Tohyama

et al.[Gong90] for the nucleonic systems. This approach, however, is severely limited by the available computing resources and has only lent itself to very few exploratory studies and comparisons with experimental observables.

A more tractable procedure is to introduce the Wigner transformation of the density matrix. Within a semiclassical approximation, numerical solutions of the equations of motion for the Wigner transform can be obtained by utilizing the test-particle method. For a purely baryonic system this approach was introduced on a mean field level by Wong[Wong82] and later utilized to study nuclear transport phenomena by Bertsch *et al.*[Bert84, Bert88a].

We follow this latter approach and perform the Wigner transformation of our equations of motion in this section.

2.3.1 The Wigner transformations

The Wigner transformations for the baryon and pion density matrices are

$$\hat{f}_b(\boldsymbol{r},\boldsymbol{p},t) = \int \rho(\boldsymbol{r}+\frac{\boldsymbol{s}}{2},m;\boldsymbol{r}-\frac{\boldsymbol{s}}{2},m')\, \mathrm{e}^{-i\boldsymbol{p}\cdot\boldsymbol{s}} d\boldsymbol{s}\ , \tag{2.76}$$

$$\hat{f}_\pi(\boldsymbol{r},\boldsymbol{k},t) = \int \rho_\pi(\boldsymbol{r}+\frac{\boldsymbol{s}}{2},m;\boldsymbol{r}-\frac{\boldsymbol{s}}{2},m')\, \mathrm{e}^{-i\boldsymbol{p}\cdot\boldsymbol{s}} d\boldsymbol{s}\ , \tag{2.77}$$

where the caret is used to remind of the fact that these quantities are still matrices with respect to the spin-isospin labels m and m'. They can be expanded as

$$\hat{f}_b(\boldsymbol{r},\boldsymbol{p},t) = \sum_{\alpha\alpha'} f_{\alpha\alpha'}(xp) \left(\frac{M^*_\alpha M^*_{\alpha'}}{E^*_\alpha(p) E^*_{\alpha'}(p)}\right)^{1/2} u^\dagger_{\alpha'}(\Pi) u_\alpha(\Pi)\ , \tag{2.78}$$

$$\hat{f}_\pi(\boldsymbol{r},\boldsymbol{k},t) = \sum_{\beta\beta'} f_{\beta\beta'}(xk) \left(\frac{1}{E_\beta(k) E_{\beta'}(k)}\right)^{1/2} v^\dagger_{\beta'}(k) v_\beta(k)\ , \tag{2.79}$$

where the summation is taken over all possible single particle states. Here v_β is the isospinor of the pion, $u_\alpha(\Pi)$ is the spin-isospinor of the baryon which has the effective

mass M_α^* and the momentum Π in accordance with the fact that the baryons are moving in scalar and vector fields. Furthermore, $\alpha = (b, m_s, m_t)$ is used to specify quantum numbers of the baryon, where $b = N$ or Δ, and m_s/m_t is the spin/isospin of the baryon. These spinors satisfy the following orthonormality conditions

$$\langle u_\alpha(\Pi)|u_{\alpha'}(\Pi)\rangle = \delta_{\alpha\alpha'} E_\alpha^*(\Pi)/M_\alpha^* \ , \tag{2.80}$$

and

$$\langle v_\beta(k)|v_{\beta'}(k)\rangle = \delta_{\beta\beta'} \ . \tag{2.81}$$

In the above equations we have used $p = (E, \boldsymbol{P})$ for the four-momentum of baryons and $k = (E_\pi, \boldsymbol{k})$ for that of pions. The effective momentum and mass of the baryon are related to the vector and scalar fields through

$$\Pi_\mu = p_\mu - U_\mu \ , \tag{2.82}$$

$$M_\alpha^* = M_\alpha + U_s \ , \tag{2.83}$$

and the energy of the baryon in the nuclear medium is given by

$$E_\alpha^* = (\Pi_i \Pi^i + M_\alpha^{*2})^{1/2} \ . \tag{2.84}$$

2.3.2 The Vlasov terms

In order to bring out the physics of the kinetic equations for the hadron density matrices more clearly, it is instructive to compare their form with the standard BUU equation. For this purpose, it is useful to recast our equations of motion on the form

$$i\frac{\partial \rho}{\partial t} - [\hat{E} + \hat{U}_{HF}, \rho] = I_{bb}^b + I_{b\pi}^b \ , \tag{2.85}$$

$$i\frac{\partial \rho_\pi}{\partial t} - [\hat{E}^\pi, \rho_\pi] = I_{b\pi}^\pi \ . \tag{2.86}$$

The left-hand sides of these two equations are the Vlasov terms, corresponding to the collisionless one-body propagation. These terms will be rewritten in the usual form below. The mean field U_{HF} in these equations has been assumed to only contain scalar and vector components. It can therefore be decomposed as

$$\hat{U}_{HF}(G) = -\alpha_\mu U^\mu(x) + \gamma_0 U_s(x) \ , \tag{2.87}$$

with $\alpha_\mu = (\gamma_0\gamma_i, \gamma_0\gamma_0) = (\alpha_i, 1)$. Considering only the diagonal elements of ρ and ρ_π in isospin space, as is usually done, we may now perform a Wigner transformation of eqs. (2.85, 2.86) and subsequently take the trace in spin space. Employing the semi-classical limit for the mean-field terms, the following equations of motion for the baryon and pion phase space distributions are then obtained[Wlbr91a], with the Vlasov terms in an explicit form

$$\begin{aligned} \frac{\partial f_b(xp)}{\partial t} + \frac{\Pi^i}{E_b^*(p)}\nabla_i^x f_b(xp) \ - \ & \frac{\Pi^\mu}{E_b^*(p)}\nabla_i^x U_\mu(x)\nabla_p^i f_b(xp) + \frac{M_b^*}{E_b^*(p)}\nabla_i^x U_s \nabla_p^i f_b(xp) \\ = \ & I_{bb}^b(xp) + I_{b\pi}^b(xp) \end{aligned} \tag{2.88}$$

for the particular state b of the baryon. For any charge state of the pion we have

$$\frac{\partial f_\pi(xk)}{\partial t} + \frac{\boldsymbol{k}\cdot\boldsymbol{\nabla}^x}{E_\pi(k)} f_\pi(xk) = I_{b\pi}^\pi(xk) \ , \tag{2.89}$$

where the collision terms are given by

$$I_{bb}^b(xp) = -i\int \mathrm{Tr} I_{bb}^b(x,1;x',1')\ \mathrm{e}^{-i\boldsymbol{p}\cdot\boldsymbol{r}} d\boldsymbol{r} \ , \tag{2.90}$$

$$I_{b\pi}^b(xp) = -i\int \mathrm{Tr} I_{b\pi}^b(x,1;x',1')\ \mathrm{e}^{-i\boldsymbol{p}\cdot\boldsymbol{r}} d\boldsymbol{r} \ , \tag{2.91}$$

and

$$I_{b\pi}^\pi(xk) = -i\int \mathrm{Tr} I_{b\pi}^\pi(x,1;x',1')\ \mathrm{e}^{-i\boldsymbol{k}\cdot\boldsymbol{r}} d\boldsymbol{r} \ . \tag{2.92}$$

2.3.3 The baryon-baryon collision terms

The collision term I_{bb}^{b} represent the rate of change of the baryon phase-space distribution function as a result of baryon-baryon collisions. To calculate the collision term, we use the spin-isospinor u_α to represent a baryon; they satisfy the orthonormality relation eq. (2.80). In this notation, the different N and Δ charge states can be considered as identical particles with different intrinsic quantum numbers α. The two-body density matrix ρ_{20}=AS$\rho(1)\rho(2)$ can then be antisymmetrized even between N and Δ. The interactions used here does not contain the exchange term between N and Δ, and so the exchange term of the matrix elements of the interaction between N and Δ automatically vanishes, due to the above orthonormality relations. Therefore, the spurious terms in ρ_{20} due to the antisymmetrization between N and Δ have no contribution to the collision terms I_{bb}^{b}. With this in mind, the calculation of I_{bb}^{b} is straightforward, although lengthy. The final result is[Wlbr91a]

$$
\begin{aligned}
I_{bb}^{b}(xp) \;=\; & \frac{\pi}{(2\pi)^9} \sum_{\alpha_1\alpha_2\alpha_3, m_b^*} \int\!\!\int\!\!\int d\boldsymbol{p}_1 d\boldsymbol{p}_2 d\boldsymbol{p}_3 \frac{M_b^* M_{\alpha_1}^* M_{\alpha_2}^* M_{\alpha_3}^*}{E_b^* E_{\alpha_1}^* E_{\alpha_2}^* E_{\alpha_3}^*} \\
& \cdot \delta(E_b^*(p) + E_{\alpha_1}^*(p_1) - E_{\alpha_2}^*(p_2) - E_{\alpha_3}^*(p_3))\delta(\boldsymbol{p} + \boldsymbol{p}_1 - \boldsymbol{p}_2 - \boldsymbol{p}_3) \\
& \cdot \langle\langle p\alpha_b p_1\alpha_1|\hat{G}|p_2\alpha_2 p_3\alpha_3\rangle\rangle \qquad (2.93) \\
& \cdot [\langle\langle p_2\alpha_2 p_3\alpha_3|\hat{G}|p\alpha_b p_1\alpha_1\rangle\rangle - \langle\langle p_2\alpha_2 p_3\alpha_3|\hat{G}|p_1\alpha_1 p\alpha_b\rangle\rangle] \\
& \cdot [f_{\alpha_2}(xp_2) f_{\alpha_3}(xp_3)\overline{f}_{\alpha_1}(xp_1)\overline{f}_b(xp) - \overline{f}_{\alpha_2}(xp_2)\overline{f}_{\alpha_3}(xp_3) f_{\alpha_1}(xp_1) f_b(xp)] \,,
\end{aligned}
$$

where

$$
\begin{aligned}
& \langle\langle p\alpha_b p_1\alpha_1|\hat{G}|p_2\alpha_2 p_3\alpha_3\rangle\rangle = \qquad (2.94) \\
& \int \langle u_\alpha(p) u_{\alpha_1}(p_1)|\hat{G}|u_{\alpha_2}(p_2) u_{\alpha_3}(p_3)\rangle e^{-i[(\boldsymbol{p}-\boldsymbol{p}_1)-(\boldsymbol{p}_2-\boldsymbol{p}_3)]\cdot\boldsymbol{r}/2} d\boldsymbol{r}.
\end{aligned}
$$

The collision term I_{bb}^{b} respects the Pauli exclusion principle as shown in the appearance of $\overline{f}_\alpha(xp) = 1 - f_\alpha(xp)$ and $\overline{f}_b(xp) = 1 - f_b(xp)$. The effective interaction $\hat{v}$, and

hence $\hat{G}$, contains the $p \leftrightarrow n$ and $N \leftrightarrow \Delta$ transition operators, and therefore all the possible collision processes are included in this collision integral. The above baryon collision term is of the same form as the NN collision term appearing in the standard BUU equations, but generalized to accommodate the four Δ states of the baryon.

2.3.4 The baryon-pion collision terms

In this section we calculate the rate of change of the hadron phase-space distribution function due to baryon-pion interactions. Let us first consider $I^b_{b\pi}$. It is given by $I^b_{b\pi}(1,1') = \langle \hat{I}^b_{b\pi}(11') \rangle$, where the collision operator is

$$\hat{I}^b_{b\pi}(11') \;=\; \hat{U}_\pi(x)\hat{\Gamma}(x,x,x') - \Gamma(x,x',x')\hat{U}_\pi(x'). \tag{2.95}$$

Taking the average of the collision operator is tedious and the details of this process can be found in Appendix A. As in the BUU equation, the collision terms can be separated into gain terms and loss terms. (The same is true for $I^b_{b\pi}$.) The physical processes represented by the gain and loss terms of $I^b_{b\pi}$ are shown in Fig.2.1. Explicitly,

$$I^b_{b\pi}(\boldsymbol{r},\boldsymbol{p},t) = I^b_{\rm gain}(xp) - I^b_{\rm loss}(xp)\,. \tag{2.96}$$

The gain term is given by

$$I^b_{\rm gain}(xp) = \tag{2.97}$$
$$\frac{\pi}{8(2\pi)^6}\sum_{\pi\alpha' m^b_s}\int\int \frac{M^*_b M^*_{\alpha'}}{E^*_b(p)E^*_{\alpha'}(p')}\frac{\langle u_{\alpha'p'}|\hat{u}(p')\hat{\underline{u}}(k)\hat{u}(p)|u_{\alpha p}\rangle \cdot \langle u_{\alpha p}|\hat{\underline{u}}(k)|u_{\alpha'p'}\rangle}{E^4_\pi(k)}$$
$$\cdot\,[\overline{f}_\pi(xk)f_{\alpha'}(xp')\overline{f}_b(xp)\delta(E^*_b(p)+E_\pi(k)-E^*_{\alpha'}(p'))\delta(\boldsymbol{p'}-\boldsymbol{k}-\boldsymbol{p})$$
$$+f_\pi(xk)f_{\alpha'}(xp')\overline{f}_b(xp)\delta(E^*_b(p)-E_\pi(k)-E^*_{\alpha'}(p'))\delta(\boldsymbol{p'}+\boldsymbol{k}-\boldsymbol{p})]\;d\boldsymbol{p'}d\boldsymbol{k}\;,$$

while the loss term is

$$I^b_{\rm loss}(xp) = \tag{2.98}$$

The collision term $I^b_{b\pi}$

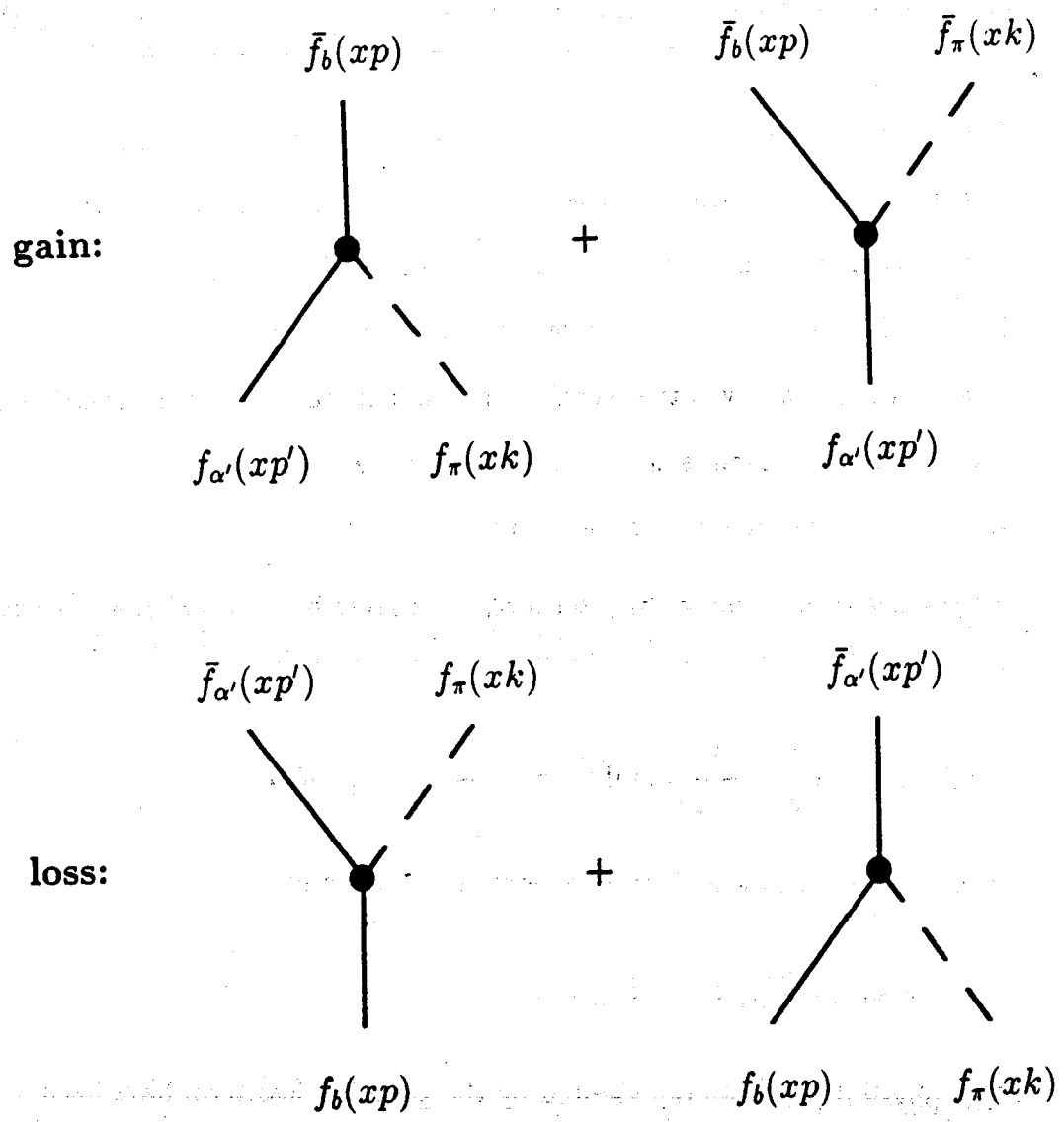

Figure 2.1: Diagrammatic representation of the gain and loss terms responsible for changing the baryon phase-space distribution $f_b(x,p)$ as a result of baryon-pion collisions. The terms on the left pertain to Δ resonances, $b = \Delta$, while those on the right are for nucleons, $b = N$.

$$\frac{\pi}{8(2\pi)^6}\sum_{\pi\alpha' m_s^b}\int\int \frac{M_b^* M_{\alpha'}^*}{E_b^*(p)E_{\alpha'}^*(p')}\frac{\langle u_{\alpha'p'}|\hat{u}(p')\underline{\hat{u}}(k)\hat{u}(p)|u_{\alpha p}\rangle\cdot\langle u_{\alpha p}|\underline{\hat{u}}(k)|u_{\alpha'p'}\rangle}{E_\pi^4(k)}$$

$$\cdot\ [f_\pi(xk)\overline{f}_{\alpha'}(xp')f_b(xp)\delta(E_b^*(p)+E_\pi(k)-E_{\alpha'}^*(p'))\delta(\boldsymbol{p}'-\boldsymbol{k}-\boldsymbol{p})$$

$$+\overline{f}_\pi(xk)\overline{f}_{\alpha'}(xp')f_b(xp)\delta(E_b^*(p)-E_\pi(k)-E_{\alpha'}^*(p'))\delta(\boldsymbol{p}'+\boldsymbol{k}-\boldsymbol{p})]\ d\boldsymbol{p}'d\boldsymbol{k}\ .$$

Here $\overline{f}_\pi(xk)=1+f_\pi(xk)$, and the subscript π has been used to specify the isospin of the pion. These are the general expressions, and the matrix elements in these equations assure that only physical processes can happen. For example, only when b specifies a nucleon do the first terms in these two equations contribute, while only when b specifies a Δ will the second terms contribute. Each of the matrix elements is a vector in spin-isospin space, as dictated by the underlined quantities, and the dot signifies a contraction with respect to these labels.

We now turn to the collision term $I_{b\pi}^\pi$. It is given by $I_{b\pi}^\pi=\langle\hat{I}_{b\pi}^\pi\rangle$, where the collision operator is

$$i\hat{I}_{b\pi}^\pi(x;x')=\frac{1}{2}\left\{\frac{1}{\hat{E}_\pi(x)}\hat{u}(x)\hat{\Gamma}(x,x',x)-\hat{\Gamma}(x',x,x')\hat{u}(x')\frac{1}{\hat{E}_\pi(x')}\right\}\ . \tag{2.99}$$

It can also be separated into gain terms and loss terms,

$$I_{b\pi}^\pi(\boldsymbol{r},\boldsymbol{k},t)=I_{\text{gain}}^\pi(xk)-I_{\text{loss}}^\pi(xk)\ . \tag{2.100}$$

The physical processes represented by the gain and loss term have been depicted in Fig.2.2. Explicitly,

$$\begin{aligned}I_{\text{gain}}^\pi(xk)\ =\ &\frac{\pi}{16(2\pi)^6}\sum_{\alpha\alpha'}\int\int\frac{M_\alpha^* M_{\alpha'}^*}{E_\alpha^*(p)E_{\alpha'}^*(p')}\\ &\cdot\ \frac{\langle u_{\alpha'p'}|\underline{\hat{u}}(k)\hat{u}(p+p')^2|u_{\alpha p}\rangle\cdot\langle u_{\alpha p}|\underline{\hat{u}}(k)|u_{\alpha'p'}\rangle}{E_\pi^4(k)}\\ &\cdot\ \delta(E_{\alpha'}^*(p')-E_\pi(k)-E_\alpha(p))\ \delta(\boldsymbol{p}'-\boldsymbol{p}-\boldsymbol{k})\\ &\cdot\ \overline{f}_\pi(xk)f_{\alpha'}(xp')\overline{f}_\alpha(xp)\ d\boldsymbol{p}d\boldsymbol{p}'\ ,\end{aligned} \tag{2.101}$$

The collision term $I^{\pi}_{b\pi}$

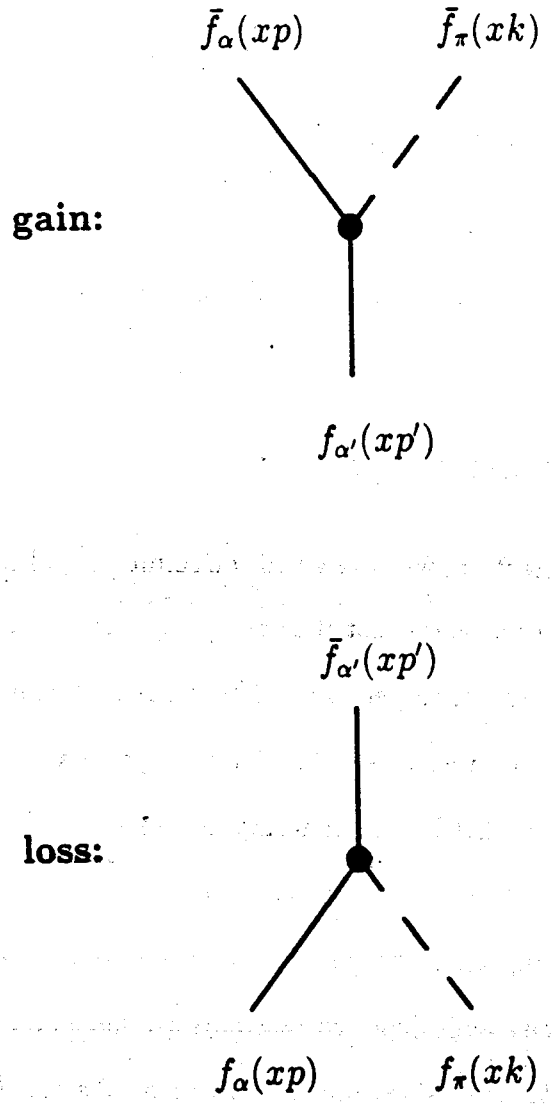

Figure 2.2: Diagrammatic representation of the gain and loss terms responsible for changing the pion phase-space distribution $f_\pi(x,k)$ as a result of baryon-pion collisions.

and

$$
\begin{aligned}
I^{\pi}_{\rm loss}(xk) \;=\; & \frac{\pi}{16(2\pi)^6}\sum_{\alpha\alpha'}\int\int \frac{M^*_{\alpha}M^*_{\alpha'}}{E^*_{\alpha}(p)E^*_{\alpha'}(p')} \\
& \cdot \frac{\langle u_{\alpha'p'}|\underline{\hat{u}}(k)\hat{u}(p+p')^2|u_{\alpha p}\rangle\cdot\langle u_{\alpha p}|\underline{\hat{u}}(k)|u_{\alpha'p'}\rangle}{E^4_{\pi}(k)} \\
& \cdot \delta(E^*_{\alpha'}(p') - E_{\pi}(k) - E_{\alpha}(p))\;\delta(\boldsymbol{p'}-\boldsymbol{p}-\boldsymbol{k}) \\
& \cdot f_{\pi}(xk)f_{\alpha}(xp)\overline{f}_{\alpha'}(xp')\;d\boldsymbol{p}d\boldsymbol{p'}. \qquad (2.102)
\end{aligned}
$$

It should be noted that the fermion suppression factors $\overline{f}_{\alpha}$ and the boson enhancement factors $\overline{f}_{\pi}$ are included in these collision terms automatically and follow from our derivation.

2.3.5 Transport equations

In the previous section, we have given the semiclassical equations of motion, eqs. (2.88, 2.89), for the phase-space distributions $f_b(xp)$ and $f_{\pi}(xp)$ for baryons (nucleons and deltas) and π mesons, respectively. The collision terms appearing in these equations of motion are presented in eq. (2.93) for baryon-baryon collisions, and in eqs. (2.97, 2.98) and (2.101, 2.102) for pion-baryon collisions. Together, these equations form a complete set of coupled transport equations for nucleons, Δ resonances, and π mesons, including all many-particle correlations up to and including the two-body level. Three-body and higher correlations are neglected. This limits the applicability of our theory to heavy-ion collisions up to only a few GeV per nucleon. For higher energies, three- and more-particle effects are expected to play a more significant role [Dani90].

In the following chapters, we will not study the full equation with both scalar and vector mean field potentials. Rather we wish to focus on the dynamics induced by the coupled collision terms for pions, Deltas and nucleons. For this purpose, we limit

ourselves to the case of the presence of only a zeroth component of the vector mean field potential to be able to compare with previous approaches.

With this assumption, eq. (2.88), the transport equation for the particular state b of the baryon (nucleon or Delta) leads to

$$\frac{\partial f_b(xp)}{\partial t} + \frac{\boldsymbol{p}}{E_b} \cdot \nabla_r f_b(xp) - \nabla_r U(x) \cdot \nabla_p f_b(xp) = I^b_{bb}(xp) + I^b_{b\pi}(xp). \tag{2.103}$$

For the pion we still have

$$\frac{\partial f_\pi(xk)}{\partial t} + \frac{\boldsymbol{k}}{E_\pi} \cdot \nabla_r f_\pi(xk) = I^\pi_{b\pi}(xk)\ . \tag{2.104}$$

The collision terms can be written in more compact forms by using of four-dimensional delta functions and introducing the square of the transition matrix element

$$\begin{aligned} & I^b_{bb}(xp) = \\ & \pi \sum_{\alpha_1\alpha_2\alpha_3, m^b_s} \int\int\int \frac{M_b M_{\alpha_1} M_{\alpha_2} M_{\alpha_3}}{E_b E_{\alpha_1} E_{\alpha_2} E_{\alpha_3}} W^b_{bb}(p_1\alpha_1, p_2\alpha_2, p_3\alpha_3, p\alpha_b) \cdot \\ & [f_{\alpha_2}(xp_2) f_{\alpha_3}(xp_3) \overline{f}_{\alpha_1}(xp_1) \overline{f}_b(xp) - \overline{f}_{\alpha_2}(xp_2) \overline{f}_{\alpha_3}(xp_3) f_{\alpha_1}(xp_1) f_b(xp)] \cdot \\ & \delta^{(4)}(p + p_1 - p_2 - p_3) \frac{1}{(2\pi)^9} d\boldsymbol{p}_1 d\boldsymbol{p}_2 d\boldsymbol{p}_3. \end{aligned} \tag{2.105}$$

Where $W^b_{bb}(p_1\alpha_1, p_2\alpha_2, p_3\alpha_3, p\alpha_b)$ is the square of the transition matrix element in baryon-baryon collisions, which determines the transition rate. Explicitly, it is given by

$$\begin{aligned} & W^b_{bb}(p_1\alpha_1, p_2\alpha_2, p_3\alpha_3, p\alpha_b) = \langle\langle p\alpha_b p_1\alpha_1 | \hat{G} | p_2\alpha_2 p_3\alpha_3 \rangle\rangle \\ & \cdot [\langle\langle p_2\alpha_2 p_3\alpha_3 | \hat{G} | p\alpha_b p_1\alpha_1 \rangle\rangle - \langle\langle p_2\alpha_2 p_3\alpha_3 | \hat{G} | p_1\alpha_1 p\alpha_b \rangle\rangle]. \end{aligned} \tag{2.106}$$

Since we are not pursuing a first principle theory at the present stage, the effect of the transition matrix element will be simulated by using of the free space cross sections as we will discuss in detail in the next chapter. In this respect, we take the same path

as all other presently available relativistic dynamical models. The collision terms due to baryon-pion interactions can be rewritten as

$$
\begin{aligned}
& I^b_{b\pi}(xp) = \\
& \frac{\pi}{8}\sum_{\pi\alpha' m^b_j}\int\int \frac{M_b M_{\alpha'}}{E_b(p)E_{\alpha'}(p')} W^b_{b\pi}(\alpha' p', \pi k, \alpha p)\cdot \\
& \{[(1+f_\pi(xk))f_{\alpha'}(xp')\overline{f}_b(xp) - f_\pi(xk)\overline{f}_{\alpha'}(xp')f_b(xp)]\delta^{(4)}(p'-k-p) \qquad (2.107)\\
& +[f_\pi(xk)f_{\alpha'}(xp')\overline{f}_b(xp) - (1+f_\pi(xk))\overline{f}_{\alpha'}(xp')f_b(xp)]\delta^{(4)}(p'+k-p)\}\cdot \\
& \frac{1}{(2\pi)^6}\, dp'dk\ ,
\end{aligned}
$$

and

$$
\begin{aligned}
& I^\pi_{b\pi}(xk) = \\
& \frac{\pi}{16}\sum_{\alpha\alpha'}\int\int \frac{M_\alpha M_{\alpha'}}{E_\alpha(p)E_{\alpha'}(p')} W^\pi_{b\pi}(\alpha p, \alpha' p', \pi k)\cdot \\
& [(1+f_\pi(xk))f_{\alpha'}(xp')\overline{f}_\alpha(xp) - f_\pi(xk)f_\alpha(xp)\overline{f}_{\alpha'}(xp')]\cdot \\
& \delta^{(4)}(p'-p-k)\frac{1}{(2\pi)^6}dpdp'. \qquad (2.108)
\end{aligned}
$$

$W^b_{b\pi}(\alpha' p', \pi k, \alpha p)$ and $W^\pi_{b\pi}(\alpha p, \alpha' p', \pi k)$ are the square of the transition matrix element for the corresponding processes, again their effect will be simulated by using of the free space cross sections and the width of the resonances. Explicitly,

$$
W^b_{b\pi}(\alpha' p', \pi k, \alpha p) = \frac{\langle u_{\alpha' p'}|\hat{u}(p')\underline{\hat{u}}(k)\hat{u}(p)|u_{\alpha p}\rangle \cdot \langle u_{\alpha p}|\underline{\hat{u}}(k)|u_{\alpha' p'}\rangle}{E^4_\pi(k)}, \qquad (2.109)
$$

and

$$
W^\pi_{b\pi}(\alpha p, \alpha' p', \pi k) = \frac{\langle u_{\alpha' p'}|\underline{\hat{u}}(k)\hat{u}(p+p')^2|u_{\alpha p}\rangle \cdot \langle u_{\alpha p}|\underline{\hat{u}}(k)|u_{\alpha' p'}\rangle}{E^4_\pi(k)}. \qquad (2.110)
$$

In summary of this chapter, we have started from a relativistic field theoretical Lagrangian of the Walecka type, including σ, ω and π mesons. By integrating over the degrees of freedom of the virtual mesons, we were able to obtain mean-field terms

for the baryon interactions. However, the pion is treated as a real particle. In this way, we are able to incorporate the formation and decay of Δ resonances.

Even though our theoretical framework fully utilizes relativistic kinematics, and although we start from a fully covariant Lagrangian, our final results do not include the true relativistic effects of retardation.

This is because we made use of the instantaneous meson exchange approximation, eq. (2.14), replacing the Green's function $G(x - x')$ by $G(\boldsymbol{r} - \boldsymbol{r}', t)\delta(t - t')$. This was done to remove the non-locality in time introduced by the elimination of the virtual meson fields.

The advantage of the transport equations as derived here is that one can represent the phase-space distribution functions for nucleons, deltas and pions by test particle distributions for the different species. With this, one should be able to extend the powerful simulation techniques developed for the non-relativistic case of the dynamical simulation of the phase-space distribution function of nucleons in heavy-ion collisions to the relativistic coupled problem for nucleons, deltas and pions. Although the transport equations presented here are derived for a system of pions, nucleons and Delta resonances, they can be easily extended to contain higher resonances, such as the N^*. In the following we will treat N^*'s in a manner similar to that for Delta resonances.

Chapter 3

Numerical Realization of the Model

3.1 Equations of motion for test particles

In this chapter, we present details of the numerical realization procedure of the hadronic transport model.

The transport equations 2.103 and 2.104 for hadronic matter, are highly coupled through the collision integrals. However, their solutions can be obtained numerically within the test particle method which was first introduced to nuclear physics by Wong[Wong82]. The details of the application of the test particle method to solve the standard BUU equation can be found in Ref. [Bert88a].

In the test particle method one discretizes the continuous distribution function with a finite number of test particles representing individual phase space cells, i.e.

$$f(\boldsymbol{r},\boldsymbol{p},t) \cong \frac{1}{N_t}\sum_i \delta(\boldsymbol{r}-\boldsymbol{r}_i)\delta(\boldsymbol{p}-\boldsymbol{p}_i) \tag{3.1}$$

where $\boldsymbol{r}_i$ and $\boldsymbol{p}_i$ are coordinates of the individual test particles. N_t is the number of test particles per nucleon. To obtain the equations of motion for the test particles corresponding to the solution of the transport eqs. (2.103 and 2.104) we take

derivatives of eq. (3.1):

$$\nabla_r f = \frac{1}{N_t}\sum_i \delta'(\boldsymbol{r}-\boldsymbol{r}_i)\delta(\boldsymbol{p}-\boldsymbol{p}_i). \tag{3.2}$$

$$\nabla_p f = \frac{1}{N_t}\sum_i \delta(\boldsymbol{r}-\boldsymbol{r}_i)\delta'(\boldsymbol{p}-\boldsymbol{p}_i), \tag{3.3}$$

$$\frac{\partial f}{\partial t} = -\frac{1}{N_t}\sum_i [\delta'(\boldsymbol{r}-\boldsymbol{r}_i)\delta(\boldsymbol{p}-\boldsymbol{p}_i)\frac{\partial \boldsymbol{r}_i}{\partial t} + \delta(\boldsymbol{r}-\boldsymbol{r}_i)\delta'(\boldsymbol{p}-\boldsymbol{p}_i)\frac{\partial \boldsymbol{p}_i}{\partial t}]. \tag{3.4}$$

Substituting the above derivatives into the transport equations (2.103 and 2.104) the equations of motion for the coordinates of test particles can be obtained. For the baryon test particles

$$\frac{d\boldsymbol{r}}{dt} = \frac{\boldsymbol{p}}{E}, \tag{3.5}$$

$$\frac{d\boldsymbol{p}}{dt} = -\nabla_r U + \boldsymbol{D}^b_{bb}(p) + \boldsymbol{D}^b_{b\pi}(p). \tag{3.6}$$

For the pion test particles, we obtain

$$\frac{d\boldsymbol{r}}{dt} = \frac{\boldsymbol{k}}{E_\pi}, \tag{3.7}$$

$$\frac{d\boldsymbol{k}}{dt} = \boldsymbol{D}^\pi_{b\pi}(k). \tag{3.8}$$

Here $\boldsymbol{D}^b_{bb}(p)$, $\boldsymbol{D}^b_{b\pi}(p)$ are the changing rate of the baryon momentum distribution due to baryon-baryon collisions and baryon-pion collisions, respectively, in accordance with the collision integrals I^b_{bb} and $I^b_{b\pi}$. $\boldsymbol{D}^\pi_{b\pi}(k)$ is the corresponding change in the pion momentum distribution due to baryon-pion collisions corresponding to the collision integral $I^\pi_{b\pi}$. They are calculated in the same manner as in the cascade models[Rand79, Cugn81, Cugn82, Cugn88], namely by discretizing the reaction time into small time steps and solving the collision integrals within each time step via a Monte Carlo simulation method. It is seen that the motion of test particles in the phase space

is governed by the mean field U and the vertex of nucleon-nucleon collisions. In the following we describe these two ingredients of the model in detail.

3.2 The nuclear equation of state

The nuclear equation of state describes the response of the nuclear matter to different temperatures and densities. Current knowledge comprehends a narrow region around the nuclear ground state.

In the present work we use a Skyrme-type density dependent mean field potential for nucleons,

$$U(\rho) = a\frac{\rho}{\rho_0} + b(\frac{\rho}{\rho_0})^\sigma. \tag{3.9}$$

The potential energy density is then given by

$$W(\rho) = \int U(\rho)d\rho = \frac{a}{2}\frac{\rho^2}{\rho_0} + \frac{b}{1+\sigma}(\frac{\rho}{\rho_0})^\sigma\rho. \tag{3.10}$$

The properties of nuclear matter are still not very well known. Only its saturation point at equilibrium, namely, density $\rho_0 = 0.17fm^{-3}$ and binding energy per nucleon E/A $=-15.75$ MeV, is well determined while even the compressibility coefficient at equilibrium is only known to lie between 210 MeV[Blaiz80] and 310 MeV[Shar88]. For high density and high temperature nuclear matter no reliable information available. Here the compressibility coefficient K of nuclear matter is defined as

$$K = 9\rho(\partial P/\partial\rho)_s, \tag{3.11}$$

where the derivative is taken adiabatically and P is the pressure. For the parameterization of the mean field given in eq. (3.9), K is given by

$$K = 9(\frac{p_f^2}{3m} + a + b\sigma). \tag{3.12}$$

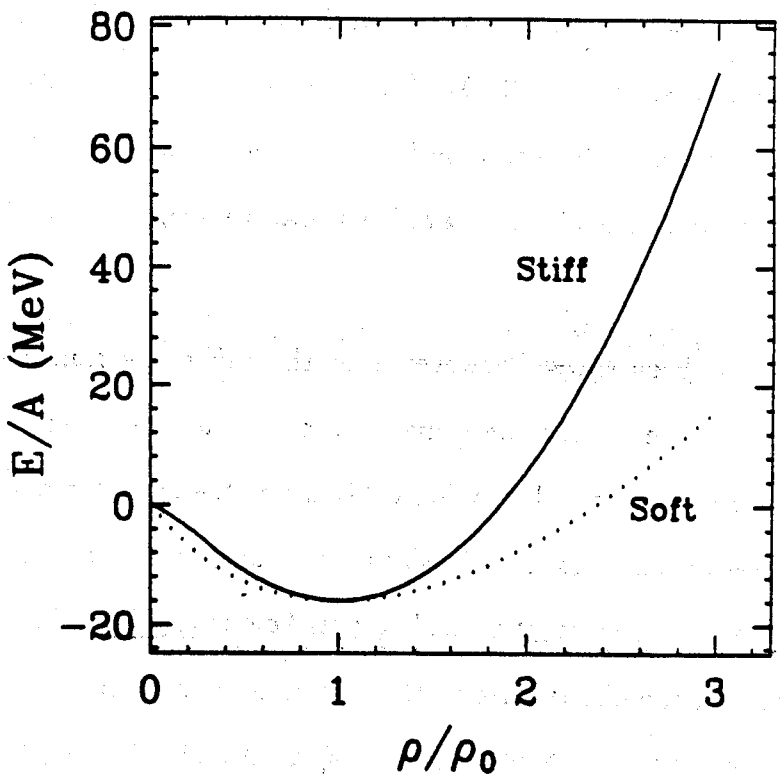

Figure 3.1: The nuclear equation of state, the solid line is for the stiff equation of state and the dotted line is for the soft one.

Here $p_f = 1.36 fm^{-1}$ is the Fermi momentum. The energy per nucleon for nuclear matter at zero temperature is given by

$$\frac{E}{A} = \frac{W(\rho)}{\rho} + \frac{3}{5}E_f(\frac{\rho}{\rho_0})^{\frac{2}{3}}, \tag{3.13}$$

where E_f=37.26 MeV is the Fermi energy. The parameters a, b and σ are then determined by the binding energy per nucleon at ρ_0, a specified compressibility coefficient K and the equilibrium condition of pressure P = 0. For the so called stiff equation of state K = 377 MeV, a = −123.6 MeV, b = 70.4 MeV and σ = 2. For the soft equation of state K= 201 MeV, a = −358.1 MeV, b = 304.8 MeV and $\sigma = \frac{7}{6}$. To see the difference between the two equation of states and their density dependence, the two equations of state have been drawn in Fig. 3.1 as a function of the nucleon density.

It has been shown, however, that the stiff momentum independent equation of state produces about the same amount of transverse momentum and similar flow angle distribution in heavy ion collisions as the available momentum dependent parameterizations, and that the soft momentum independent equation of state produces less transverse momentum and smaller flow angles[Gale87a]. We will study the sensitivity of the observables to the variation of the momentum-independent equation of state. The mean field potentials of the Δ and N^* are still very uncertain[Gino78]. However, relativistic heavy ion collisions are expected to provide information about these potentials[Siem88, Siem89]. In the following we assumed that the potential energies of the Δ and N^* are the same as that of nucleons.

3.3 Elementary nucleon-nucleon cross sections

3.3.1 Elastic scattering channels

We have taken into account the following elastic scattering channels

$$N + N \rightarrow N + N, \tag{3.14}$$

$$N + \Delta \rightarrow N + \Delta, \tag{3.15}$$

$$N + N^* \rightarrow N + N^*, \tag{3.16}$$

$$\Delta + \Delta \rightarrow \Delta + \Delta, \tag{3.17}$$

$$N^* + N^* \rightarrow N^* + N^*, \tag{3.18}$$

$$N^* + \Delta \rightarrow N^* + \Delta. \tag{3.19}$$

Where the nucleon N, the Δ resonance and the N^* resonance can be in any charge state allowed by the charge conservation law. Here we adopt the well known Cugnon's parameterization for nucleon-nucleon elastic cross sections, both for the angular distribution and for the total cross section. Since no information about the collision between a nucleon and a baryon resonance or the collision between two baryon resonances is available, we assumed that all the elastic scattering channels have the same cross section. The total cross section is parameterized as

$$\begin{aligned} \sigma_{el}(\sqrt{s}) &= 55, \quad (\sqrt{s} < 1.8993), \\ \sigma_{el}(\sqrt{s}) &= \frac{35}{1 + 100(\sqrt{s} - 1.8993)} + 20, \quad (\sqrt{s} > 1.8993). \end{aligned} \tag{3.20}$$

In this parameterization, $\sqrt{s}$ is the center of mass energy of nucleon-nucleon collisions and measured in GeV and σ is in mb.

The differential cross section is given by

$$\frac{d\sigma}{dt} = ae^{bt}. \tag{3.21}$$

Where t is the negative of the square of the momentum transfer in the C.M.S. and b is parameterized as

$$b(\sqrt{s}) = \frac{6[3.65(\sqrt{s} - 1.866)]^6}{1 + [3.65(\sqrt{s} - 1.866)]^6}. \tag{3.22}$$

3.3.2 Inelastic scattering channels

The following inelastic scattering channels have been included in the model

$$p + p \leftrightarrow n + \Delta^{++}, \tag{3.23}$$

$$p + p \leftrightarrow p + \Delta^{+}, \tag{3.24}$$

$$n + p \leftrightarrow p + \Delta^{0}, \tag{3.25}$$

$$n + p \leftrightarrow n + \Delta^{+}, \tag{3.26}$$

$$n + n \leftrightarrow p + \Delta^{-}, \tag{3.27}$$

$$n + n \leftrightarrow n + \Delta^{0}, \tag{3.28}$$

$$p + p \leftrightarrow p + N^{*+}, \tag{3.29}$$

$$n + p \leftrightarrow p + N^{*0}, \tag{3.30}$$

$$n + p \leftrightarrow n + N^{*+}, \tag{3.31}$$

$$n + n \leftrightarrow n + N^{*0}. \tag{3.32}$$

Δ and N^* production cross sections for each charge state in all of the above inelastic channels can be estimated by using of VerWest and Arndt's isospin decomposition formula[Verw82] for pion production in nucleon-nucleon collisions.

According to VerWest and Arndt the reaction cross section for single pion production in nucleon-nucleon collisions can be reduced to four independent isospin cross sections σ_{if} with $i, f = 1$ or 0, here i and f are the initial and final isospin of the two

nucleon system. Explicitly,

$$\sigma(p+p\rightarrow p+p+\pi^0) = \sigma_{11}, \tag{3.33}$$

$$\sigma(p+p\rightarrow p+n+\pi^+) = \sigma_{10}+\sigma_{11}, \tag{3.34}$$

$$\sigma(n+p\rightarrow p+n+\pi^0) = \frac{1}{2}(\sigma_{10}+\sigma_{01}), \tag{3.35}$$

$$\sigma(n+p\rightarrow n+n+\pi^+) = \frac{1}{2}(\sigma_{11}+\sigma_{01}), \tag{3.36}$$

$$\sigma(n+p\rightarrow p+p+\pi^-) = \frac{1}{2}(\sigma_{11}+\sigma_{01}). \tag{3.37}$$

Assuming that pions are produced through the intermediate state of Δ and N^* resonances, the following parameterization for the isospin cross section σ_{if} results in a good fit to the experimental single pion production data of nucleon-nucleon collisions.

$$\sigma_{if}(\sqrt{s}) = \frac{\pi(\hbar c)^2}{2p^2}\alpha(\frac{p_r}{p_0})^\beta \frac{m_0^2\Gamma^2(q/q_0)^3}{(s^*-m_0^2)^2+m_0^2\Gamma^2}, \tag{3.38}$$

where α, β, m_0 and Γ are parameters, it has been listed in table 3.1. s is the square of the center of mass energy. Other quantities in the parameterization are defined as

$$p^2 = \frac{s}{4}-M_N^2, \tag{3.39}$$

$$s_0 = (M_N+m_0)^2, \tag{3.40}$$

$$p_0^2 = \frac{s_0}{4}-M_N^2, \tag{3.41}$$

$$p_r^2(s) = \frac{1}{4s}[s-(M_N-\langle M\rangle)^2][s-(M_N+\langle M\rangle)^2], \tag{3.42}$$

$$q^2(s^*) = \frac{1}{4s^*}[s^*-(M_N-M_\pi)^2][s^*-(M_N+M_\pi)^2], \tag{3.43}$$

$$q_0 = q(m_0^2), \tag{3.44}$$

$$s^* = \langle M\rangle^2, \tag{3.45}$$

$$\langle M(s)\rangle = M_0+(\arctan(Z_+)-\arctan(Z_-))^{-1}(\frac{\Gamma_0}{4})\ln(\frac{1+Z_+^2}{1-Z_-^2}). \tag{3.46}$$

Where

$$Z_+ = (\sqrt{s}-M_N-M_0)\frac{2}{\Gamma_0}, \tag{3.47}$$

Table 3.1: Isospin cross section parameters

parameter	σ_{11}	σ_{10}	σ_{01}
α	3.772	15.28	146.3
β	1.262	0	0
m_0(MeV)	1188	1245	1472
Γ(MeV)	99.02	137.4	26.49

$$Z_- = (M_N + M_\pi - M_0)\frac{2}{\Gamma_0}, \tag{3.48}$$

for Δ resonance M_0=1220 MeV, Γ_0=120 MeV and for N^* resonance M_0=1430 MeV, Γ_0=200 MeV.

To gain some familarity with the energy dependence of the isospin cross section, the isospin cross section have been calculated and plotted in Fig. 3.2 for a nucleon with kinetic energy E_k to collide with a nucleon at rest in the laboratory frame.

As shown in ref. [Wolf90], in terms of the isospin cross sections the inelastic cross sections can be estimated as

$$\sigma(p+p \to n+\Delta^{++}) = \sigma_{10} + \frac{1}{2}\sigma_{11}, \tag{3.49}$$

$$\sigma(p+p \to p+\Delta^{+}) = \frac{3}{2}\sigma_{11}, \tag{3.50}$$

$$\sigma(n+p \to p+\Delta^{0}) = \frac{1}{2}\sigma_{11} + \frac{1}{4}\sigma_{10}, \tag{3.51}$$

$$\sigma(n+p \to n+\Delta^{+}) = \frac{1}{2}\sigma_{11} + \frac{1}{4}\sigma_{10}, \tag{3.52}$$

$$\sigma(p+p \to p+N^{*+}) = 0, \tag{3.53}$$

$$\sigma(n+p \to p+N^{*0}) = \frac{3}{4}\sigma_{01}, \tag{3.54}$$

$$\sigma(n+p \to n+N^{*+}) = \frac{3}{4}\sigma_{01}. \tag{3.55}$$

These cross sections have been shown in Fig. 3.3 and Fig. 3.4. Cross sections for the n + n channels can be obtained from that of p + p channels by isospin symmetry. The differential cross sections for the inelastic collisions have been assumed to be isotropic in the nucleon-nucleon center of mass frame.

The reabsorption cross section for baryon resonances have been obtained from the detailed balance. Explicitly, for N^* resonance

$$\sigma(n + N^{*+} \rightarrow n + p) = \frac{p_f^2}{p_i^2}\sigma(p + n \rightarrow n + N^{*+}), \tag{3.56}$$

$$\sigma(p + N^{*0} \rightarrow n + p) = \frac{p_f^2}{p_i^2}\sigma(p + n \rightarrow p + N^{*0}). \tag{3.57}$$

For Δ resonance

$$\sigma(\Delta^+ + p \rightarrow p + p) = \frac{1}{4} \cdot \frac{p_f^2}{p_i^2} \cdot \sigma(p + p \rightarrow \Delta^+ + p), \tag{3.58}$$

$$\sigma(\Delta^{++} + n \rightarrow p + p) = \frac{1}{4} \cdot \frac{p_f^2}{p_i^2} \cdot \sigma(p + p \rightarrow \Delta^{++} + n), \tag{3.59}$$

$$\sigma(\Delta^+ + n \rightarrow p + n) = \frac{1}{2} \cdot \frac{p_f^2}{p_i^2} \cdot \sigma(p + n \rightarrow \Delta^+ + n), \tag{3.60}$$

$$\sigma(\Delta^0 + p \rightarrow p + n) = \frac{1}{2} \cdot \frac{p_f^2}{p_i^2} \cdot \sigma(p + n \rightarrow \Delta^0 + p). \tag{3.61}$$

By using isospin symmetry and averaging over the isospin degree of freedom the above relations reduce to

$$\sigma(N + \Delta \rightarrow N + N) = \frac{1}{8} \cdot \frac{p_f^2}{p_i^2} \cdot \sigma(N + N \rightarrow N + \Delta). \tag{3.62}$$

Here p_f is the momentum in the final NN channel in the C.M. of the colliding particles. This assumes that the resonance is narrow; in general eq.(3.62) underestimates the absorption rate of low-energy Δ's[Dani91].

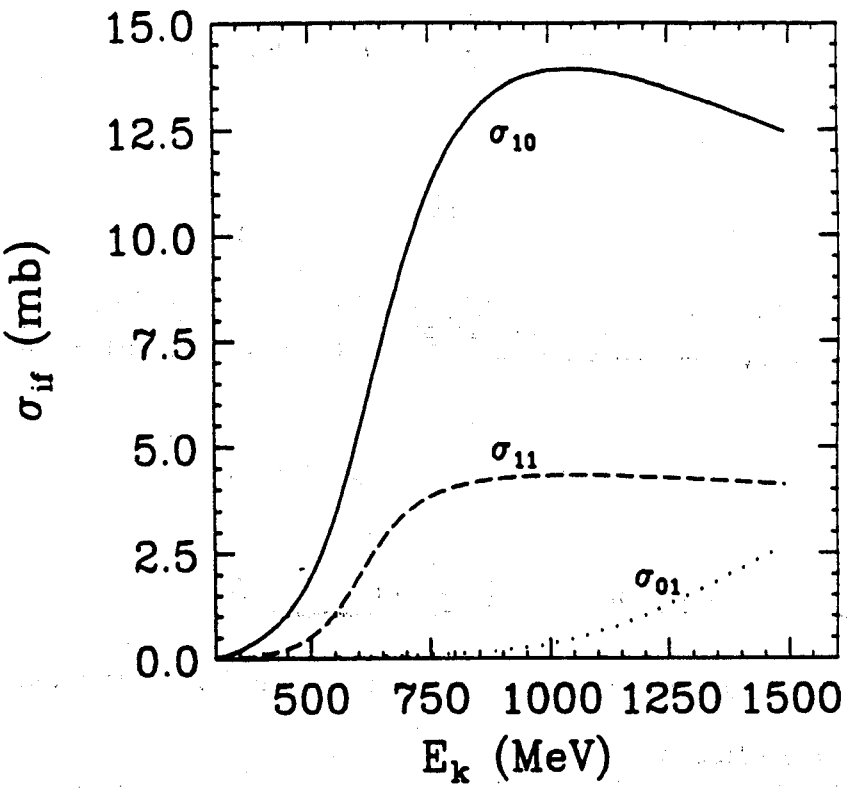

Figure 3.2: Energy dependence of the isospin cross sections

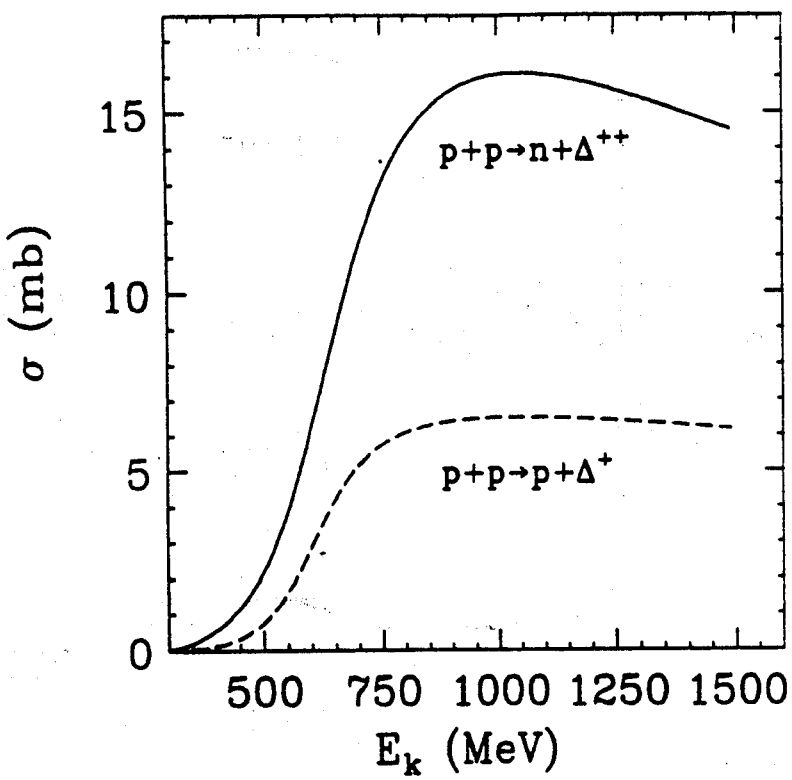

Figure 3.3: Energy dependence of the Δ production cross section in p + p collisions

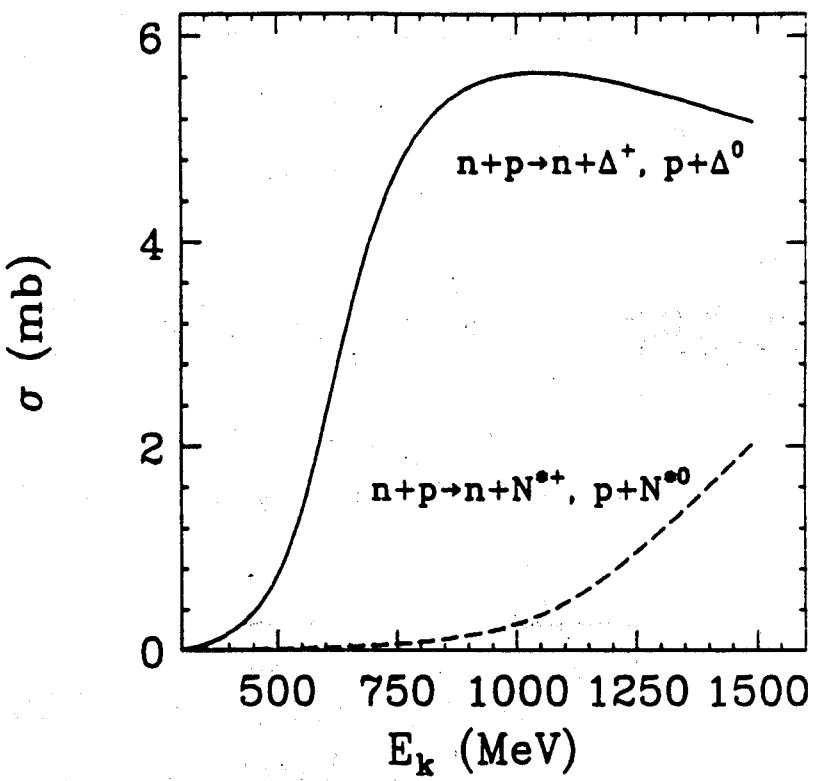

Figure 3.4: Energy dependence of the Δ and N^* production cross section in n + p collisions

3.3.3 Direct pion production channels

Direct processes for pion production of the form

$$N_1 + N_2 \rightarrow N_3 + N_4 + \pi \tag{3.63}$$

account about 20 percent of the total pion production cross section[Kita86]. However, the energy dependence of the direct pion production cross section is unknown. We will set the percentage of the direct process in the total inelastic cross section as a free parameter, meanwhile, reduce the Δ and N^* production cross section estimated in the previous section by this percentage, so that by turning on or off and adjusting this parameter we can study the effect of the direct processes on the experimental observables. The kinematics of the three-body final state is not easy to treat and one usually assumes that the pion takes all of the available kinetic energy in the nucleon-nucleon center of mass frame of the initial state[Kita86, Aich85]. Another way of determining the momentum distribution of the three-body final state is to use the Fermi statistical model for pion production[Ferm54]. The essential assumption in this model is that the production of pions in nucleon-nucleon collisions is governed by statistics rather than by dynamics, with cross sections determined by the available phase space subject to conservation laws. In the C.M.S. of the two initial nucleons the momentum distribution for one of the three particles in the direct process is given by [Bloc56]

$$\begin{aligned}\frac{dP}{dp_1} &= \frac{2\pi^2}{3}p_1^2\{[1-\frac{2(m_2^2+m_3^2)}{(E-E_1)^2-p_1^2}+\frac{(m_2^2-m_3^2)^2}{((E-E_1)^2-p_1^2)^2}]^{1/2}\} \\ &\cdot\{3(E-E_1)^2[1-\frac{(m_2^2-m_3^2)^2}{((E-E_1)^2-p_1^2)^2}] \\ &-p_1^2[1-\frac{2(m_2^2+m_3^2)}{(E-E_1)^2-p_1^2}+\frac{(m_2^2-m_3^2)^2}{((E-E_1)^2-p_1^2)^2}]\}.\end{aligned} \tag{3.64}$$

The maximum of p_1 is given by

$$(p_1)_{max} = \frac{\{[E^2 - (m_1 + m_2 + m_3)^2][E^2 - (m_1 - m_2 - m_3)^2]\}^{1/2}}{2E}, \tag{3.65}$$

where $E = \sqrt{s}$ is the total energy of the system. The momentum distribution of the other two nucleons can be obtained from the energy-momentum conservation. We have developed a Monte Carlo procedure to simulate the three-body momentum distribution. In Fig. 3.5 we compare the pion kinetic energy distribution obtained from the above equation and that from the Monte Carlo procedure for nucleon-nucleon collisions at the center of mass energy of 3 GeV. It is seen that the momentum distribution of the three-body final state can be simulated satisfactorily.

Taking the cross section for the direct pion production as 20 percent of the total inelastic cross section, independent of the center of mass energy of the nucleon-nucleon collisions, we find that the calculated pion spectrum for a nucleus-nucleus at $E/A \simeq$ 1GeV is rather unchanged from that assuming all pions are produced through the intermediate state of Δ and N^* resonances[Liba91a]. To avoid the ambiguity caused by the unknown energy dependence of the direct process and to compare with other model calculations we will neglect the direct process in the following calculations.

3.3.4 The pion-nucleon resonance and decay

In the model we allow the decay of baryon resonances and the pion-nucleon resonance of the form

$$\Delta \leftrightarrow \pi + N \ , \ N^* \leftrightarrow \pi + N. \tag{3.66}$$

Where Δ, N^*, π and nucleon can be in any charge state allowed by charge conservation. The branching ratio of the possible final state is determined by the appropriate

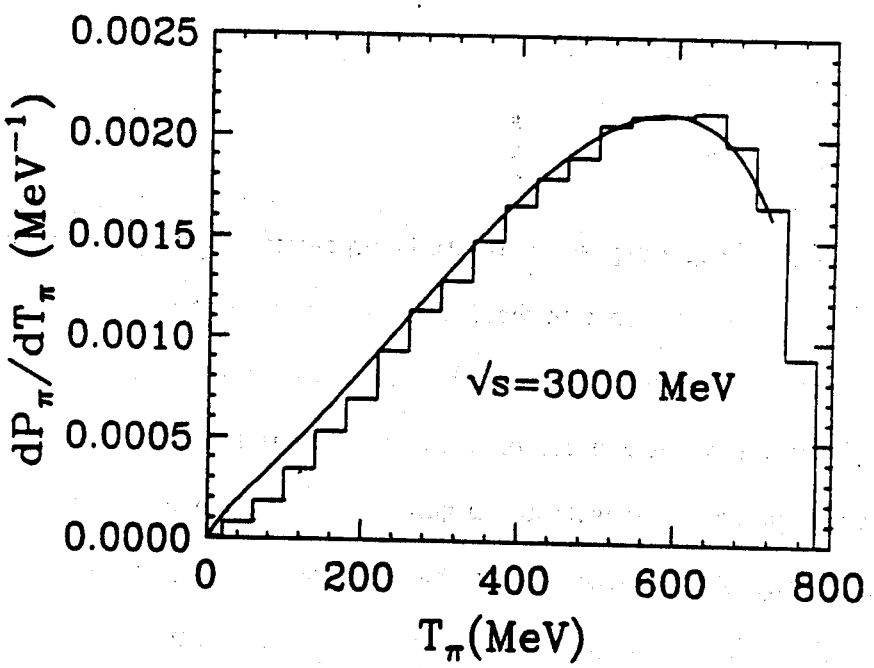

Figure 3.5: Pion kinetic energy distribution in the direct process. The solid line is from Fermi statistical model and the histogram is from the Monte Carlo simulation

Clebsch-Gordan coefficients. The mass of the baryon resonance fromed in the pion-nucleon resonance is uniquely determined by the reaction kinematics. The width for the Δ resonance is parameterized following Kitazoe et al.[Kita86] as

$$\Gamma(q) = \frac{0.47\, q^3}{\left(1 + 0.6\,(q/m_\pi)^2\right) m_\pi^2}, \tag{3.67}$$

where q is the momentum of the pion in the Δ rest frame. For N^* resonance a constant width of 200 MeV has been used[Verw82].

During each time step of duration dt, the decay probability of the Δ's and N^*'s present in the system is determined by an exponential law using the proper time obtained from their widths,

$$P_{decay} = 1 - e^{-dt/\tau}\ ,\ \tau = \frac{\hbar}{\Gamma}. \tag{3.68}$$

Since one of our purposes is to study properties of the pion spectrum in heavy ion collisions, it is necessary to discuss how the pion spectrum in a single nucleon-nucleon collision is calculated. The Δ or N^* resonance is assumed to be produced isotropically in the nucleon-nucleon center of mass frame and we also assume that the decay of the resonance has an isotropic angular distribution in the rest frame of the resonance. The decay of the resonance is then calculated using the Monte Carlo integration technique. This leads to a pion spectrum in the rest frame of the resonance which is finally Lorentz transformed into the desired frame. As an illustration, we show in Fig. 3.6 the contribution to the pion spectrum from the Δ resonance (dotted histogram), N^* resonances (dashed histogram) and the direct process (solid histogram) in nucleon-nucleon collisions at the center of mass energy of 3 GeV. The spectra from the three processes are normalized to 1, respectively.

The cross section for the pion-nucleon resonance is also parameterized using the Breit-Wigner formula with the maximum cross section from the experimental

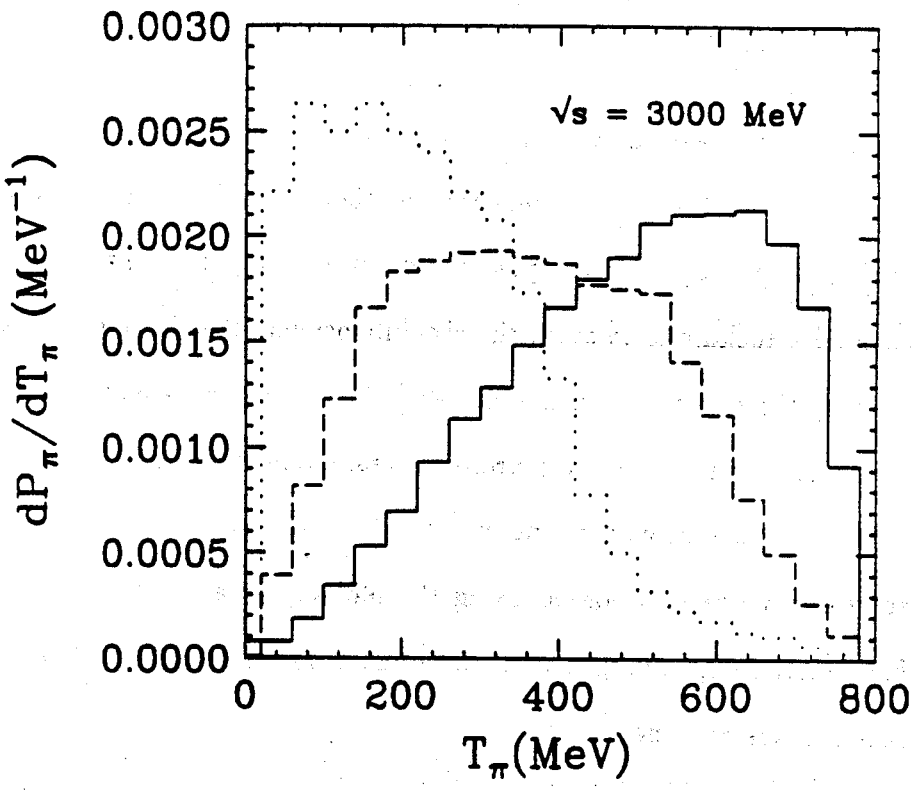

Figure 3.6: Pion spectrum in nucleon-nucleon collisions. The solid histogram is the spectrum from the direct process. The dashed histogram is the spectrum from the N^* decay and the dotted histogram is that from the Δ decay.

data[Part88],

$$\sigma_{\max}(\pi^+ + p \rightarrow \Delta^{++}) = \sigma_{\max}(\pi^- + n \rightarrow \Delta^-) = 200 \text{ mb.} \quad (3.69)$$

$$\sigma_{\max}(\pi^0 + p \rightarrow \Delta^+) = \sigma_{\max}(\pi^0 + n \rightarrow \Delta^0) = 135 \text{ mb.} \quad (3.70)$$

$$\sigma_{\max}(\pi^- + p \rightarrow \Delta^0) = \sigma_{\max}(\pi^+ + n \rightarrow \Delta^+) = 70 \text{ mb.} \quad (3.71)$$

$$\sigma_{\max}(\pi^- + p \rightarrow N^{*0}) = \sigma_{\max}(\pi^0 + n \rightarrow N^{*0}) = 50 \text{ mb.} \quad (3.72)$$

$$\sigma_{\max}(\pi^+ + n \rightarrow N^{*+}) = \sigma_{\max}(\pi^0 + p \rightarrow N^{*+}) = 50 \text{ mb.} \quad (3.73)$$

3.3.5 Pauli blocking for fermions and enhancement factors for bosons

The phase-space occupation factors for the final state of the fermions, $1 - f_b(xp)$, are treated via a Monte-Carlo rejection method. Since the computation of all possible final-state phase-space occupation factors is a very time-intensive task, we have developed a technique to store the six-dimensional phase-space occupation probability at every time step on a lattice[Baue90]. In this way we are able to use a large number of test particles (> 100) to represent a real particle in the reaction of two heavy nuclei while using a reasonable amount of CPU time. BUU-type of calculations for heavy system have been hindered using the old way of evaluating Pauli blocking factors. For reactions involving intermediate mass nuclei, as many as 400 test particles per real particle have been used.

The final state phase-space occupation probability factors for bosons, $1 + f_\pi(xp)$, cannot be treated by conventional rejection methods, because the possible range of values of this function is not between 0 and 1. However, it is possible to introduce a cutoff, F, such

$$F > \max(1 + f_\pi(xp))$$

for all coordinate values (x, p) during the course of the nuclear collision. By

multiplying the interaction matrix element by F and dividing $(1 + f_\pi(xp))/F$ one can use the conventional rejection technique on this scaled occupation probability factor[Wlbr91a, Welk91].

In the present calculation the mean boson phase space occupation probabilities are on the order of $\langle f_\pi \rangle \approx 5 \cdot 10^{-2}$, because we have, for example, ≈ 50 pions of three different isospin substates distributed over a total phase space volume of $\approx 400\, h^3$ for central La + La collisions at 1.35 GeV/nucleon beam energy. Thus the effect of stimulated emission of pions due to the effect of the boson enhancement factor is negligible in the case studied here. In nucleus-nucleus collisions at CERN-energies, however, this may not be the case. Depending on the assumptions for pion freeze out and expansion of the hadronic system, pion phase space occupation probabilities may become comparable to 1, and one may introduce a non-zero chemical potential for pions. Kataya and Ruuskanen[Kata90] have shown that then one can also obtain a concave p_t spectrum for negative pions due to this effect.

Chapter 4

Pion production dynamics

In this chapter we study the dynamics of pion production. In relativistic heavy ion collisions of beam energy around 1 GeV/nucleon about one half of the nucleon-nucleon collision cross sections are inelastic, mainly through pion production. Pion production may reveal interesting properties of the reaction dynamics.

To gain some insight into the dynamical properties of relativistic heavy ion collisions and to get some familiarity with the dynamical characteristics of our model, we show in Fig. 4.1 the time evolution of the accumulated total number of baryon-baryon collisions and the reaction rates for several relevant collision processes. In the model explicit isospin degrees of freedom have been used, the quantities shown in the figure are the sums over all possible isospin channels.

The particular choice of the system Ca+Ca at a beam energy of E/A=1.8 GeV and impact parameter b=0 is made in order to compare with Cugnon's cascade calculation[Cugn81, Cugn82, Cugn88]. The overall time dependence of the total collision number and reaction rates is similar to that of the cascade calculation. The accumulated baryon-baryon collision numbers saturates at around 10-15 fm/c. After this time, mainly Δ decays and pion reabsorptions are present. We see that the Δ destruction processes, $N\Delta \rightarrow NN$ and $\Delta \rightarrow N\pi$, set in slightly later than the

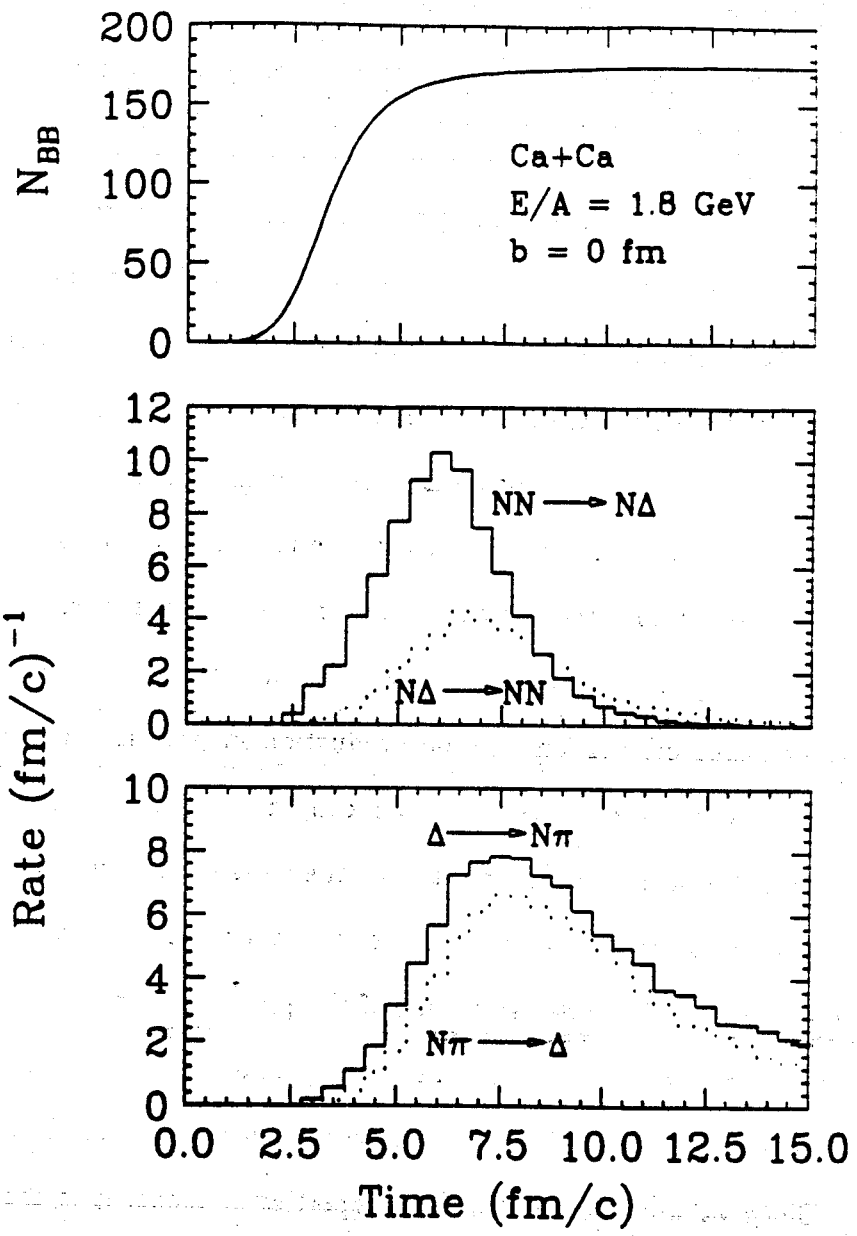

Figure 4.1: Upper figure: Accumulation of the total number of baryon-baryon collisions in the reaction of Ca+Ca at E/A = 1.8 GeV and impact parameter b = 0 fm. Lower figure: Time evolution of the reaction rate for the specified processes in the same reaction.

$NN \rightarrow N\Delta$ process, because the former processes need an appreciable accumulation of Δ's, and also because the Δ has a finite lifetime. The Δ decay rate is always higher than that of the formation of this resonance.

It is of interest to note the quantitative differences between our model calculations and the cascade model calculations. The saturated number of total baryon-baryon collisions calculated in the present model is about 15 percent smaller than that of the cascade model. This is mainly due to the better treatment of the Pauli blocking factor and the inclusion of the mean field in our model. The time integrated cross section for the Δ reabsorption process ($N\Delta \rightarrow NN$) in the present model is about twice of that in the cascade model. Consequently, the total number of pions observed in the final state is about 30 percent less than that in the cascade model. A later modified cascade calculation[Cugn88] shows that the discrepancies between the experimental data and the cascade calculation on pion production in proton, pion and heavy ion induced reactions can be removed if one artifically multiplies the cross section $\sigma(N\Delta \rightarrow NN)$ by a factor of three without changing the cross section $\sigma(NN \rightarrow N\Delta)$. This has been explained as an indication of the enhancement of the pion reabsorption in nuclear medium and the underestimation of the pion reabsorption in their model. However, in our calculation the medium effect explanation is not necessary, and the total pion production cross sections are in agreement with data (see below).

Since we are interested in the properties of pions, it is crucial to know the time evolution of the source of the pions. In Fig. 4.2 the population of free pions and pions still bound inside excited baryons (unborn pions) is displayed for the system La+La at a beam energy of 1350 MeV per nucleon and b=1fm. It is seen that the total number of pions, Δ's and N*'s freezes out at around t=20 fm/c at a value which is in good agreement with experimental data[Harr87]. The overall time dependence of our bound and unbound pion multiplicities is similar to the one obtained from the

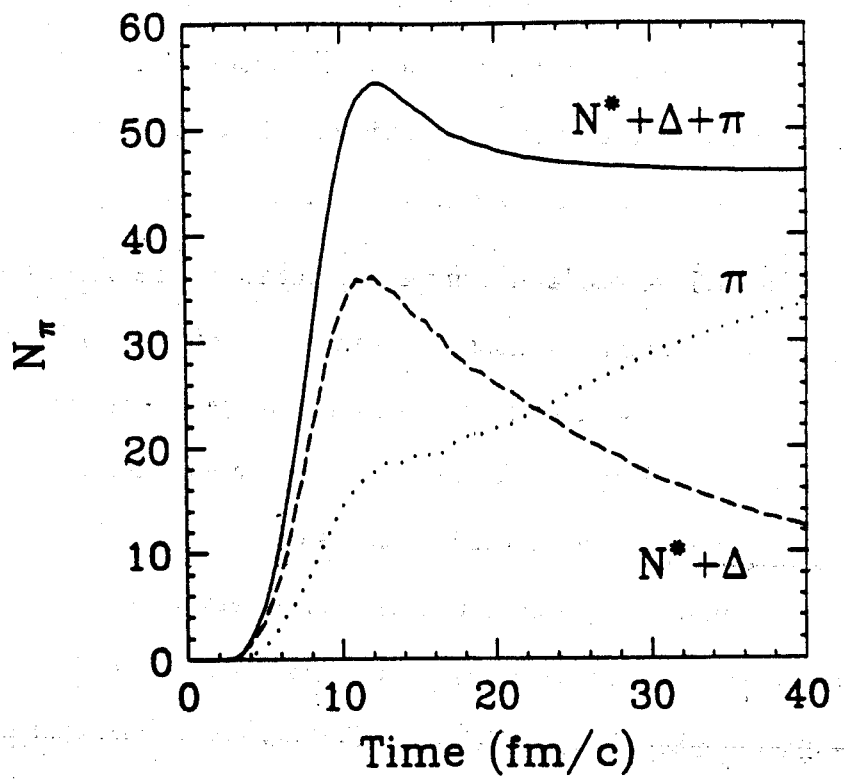

Figure 4.2: Time evolution of the population of free pions, Δ's and N^*'s in central collisions of La + La at E/A = 1350 MeV.

cascade calculation.

In Fig. 4.3 we study the beam energy dependence of the time evolution of the pion multiplicity. First, we note that the reaction time scale is getting shorter as the beam energy is increased. Secondly, the final pion multiplicity is proportional to the beam energy.

In Fig. 4.4, We compare the final pion multiplicity with that of the experimental data for central collisions of La+La. The round plot symbols on the solid line are our calculated results, and the square symbols with error bars are the experimental data[Harr87]. A good agreement can be seen in the whole energy range. Similarly good results have been obtained with a VUU-model[Moli87]. In Ref. [Moli87] a comparison of the data to existing cascade model calculations is shown as well, and a clear overprediction is observed for the cascade model.

In Fig. 4.5 we display the mass dependence of the time evolution of the pion multiplicity in central collisions at a beam energy of 1.5 GeV/nucleon. It is seen that the reaction time scale is rather insensitive to the size of the colliding system .The final pion multiplicity as a function of 2A, which approximates the mass number of the participant region in central collisions, has been shown in Fig. 4.6. It is seen that the total pion multiplicity is almost linear with respect to 2A. This is in accordance with the experimental findings[Harr87]. The linear dependence of the pion multiplicity on the mass number of the participant region reflects the fact that pion production is a bulk nuclear matter probe rather a surface probe.

The impact parameter dependences of the time evolution of the pion population and the final pion multiplicity have been shown in Fig. 4.7 and Fig. 4.8 for the reaction of Ar + Kcl at a beam energy of 1800 MeV per nucleon. It is seen that for central collisions at an impact parameter $b \leq 1$ fm, the time scale for pion production and

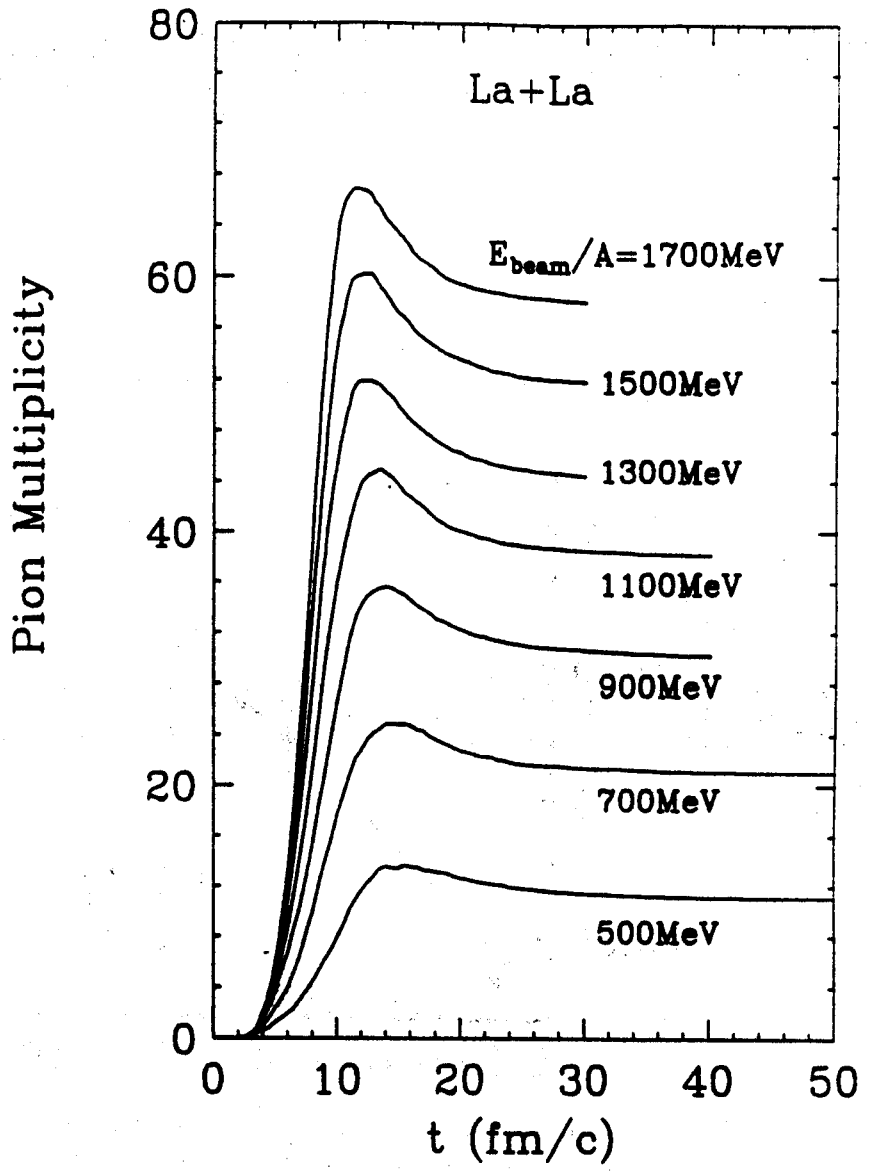

Figure 4.3: Beam energy dependence of the time evolution of the pion multiplicity in central collisions of La + La

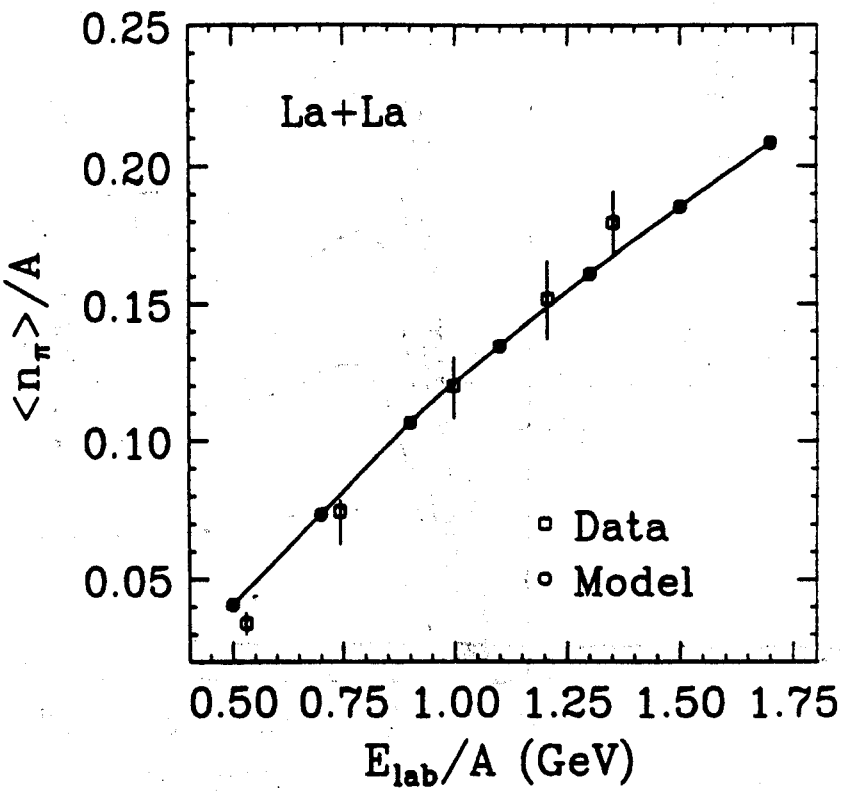

Figure 4.4: Excitation function of the pion multiplicity in central collisions of La + La. The squares are the experimental data of Ref. [Harr87], and the round plot symbols on the solid line are the model calculations.

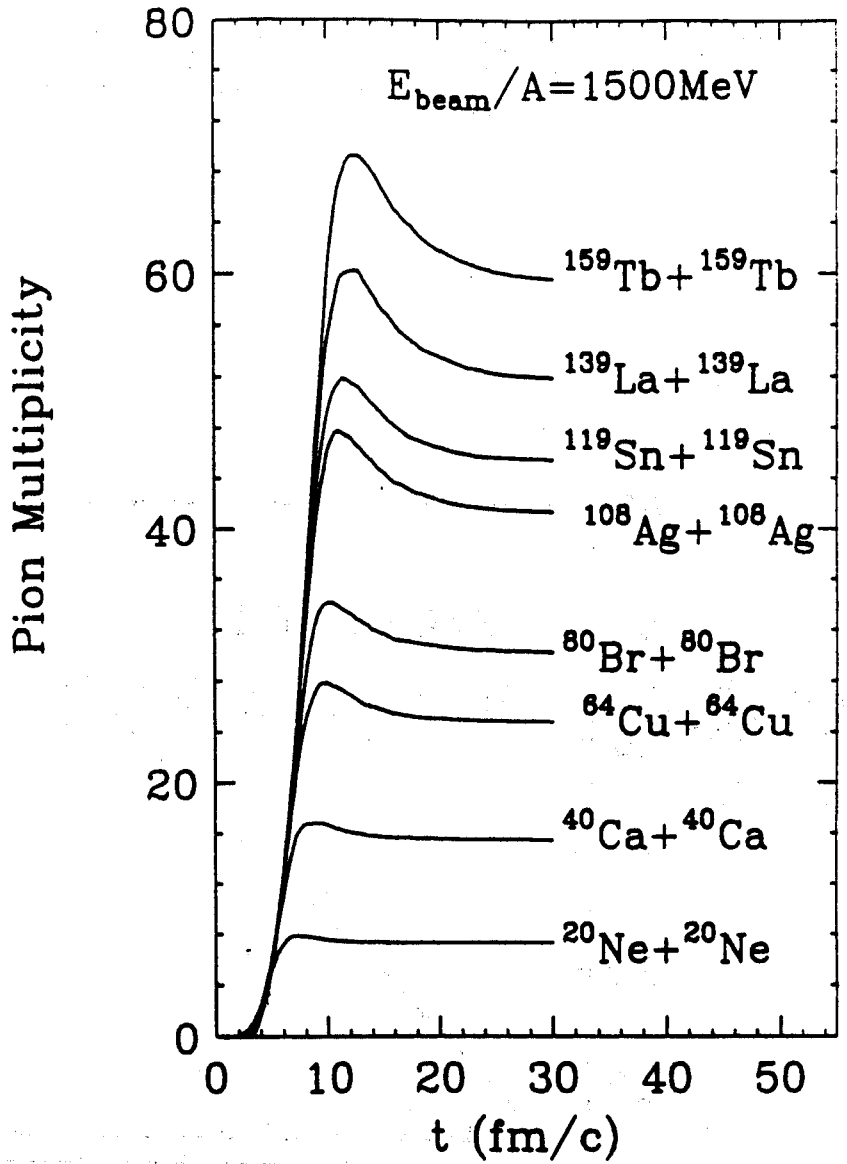

Figure 4.5: Mass dependence of the time evolution of the pion multiplicity in central collisions

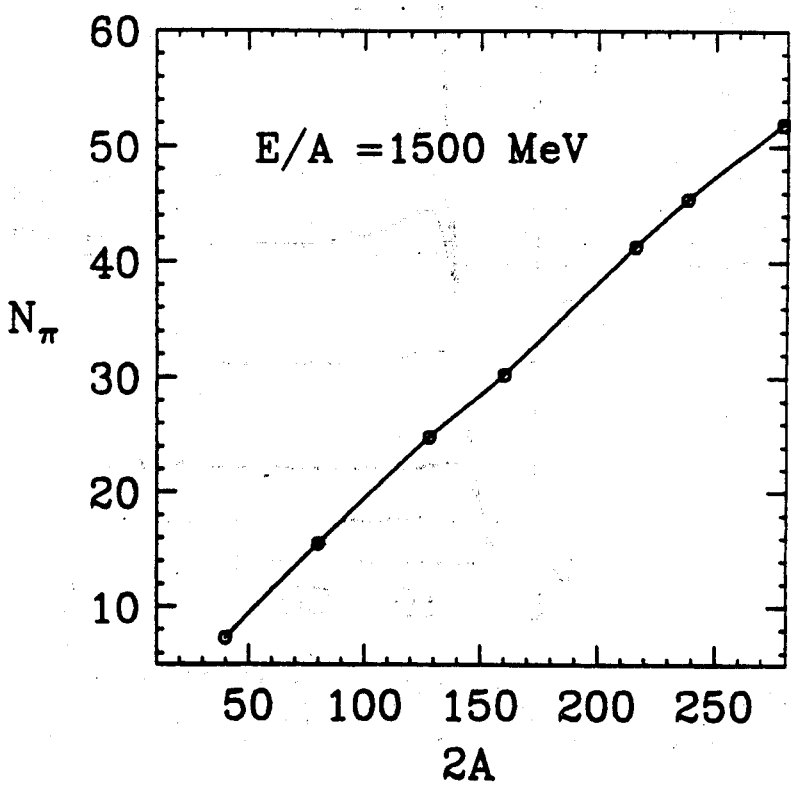

Figure 4.6: Mass dependence of the pion multiplicity

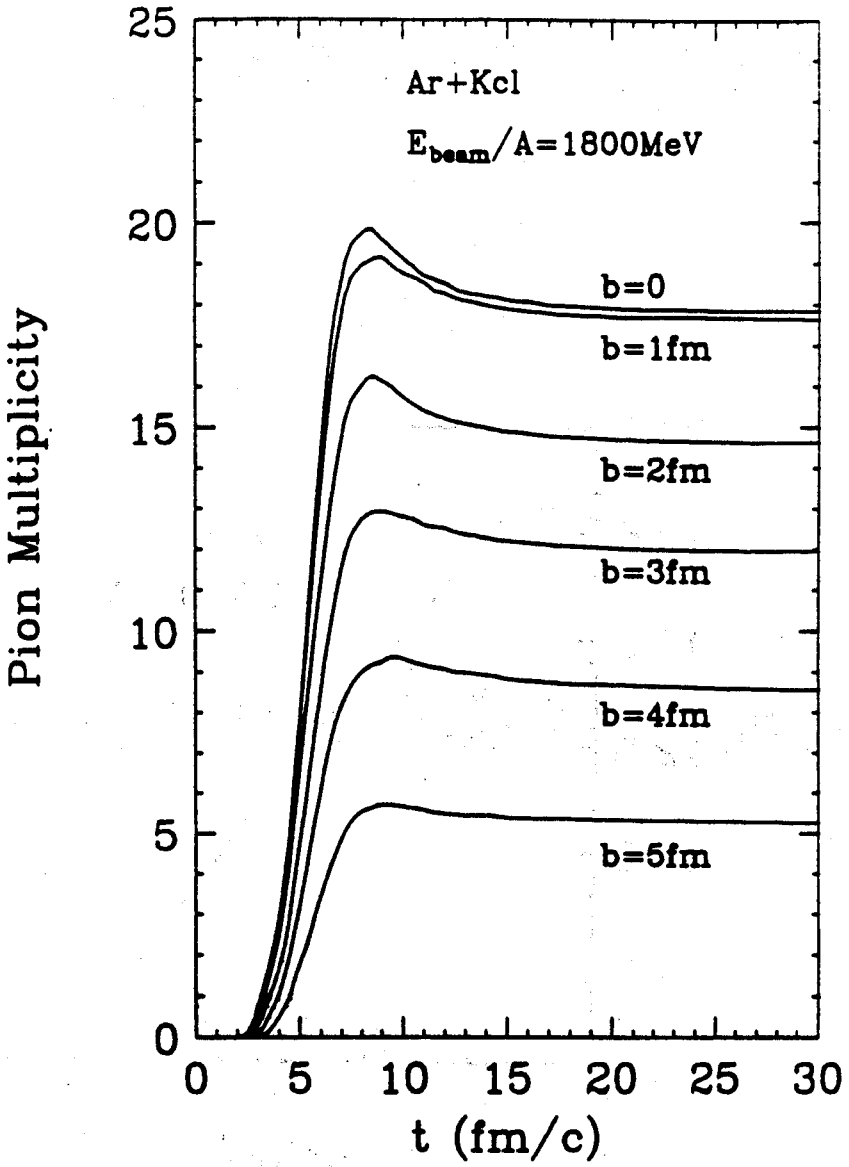

Figure 4.7: The impact parameter dependence of the pion production in Ar + Kcl reaction at the beam energy of 1800 MeV per nucleon

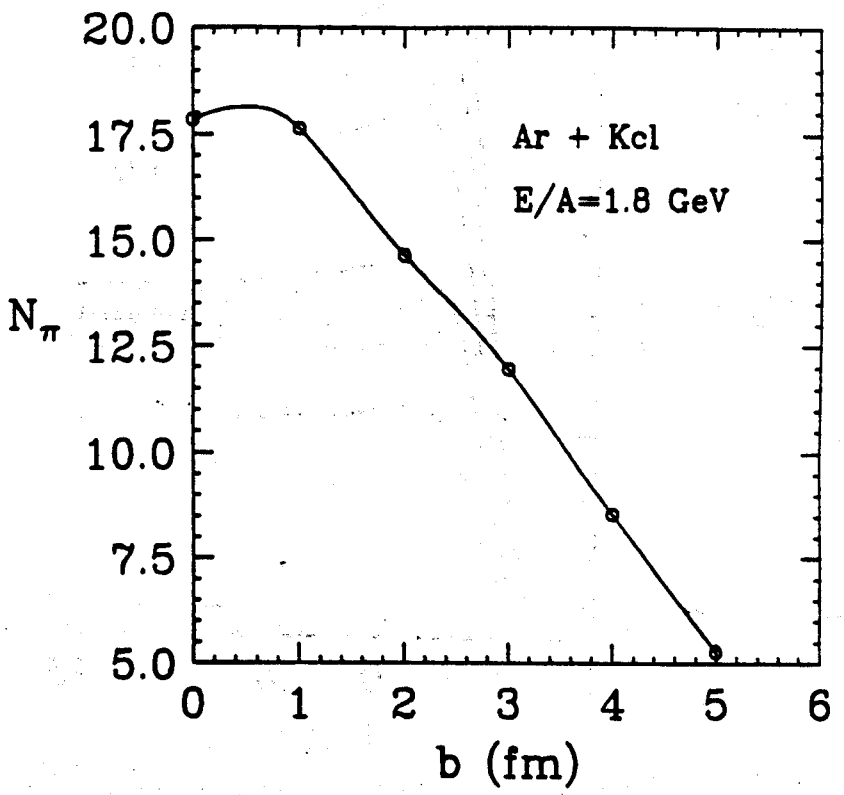

Figure 4.8: The impact parameter dependence of the pion multiplicity in Ar + Kcl reaction at the beam energy of 1800 MeV per nucleon

the final pion multiplicity are insensitive to the impact parameter because of the complete overlap of the projectile and the target. For larger impact parameters the pion production takes longer time, and the final pion multiplicity decrease linearly with the increasing impact parameter. This is in consistence with the mass and the energy dependence.

Due to the energy degradation in the reaction process, inelastic nucleon-nucleon collisions mainly occur in the early stage of the reaction. In the later expansion phase of the reaction only the resonance decay and the pion-nucleon resonance persist. The relative time dependence of these processes has been shown in Fig. 4.1. This property of the pion production dynamics cause the saturation of pion multiplicity in the expansion phase of the reaction. The saturation of the pion multiplicity can be seen clearly in Fig. 4.3 and Fig. 4.5. This property was first observed in Cugnon's cascade model calculation. Since then it has stimulated a lot of studies of properties of the compressional phase of heavy ion collisions using of the pion multiplicity. One typical example is the effort of extracting the nuclear equation of state from the excitation function of the pion multiplicity by assuming the discrepancy between the experimental data and the cascade model prediction comes completely from the lack of compression energy in the model[Stoc82, Harr87]. More elaborated models like the Boltzmann-Uehling-Uhlenbeck transport model (BUU)[Bert84, Bert88a, Krus85] and the Quantum Molecular Dynamics model (QMD)[Aich91], which include the mean field in addition to the two-body collisions, found that the sensitivity of the pion multiplicity is not so obvious, especially when momentum dependent forces are taken into account[Gale87c]. One therefore has been investigating experimentally other global properties of pions like pion spectra and pion flow. In the following two chapters we will concentrate on the study of pion spectra and pion flow, respectively.

Chapter 5

The concave shape of pion spectra

Some features of the pion kinetic energy spectrum in relativistic heavy ion collisions are expected to provide information about the space-time dynamics of the reaction. One interesting feature observed is that pion spectra in central heavy ion collisions show a concave shape on a logrithmic scale, which can be well fitted by a superposition of two Boltzmann distributions with widely different slope parameters. This phenomenon has been observed in Ar+KCl collisions at a beam energy of 1.8 GeV per nucleon[Broc84] and La+La at E/A = 1.35 GeV [Odyn88]. Preliminary results from Au+Au at E/A = 1.15 GeV[Chas90] also show this feature. A typical example of the concave shape of the pion spectrum has been given in Fig. 5.1 for the reaction of Ar + Kcl at a beam energy of 1.8 GeV/nucleon. Plot symbols with error bars are the experimental data, the solid curve is the Maxwell-Boltzmann distribution with a temperature of 63 MeV. It is seen that the experimental spectrum deviates from the Maxwell-Boltzmann thermal distribution for the total energies of pions larger than 0.5 GeV.

In ultrarelativistic heavy ion collisions and proton induced reactions, pion transverse momentum spectra also show a concave shape[Harr89]. This has generated a lot of interest, and the origin of this phenomenon has been vigorously debated in the literature[Shur88, Leeh89, Kusn89, Kata90, Brow91]. Therefore, the understanding of

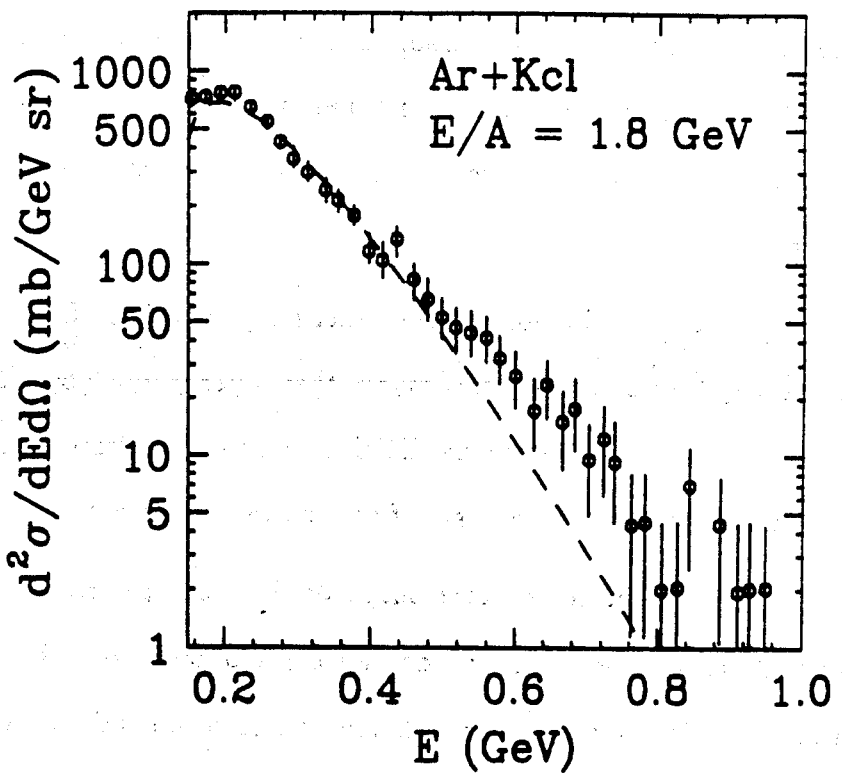

Figure 5.1: The concave shape of the pion spectrum in Ar + Kcl reaction at a beam energy of 1.8 GeV/nucleon. The experimental data shown by the plot symbols are from ref. [Broc84], the solid curve is the one-temperature fit to the experimental data with a temperature of T=63 MeV.

the mechanism that causes the concave shape of the pion kinetic energy spectra in relativistic heavy ion collisions may shed some light on the origin of the concave shape of the pion transverse momentum spectra in ultrarelativistic nuclear collisions[Liba91a].

In relativistic heavy ion collisions of beam energies around 1 GeV/nucleon, several hypotheses have been made by the groups who discovered this effect in order to explain their experimental results. These include the superposition of thermal pions and the pions from the final state Δ decays, higher resonances[Broc84] and the effect of baryon flow on the pions[Chas90]. Based on a simplified hydrodynamical model calculation[Hahn88], it was also conjectured that the concave shape of the pion spectra may come from an isotropic hydrodynamical expansion of the hot compressed nuclear matter.

The cascade model predicts purely thermal pion spectra[Broc84], although it has been very successful in predicting many other experimental observables in relativistic heavy ion collisions. The original BUU model uses the frozen Delta approximation and also fails to explain the origin of the concave shape of the pion spectra[Chas90].

We propose that the concave shape of the pion spectra is a result of different contributions of Δ resonances produced early and late during the course of the heavy ion collision. In the following we explore this idea in detail and compare our model calculations with the available experimental data.

5.1 Mechanisms for the concave shape of pion spectra

In this section, we apply our model to study the mechanism that causes the concave shape of pion spectra in central heavy ion collisions at beam energies around 1 GeV per nucleon.

5.1.1 Model calculation for the pion spectrum

In Fig. 5.2, we show the number of pions per energy interval for the La+La reaction, $\frac{1}{PE}dN/dE$, as a function of the pion kinetic energy, where P is the momentum and E is the total energy of the pions.

The time chosen for the figure, t=20 fm/c after the start of the calculation: by this time most of the baryon-baryon collisions have ceased, but a large fraction of the excited baryons produced have not decayed yet. The real pions which are not bound in resonances are represented by the solid histogram. For a thermally equilibrated dilute pion gas at a temperature T, we can use the Boltzmann distribution function

$$\frac{1}{PE}\frac{dN}{dE} = c \cdot \exp(-E_{\rm kin}/T). \tag{5.1}$$

As we can observe from Fig. 5.2, the free pions at 20 fm/c can be well described with a Boltzmann distribution of temperature 78 MeV (straight line fit).

By assuming sudden decay of all Δ's and N^*'s present at 20 fm/c, the contribution to the pion spectrum from bound pions can be obtained. These are shown by the dashed histogram. It is clear, that these pions do not show the same temperature as the pions which are already free at this time, but indicate a lower temperature.

If we superimpose the two contributions to the pion spectrum, we obtain the result which is represented by the round plot symbols. The error bars are of statistical nature since we solve the transport equations (eqs. 2.103 and 2.104) with a Monte Carlo integration procedure. The concave shape obtained in this way clearly hints at a pion spectrum with a two-temperature appearance. The low temperature is about 50 MeV for pions with $E_{\rm kin} \leq 0.2$ GeV and the higher one is about 78 MeV for pions with $E_{\rm kin} \geq 0.2$ GeV.

Different contributions to the pion spectrum at t = 40 fm/c is shown in Fig. 5.3.

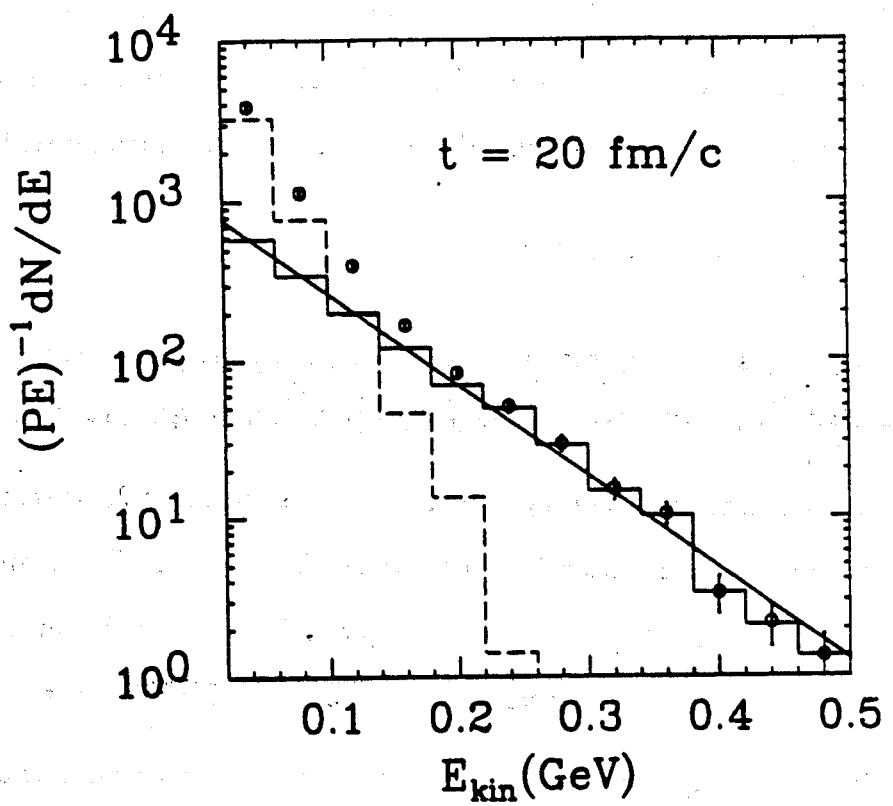

Figure 5.2: Calculated contribution to the pion spectrum from pion already free (solid histogram) and still bound in baryonic resonances (dashed histogram) as well as their sum (circles) at t = 20 fm/c. The straight line is a thermal distribution with a temperature of 78 MeV.

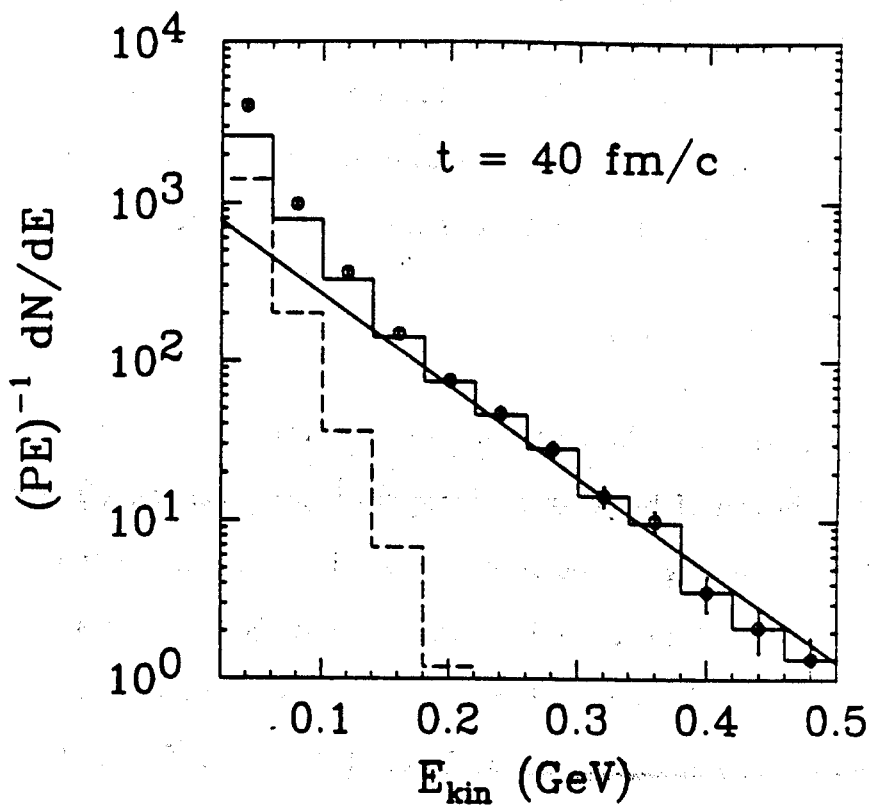

Figure 5.3: Calculated contribution to the pion spectrum from pion already free (solid histogram) and still bound in baryonic resonances (dashed histogram) as well as their sum (circles) at t = 40 fm/c.

We note that the total pion spectrum obtained at t = 20 fm/c (Fig. 5.2) is almost the same as that obtained at t = 40 fm/c when we stop our calculation. The reason for this is that between these two time instances the Δ's and N^*'s are almost moving freely during this expansion phase before they decay.

5.1.2 Concave pion spectra

What is the reason for the pions that are still bound at t=20 fm/c or 40 fm/c to show a lower temperature? We attempt to answer this question in Fig. 5.4 and Fig. 5.5. The upper part of Fig. 5.4 shows the rate of processes

$$N + N \rightarrow N + \Delta \tag{5.2}$$

during the La + La reaction. The lower part of the figure displays the probability distribution of baryon-baryon center of mass energies, $\sqrt{s}$, for two different time intervals during the course of the heavy ion reaction, as extracted from the computer calculation. The dashed histogram corresponds to all baryon-baryon collisions of the type Eq. 5.2 during the initial compressional phase of the reaction (dashed hatched area in the upper part of the figure), t $\leq$ 6 fm/c. The solid histogram corresponds in the same way to all collisions for t $\geq$ 12 fm/c (solid hatched area). We see that the center of mass energy distribution in the early stage of the reaction peaked at a higher energy than that in the later stage of the reaction. To be more quantitative on the energy degradation in the reaction process, we show in Fig. 5.5 the average center of mass energy of nucleon-nucleon collisions of the type Eq. 5.2.

We can clearly see that the early baryon-baryon collisions are on average more energetic than the later ones. This is because the central rapidity region is initially free of baryons, but is increasingly more populated as the reaction proceeds. To ease the understanding of the dynamical effect we illustrate schematically the rapidity

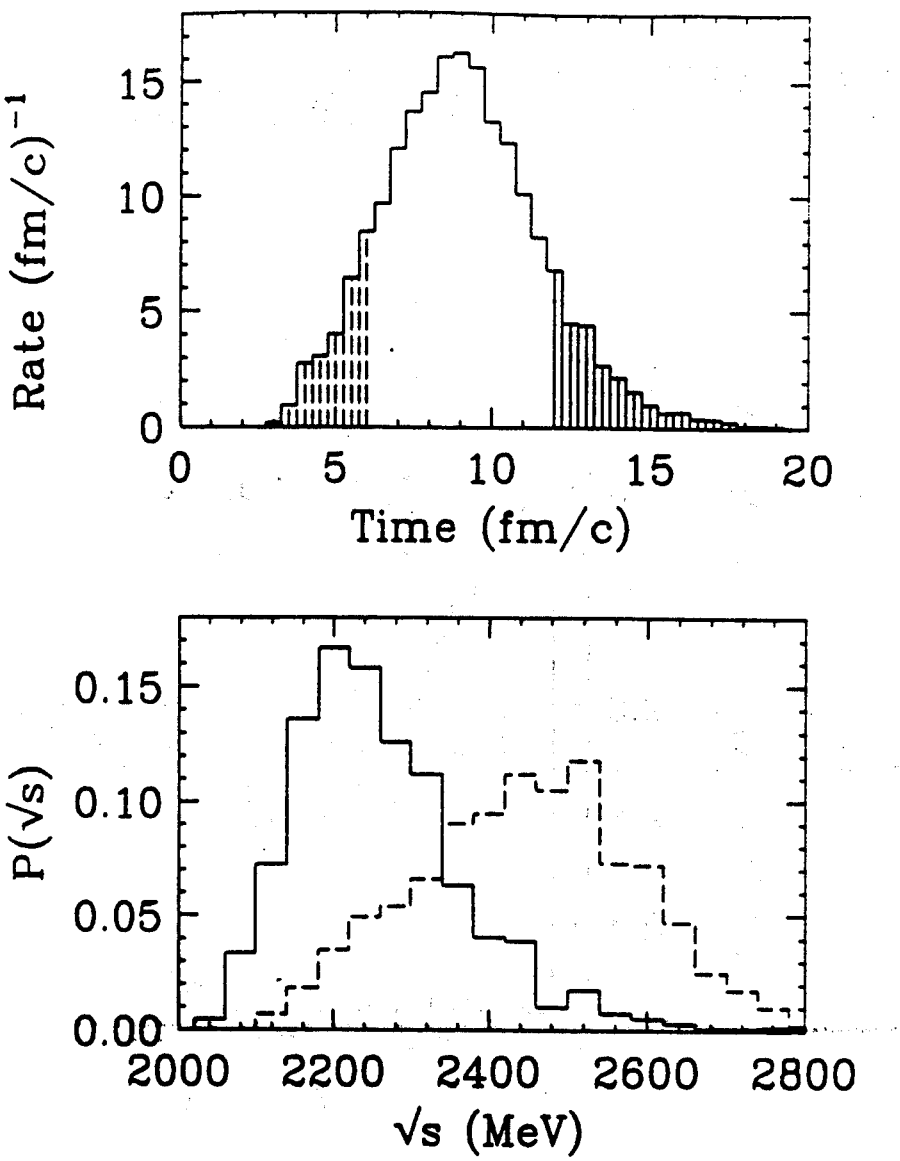

Figure 5.4: Upper part: Rate of Δ production during the La + La reaction. Lower part: Probability distribution for the C.M.S. energy of nucleon-nucleon collisions. The solid histogram is for $t \geq 12$ fm/c and the dashed histogram is for $t \leq 6$ fm/c.

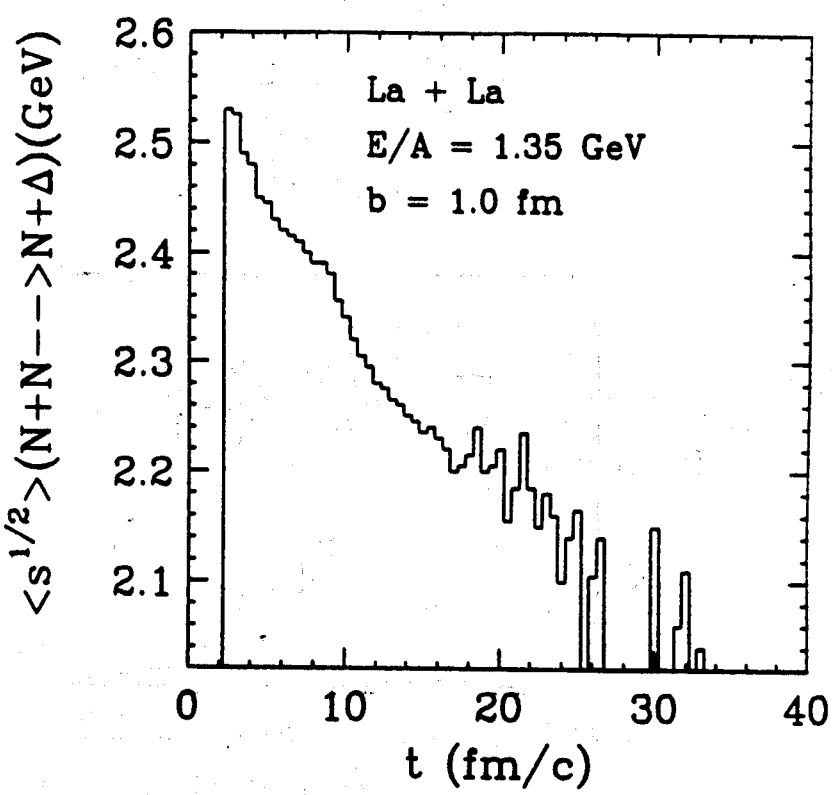

Figure 5.5: The time dependence of the average center of mass energy of nucleon-nucleon collisions in which baryon resonance can be produced during the reaction of La + La at a beam energy of 1.35 GeV/nucleon and an impact parameter of 1.0 fm.

distribution of nucleons in the reaction process in Fig. 5.6. A subsequent interaction of a nucleon at central rapidity with a nucleon at target or projectile rapidity thus becomes more and more probable towards the later time in the reaction. Since it is less energetic than a reaction of a nucleon at projectile rapidity and one at target rapidity (the only kind possible in the initial stage of the reaction), the Δ's produced later are less energetic than the ones produced earlier, and the different contributions to the kinetic energy spectrum of the pions can be understood.

The pion spectra shown in Fig. 5.2 are the results of the full dynamical evolution of the system, and this also includes the reabsorption of pionic excitations. We therefore have to ask what the effect of pion reabsorption and rescattering on the pion spectrum is.

In the present model pions can be reabsorbed through the two-step mechanism, namely, $N\pi \rightarrow \Delta(N^*)$ and $N\Delta(N^*) \rightarrow NN$. To illustrate the effect of pion reabsorption and rescattering on the pion spectrum, we compare in Fig. 5.7 the primordial π^- spectrum with the final one obtained at t=40 fm/c from the full dynamical evolution for the La+La reaction. The primordial pions are obtained by recording the momentum, mass and isospin of all Δ's and N^*'s when they are first produced during the course of the reaction, and by calculating the pion spectrum which would be obtained if all of these baryonic resonances were to decay right after they are formed, and the resulting pions would propagate without further interaction from then on. The primordial pions are represented by the round plot symbols on the solid histogram and the final pions are represented by the plot symbols on the dotted histogram.

We first notice the large difference in the normalizations of the two histograms: The number of finally escaping pions is only on the order of 10% to 20% of the total number of pionic excitations generated during the course of the heavy ion reaction.

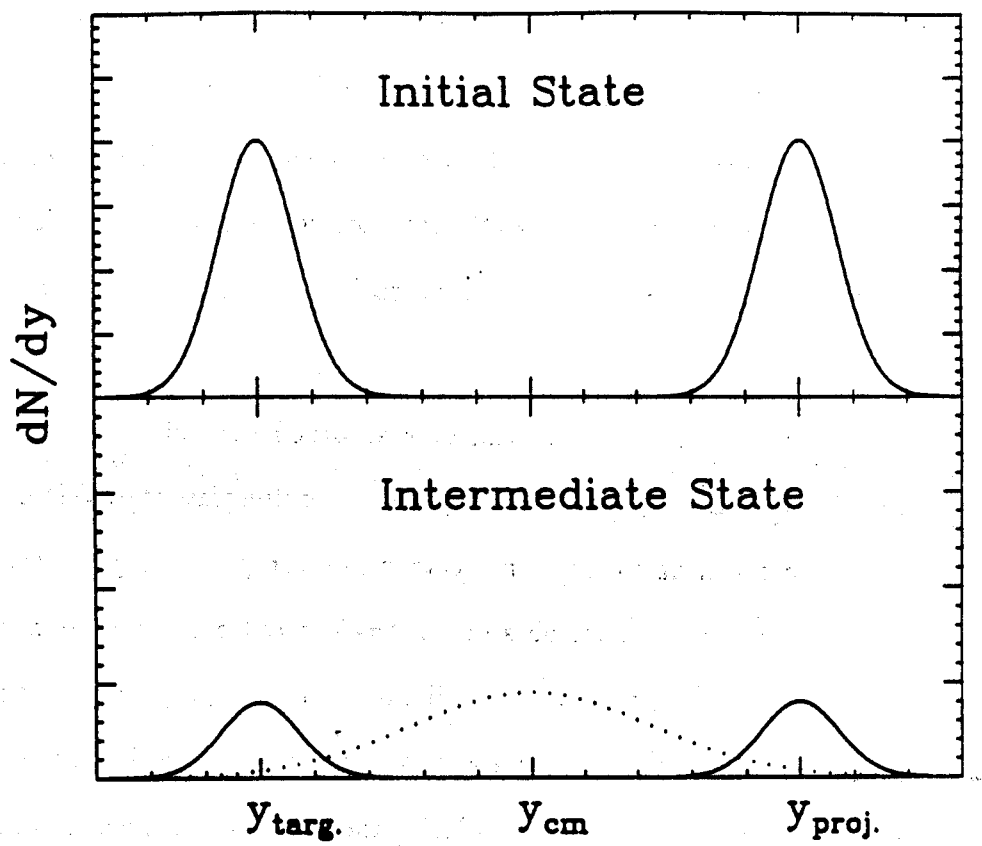

Figure 5.6: Schematic illustration of the rapidity distribution of nucleons. The upper window shows the rapidity distribution of nucleons in the initial state. The lower window shows the rapidity distribution during the reaction process. The dotted curve shows nucleons having been scattered into mid-rapidity range.

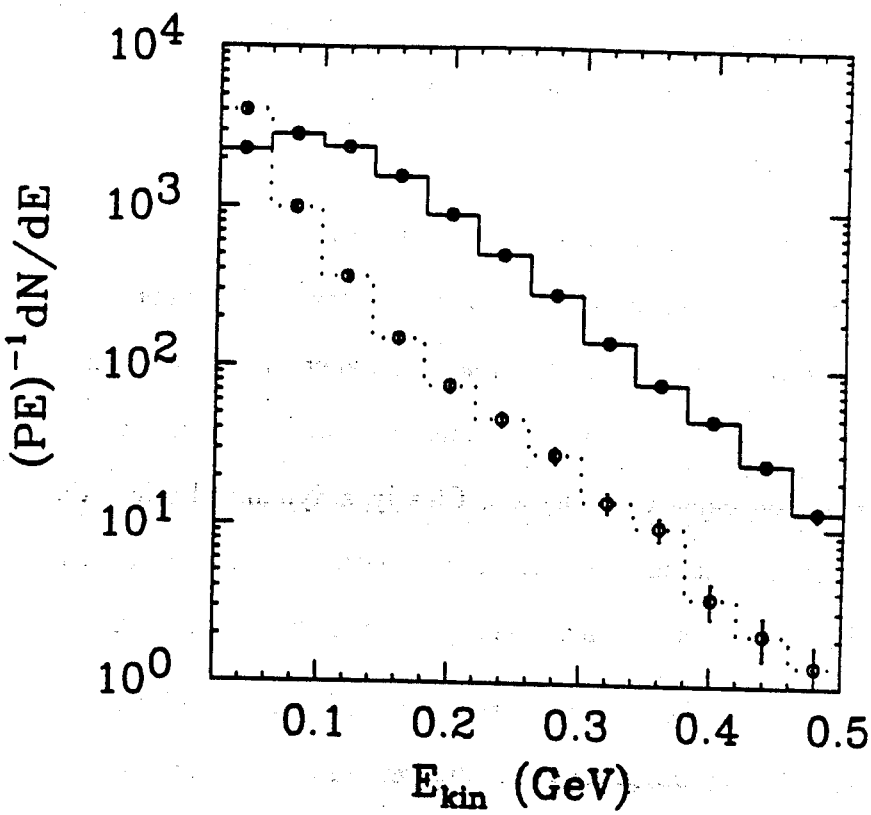

Figure 5.7: Comparison between the spectra of primordial pions (solid histogram) and final pions(dotted histogram).

Second, we see that the primordial pion spectrum does not show the concave shape observed in the final distribution. Due to the effect described above, the primordial pion spectrum is, however, not quite of the Boltzmann type as predicted by the thermal equilibrium model calculations[Hahn88, Pirn79, Barz81]. The reason for this additional shape change lies in the energy dependence of the elementary pion absorption cross sections obtained from detailed balance. High energy pions with kinetic energy larger than 0.2 GeV are rescattered or reabsorbed at a higher rate than low energy ones.

In addition, pion absorption is a two-step process and thus dependent on the square of the nucleon-density. This also favors the reabsorption of the higher energy pions produced early in the reaction (when the baryon density was high) over the reabsorption of lower energy pions produced later in the heavy ion reaction (when the baryon density was lower). Clearly, a dynamical calculation of pion reabsorption is thus essential for the correct explanation of pion energy spectra, and a calculation utilizing an energy independent pion mean free path in nuclear matter is insufficient.

From the above arguments based on Figs. 5.4 and 5.7, it is clear that we do not have only two contributions of different temperature to the pion spectrum, but rather a continuous change from the initial high temperature contribution to the final low temperature. The formation of the concave shape of the pion spectra is due to the gradual change of mean energies of the formed baryon resonances and the gradual change of reabsorption conditions during the course of the reaction.

In the study of pion spectra in relativistic heavy ion collisions an important question is to what extent the slope of pion spectra reflects the true temperature of the system in the early high-compression phase of the reaction. From the comparison of the two spectra shown in Fig. 5.2 and Fig. 5.7, we see that the higher temperature extracted from the pion spectra in the final state more accurately reflects properties

of the system in its early phase. However, one should use caution in applying the term "temperature", because what we observe is not the consequence of an equilibrated system, but rather of a non-equilibrium transport process of a system on its path towards kinetic equilibration.

Within the present transport model, one can also test the other hypotheses made to explain the concave shape of the pion spectra. By studying the dependence of the shape of the pion spectra on the nuclear equation of state, we can study the effect of the baryon collective flow on the pion spectra. It is found that nuclear collective flow are very sensitive to the nuclear equation of state. With a stiff nuclear equation of state one predicts a higher average transverse momentum in the reaction plane and a larger flow angle for nucleons[Bert88b]. Within the present model calculations, it is found that pion spectra calculated with a stiff nuclear equation of state and a soft nuclear equation of state are not distinguishable within the statistical error bars. It indicates that one should at most expect a small effect on the pion spectra from the baryon collective flow.

The effect of higher resonances on the pion spectrum, such as that of $N^*(1440)$'s included in the present model, has been studied by turning off the reaction channels involving N^*'s. It is found that the presence of N^*'s has only a very small effect due to their small production cross sections in the energy range of interest here. This finding is in agreement with that of Randrup from the study of the hadronic matter equilibration process[Rand79]. It was found that as long as the beam energy remains on the order of 1 GeV/nucleon it suffices to include only the Δ resonance. However, at higher energies, $E_{beam} \geq 2$ GeV/nucleon, higher baryon resonances as well as direct multiple pion production grow increasingly important in the reaction process, and their effects on the pion spectra remains to be explored.

5.1.3 Comparison with experimental data

In Fig. 5.8, we compare our model calculation with experimental data for central (b < 2.8 fm) reactions of La + La at a beam energy of 1350 MeV per nucleon. The experimental π^- number distribution, $(PE)^{-1}dN/dE$ at 90 ± 30 degrees in the center of mass of the target and projectile, is shown as a function of pion kinetic energy and represented by the round plot symbols. The data can be well fit by a two-temperature fit of the form

$$(PE)^{-1}dN/dE = A_1 \exp(-E_{kin}/T_1) + A_2 \exp(-E_{kin}/T_2), \tag{5.3}$$

with a χ^2 per degree of freedom of 0.9 (T_1 =45 MeV and T_2 =101 MeV), whereas the minimum χ^2 per degree of freedom is 3.4 for a one-temperature fit with T = 58 MeV[Odyn88]. For comparison, the one-temperature fit (T = 49 MeV) to the data is shown with the dashed line. Our calculations are represented by the histogram. Calculation and data both show a clear deviation from the one temperature fit. The data are in reasonable agreement with our calculation. A slight tendency of under-predicting the higher energy pions of energy $E_{kin} \geq 0.4$ GeV is noticed. One of the reasons is that a semiclassical momentum distribution has been used to initialize the nucleons; therefore the calculation lacks the quantum high momentum components. This is a problem our model shares with all the other semiclassical dynamical models.

In the lowest energy bin, we overpredict the data by a factor of 2-3, which is due to the fact that the detailed balance of eq. 3.56-eq. 3.61 was derived assuming that the baryon resonance has a zero energy width. As we will discuss in Chapter 7, the use of this detailed balance underpredicts the reabsorption of low energy Δ's. Using a new detailed balance which takes into account the finite width of the baryon resonance, the low wnergy part of the pion spectrum can well reproduce that of the experimental data.

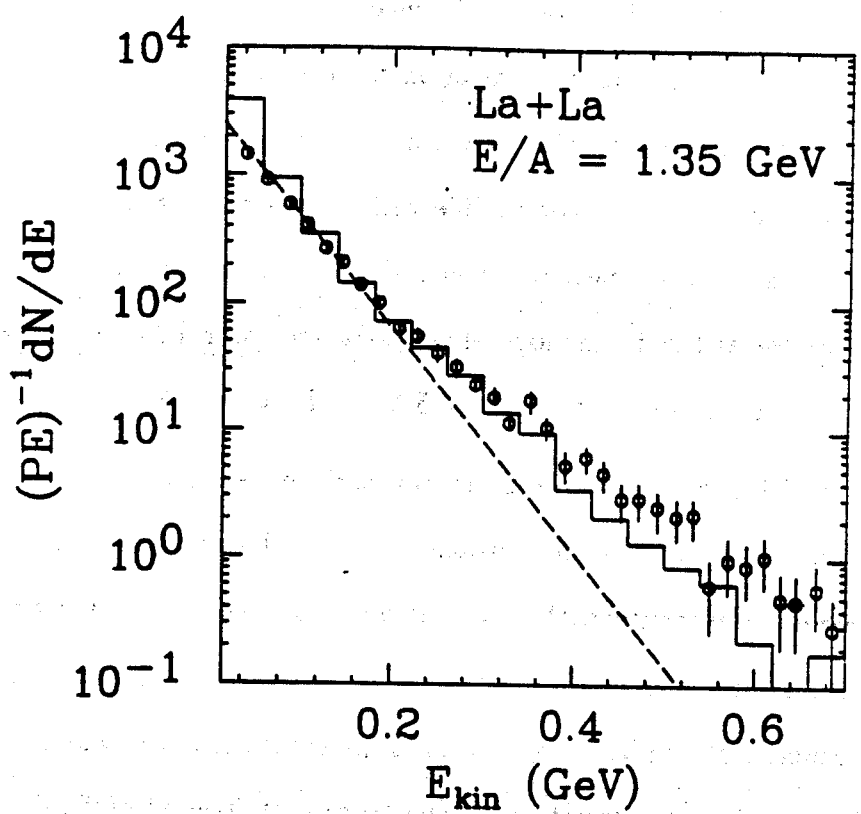

Figure 5.8: Comparison between calculations (histogram) and the experimental data of ref. [Odyn88] (plot symbols). The dashed line is the one-temperature fit to the experimental data with temperature T = 49 MeV.

To show the change in apparent temperature as a function of the kinetic energy of the pions, we introduce a local slope[Shur88, Baue91b]

$$T_l = -\left(\frac{d}{dE}\ln[\frac{1}{pE}\frac{d\sigma}{dE}]\right)^{-1} \tag{5.4}$$

and plot it as a function of E_{kin}.

In Fig. 5.9 we perform such an analysis and compare our calculations (histgrams) with the experimental data (circles). The errors bars were in both cases obtained by taking forward and backward difference formulas to compute T_l and using the difference in the results as an indication for the errors. It is clear that data and calculations are in good agreement within the error bars, and that they both show a change in local slope not compatible with a one-temperature picture. In this figure, a one-temperature spectrum would show up as a straight horizontal line. For comparison, we also show the local slope extracted from the best two-temperature fit according to eq. 5.3 to the data (T_1 =45 MeV, T_2 = 101 MeV, and A_1/A_2 = 5.0).

In Fig. 5.10, we perform another comparison between our calculation and the experimental data for central collisions of Ar+KCl at a beam energy of E/A = 1.8 GeV. This is the experimental data set in which the two-temperature structure of the pion spectrum was first found [Broc84]. Again, the experimental data are displayed by the round plot symbols, and the solid histogram is our calculation. The dashed curve is a one-temperature fit to the spectrum with T = 63 MeV.

As can be seen from the figure, the pion energy spectrum shows a deviation from the simple exponential law for pion energies greater than 0.5 GeV. A fit with two slope parameters (T_1 = 58 MeV and T_2 = 110 MeV) reproduces the whole spectrum. Similar to the situation in La + La reactions shown in Fig. 5.8, experimental data and model calculation agree quite well.

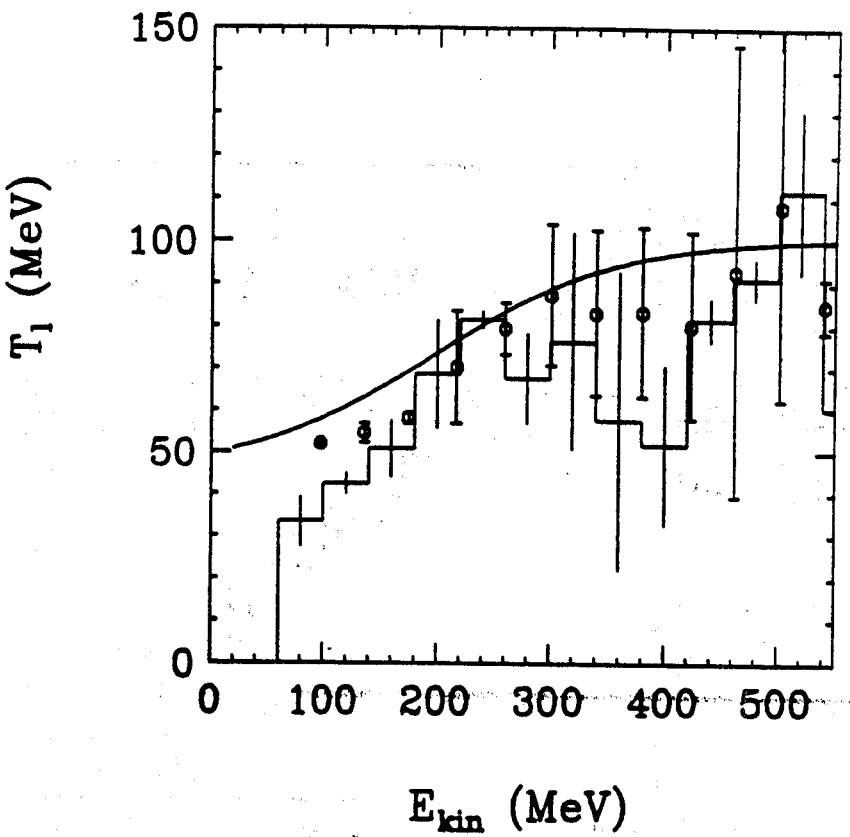

Figure 5.9: Local slope T_l as a function of the pion kinetic energy for the central collision of La + La at E/A = 1350 MeV. Circles are the experimental data and the histogram is the model calculation. The solid line represents T_l as extracted from the two-temperature fit to the experimental data.

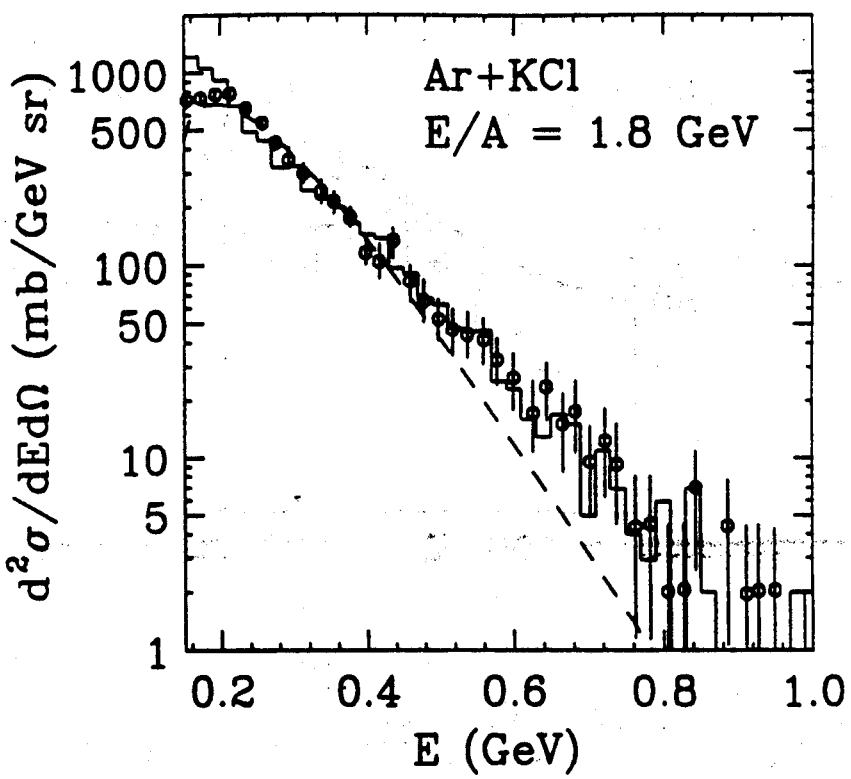

Figure 5.10: Comparison between calculations (histogram) and the experimental data of ref. [Broc84] (plot symbols). the dashed line is the one-temperature fit to the experimental data with temperature T=63 MeV.

It is well known that the cascade models with Δ resonances and their decays predict a single exponential spectrum. In principle, the main differences between our hadronic transport model and the cascade models are the inclusion of the mean field for baryons and a more proper treatment of the Pauli blocking in the present model.

The agreement between our model calculations and the available experimental data indicates that to correctly describe the experimental observables in heavy ion collisions of 1-2 GeV/nucleon beam energies, it is necessary to include the mesonic degrees of freedom explicitly, while still keeping the baryon mean field. This is because in this energy domain the long range nucleon-nucleon interactions are still sufficiently significant that the particles are not free but moving in a varying mean field both in space and time.

5.2 Systematics of pion spectra

From our previous discussions, we see that what is important for reproducing the experimentally observed concave shape of the pion spectra is the correct description of the effects of the reaction dynamics on pion production and absorption. Pions in the high temperature component are mainly produced in the early high-compression phase of the reaction, probably during the first one or two nucleon-nucleon collisions per nucleon. On the other hand, low energy pions are mainly produced in the late expansion phase of the reaction. Pion spectra therefore indeed carry interesting information about the space-time dynamics of heavy ion collisions. More of this information can be obtained by studying the dependence of the shape of the pion spectra on the beam energy, mass and impact parameter.

Since the systematic experimental study of the concave shape of the pion spectra is underway on SIS/GSI by the KaoS collaboration,[Oesc89] it is therefore interesting to

study these systematics based on our model calculations also. Moreover, a comparison between the two systematic studies will further determine the mechanism that causes the concave shape of the pion spectra and further test our model ingredients.

5.2.1 Energy dependence

We first study the energy dependence of the shape of the pion spectra in central collisions of La+La. In experiments one usually measures the pion spectrum at around 90 degrees in the C.M. system in order to avoid the 'corona effect',[Broc84] so that reliable information about the dynamics and properties of the hot and dense matter in the participant region can be extracted. All the spectra presented in the following are then calculated in the C.M. system at 90±30 degrees in accordance with the experimental situation of the KaoS collaboration.[Oesc89]

Pion spectra in central collisions have been calculated for beam energies from 0.5 GeV/nucleon to 2.1 GeV/nucleon; typical ones are displayed in the upper part of Fig. 5.11. Pion spectra at beam energies below 0.7 GeV/nucleon can be well described by a one-temperature Boltzmann distribution. This is because in this energy range the nucleon-nucleon inelastic cross section is small, only the first collision of a nucleon with target rapidity and a nucleon with projectile rapidity can effectively produce pions. For beam energies greater than 0.7 GeV/nucleon, if one fits the lower energy part of the spectrum with a single exponential distribution it is seen that the deviation of the spectrum from the single exponential distribution increases as the beam energy increases up to around 1.5 GeV/nucleon. The general feature observed here is in agreement with the experimental findings.[Odyn88] However, the tendency is not so obvious at beam energies above 1.5 GeV/nucleon. As can be seen the slope of high energy pions also increases as the beam energy increases. As we have discussed in the last section, pions in this high "temperature" component are produced in the early

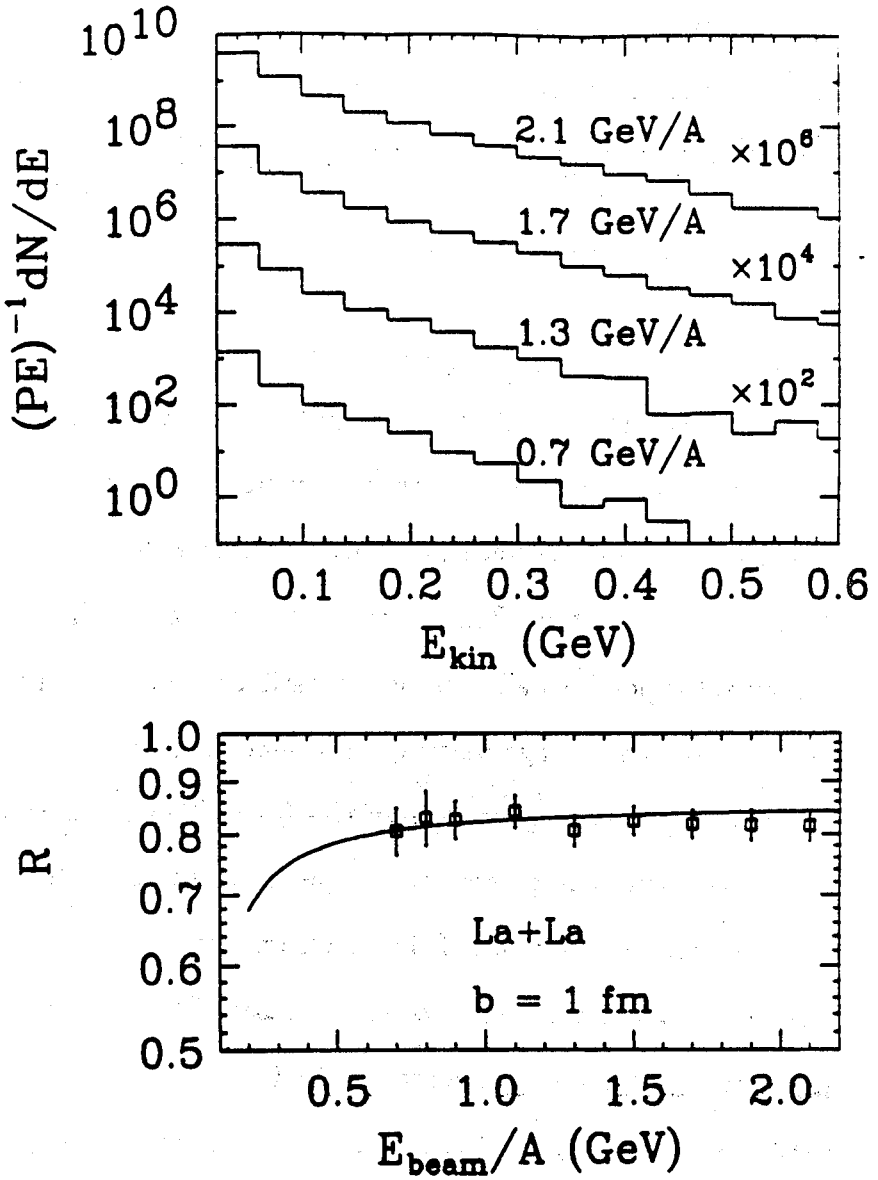

Figure 5.11: Upper figure: Calculated energy dependence of the pion spectra at 90±30 degrees in the center of mass frame for La+La reactions at impact parameter b = 1 fm. Lower figure: Energy dependence of the shape parameter R of the pion spectra shown in the upper figure. The solid line represents the analytic scaling function of equation 5.6.

high-compression phase of the reaction. The slope of the high-energy pions reflects the amount of energy deposited in the participant region via baryon excitations, which is monotonically increasing with beam energy.

5.2.2 Mass dependence

In Fig. 5.12, the upper part shows our predictions on the mass dependence of the pion spectrum. All calculations are performed for symmetric systems at a beam energy of 1.5 GeV per nucleon and an impact parameter of 1 fm. For light systems, such as C+C and Ne+Ne (not shown), the spectra can be well described by a one-temperature Boltzmann distribution. The reason for this is that, for light systems the size of the participant region is small which is compatible with the mean free path of the nucleon, and therefore on average particles only suffer one collision during the course of the reaction. For heavier systems from Ca+Ca to Tb+Tb, the situation is different. If one fits the lower energy part of the spectrum with a single exponential distribution one sees that the deviation of the spectrum from the single exponential distribution increases as the mass of the system increases. This feature of the mass dependence also agrees with the experimental results[Chas90]. Looking at the experimental pion spectra shown in Figs. 5.8 and 5.10, the deviation of the spectrum from the single exponential law in La+La is much larger than that in Ar+KCl, given the fact that the beam energy per nucleon in the La+La reaction is 450 MeV smaller than in the reaction of Ar+KCl. We also observed that the slope of high- energy pions is almost independent of the mass of the colliding nuclei.

5.2.3 Impact parameter dependence

Little knowledge of the impact parameter dependence of the pion spectra is presently available from experimental data. The KaoS collaboration has thus planned to study

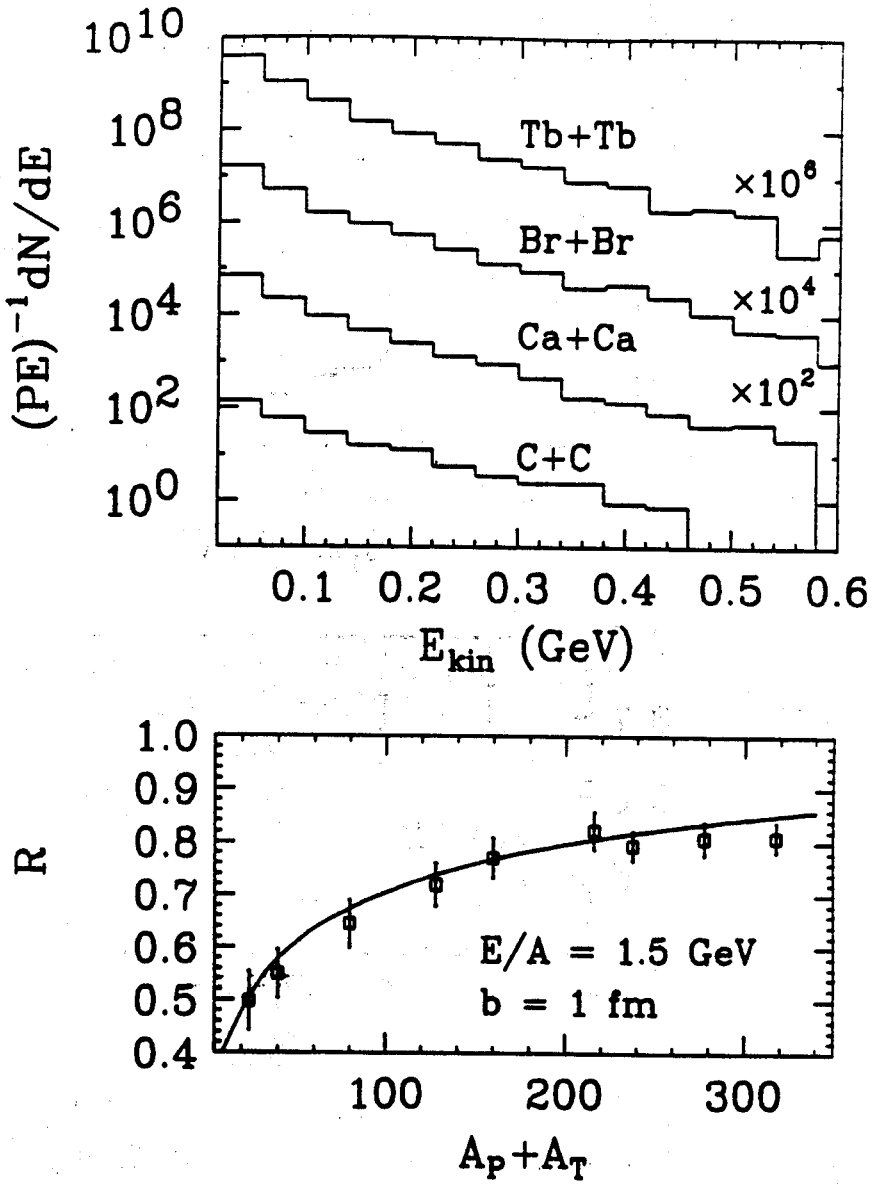

Figure 5.12: Upper figure: Calculated mass dependence of the pion spectra at 90 ± 30 degrees in the center of mass frame for a beam energy of 1.5 GeV/nucleon and impact parameter b = 1 fm. Lower figure: Mass dependence of the shape parameter R of the pion spectra shown in the upper figure. The solid line represents the analytic scaling function of equation 5.6.

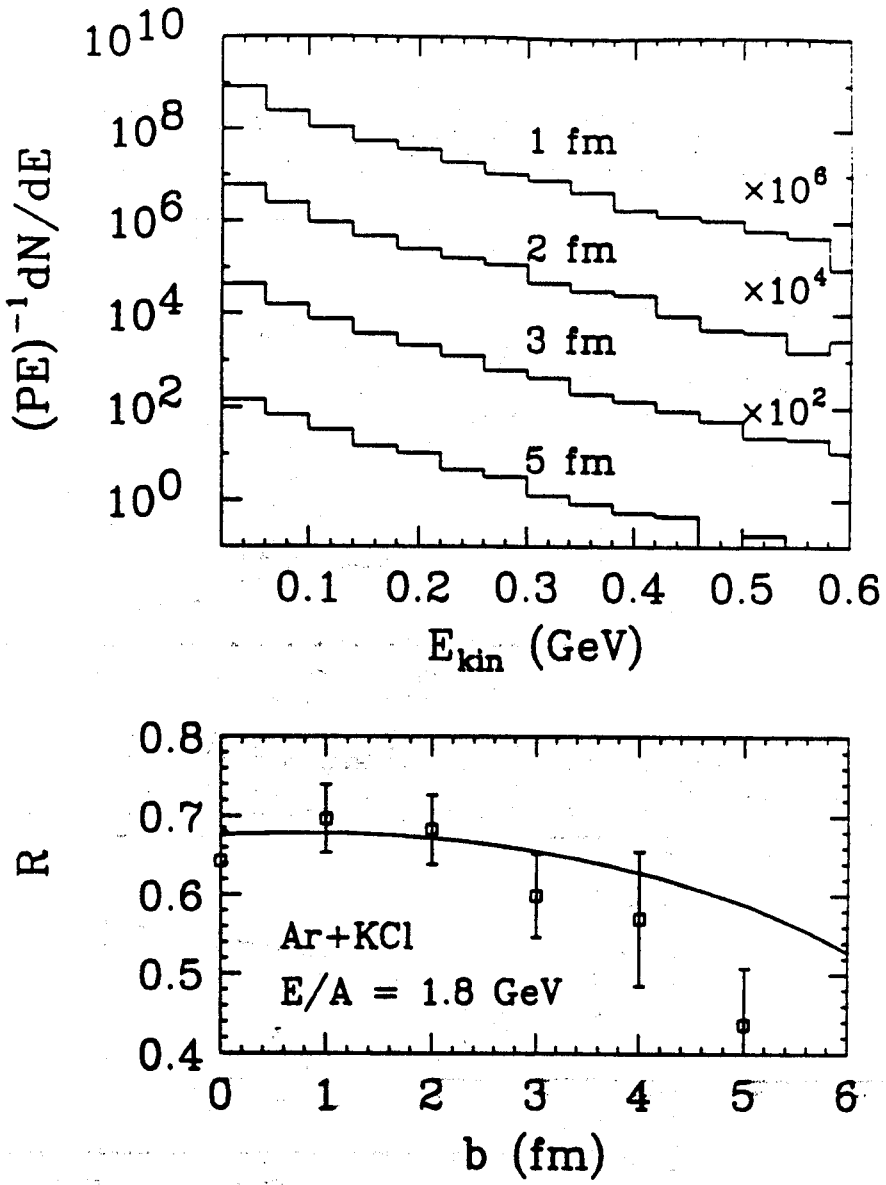

Figure 5.13: Upper figure: Calculated impact parameter dependence of the pion spectra at 90 ± 30 degrees in the center of mass frame for Ar+KCl reactions at beam energy of 1.8 GeV/nucleon. Lower figure: Impact parameter dependence of the shape parameter R of the pion spectra shown in the upper figure. The solid line represents the analytic scaling function of equation 5.6.

this dependence. In particular, a change in the slope of high-energy pions with centrality might indicate a thermal origin for these pions, while a similar slope would favour a dynamical decay process. Our predictions of the impact parameter dependence of the pion spectrum are shown in the upper part of Fig. 5.13. The reaction of Ar+KCl at a beam energy of 1.8 GeV per nucleon has been chosen. It can be seen that the spectra are almost parallel to each other and show a concave shape for impact parameters smaller than 3fm. For impact parameters larger than 5fm the spectra show only one temperature component. This is, because at large impact parameters too few particles are inside the collision zone, and pions are produced in first collisions only.

In experiments the centrality of the reaction are usually measured in terms of the charged particle multiplicity, in this case charged pions. In our model calculations there is the impact parameter and the multiplicity of charged pions in the final state. It will therefore be possible to make a direct comparison between our calculations and the coming experimental data from the KaoS collaboration.

5.3 Approximate analytic scaling function

To describe the shape of the pion spectrum quantitatively and further study its dependence on beam energy, mass and impact parameter we perform a least square fit to the spectrum with a two-temperature distribution function of eq. 5.3 and define the shape parameter as

$$R = \frac{A_1 T_1}{A_1 T_1 + A_2 T_2}. \tag{5.5}$$

With T_1 we refer to the lower temperature in the two temperature fit. It should be noted that this temperature is not the same as obtained by fitting the lower energy

part of the spectrum with a single exponential function. R represents approximately the fraction of the pion yield from the first exponential[Odyn88].

The shape parameters as extracted from our computer calculations are plotted in Figs. 5.11, 5.12, and 5.13 as functions of beam energy, mass and impact parameter, respectively. The energy dependence of the shape parameter is rather flat. As a function of the total mass of the system, R increases from about 0.5 to 0.8 when the total masses of the system grows from 24 to 160. For heavier systems, R saturates at around 0.8. For Ar+KCl collisions at a beam energy of 1.8 GeV per nucleon, the shape parameter is about 0.7 for impact parameters smaller than 2 fm; it then decreases to about 0.4 at $b = 5$ fm.

In order to understand the scaling behaviour of the shape parameter R we may attempt to formulate approximate scaling laws, based on our knowledge of the mechanism that causes the concave shape of the pion spectra. As we have discussed previously, pions in the higher temperature component are mainly produced in the early high-compression phase during the course of the reaction. To obtain an approximate scaling function we assume that pions in the higher temperature component are completely from first collisions in the early phase of the reaction. This approximation is valid for beam energies which are not too high. To contribute to the lower energy component, at least one of the colliding nucleons has to have had at least one previous collision to transport it into the 'mid-rapidity source'. We use Poisson statistics for the probability distribution of the number of nucleon-nucleon collisions. Under these simplifying assumptions, the scaling function for the shape parameter is given by

$$R = \frac{1 - e^{-\overline{n}} - \overline{n}e^{-\overline{n}}}{1 - e^{-\overline{n}}}. \tag{5.6}$$

Here, the numerator represents the probablity to have had at least two collisions, whereas the denominator is the probability for nucleons to have had at least one col-

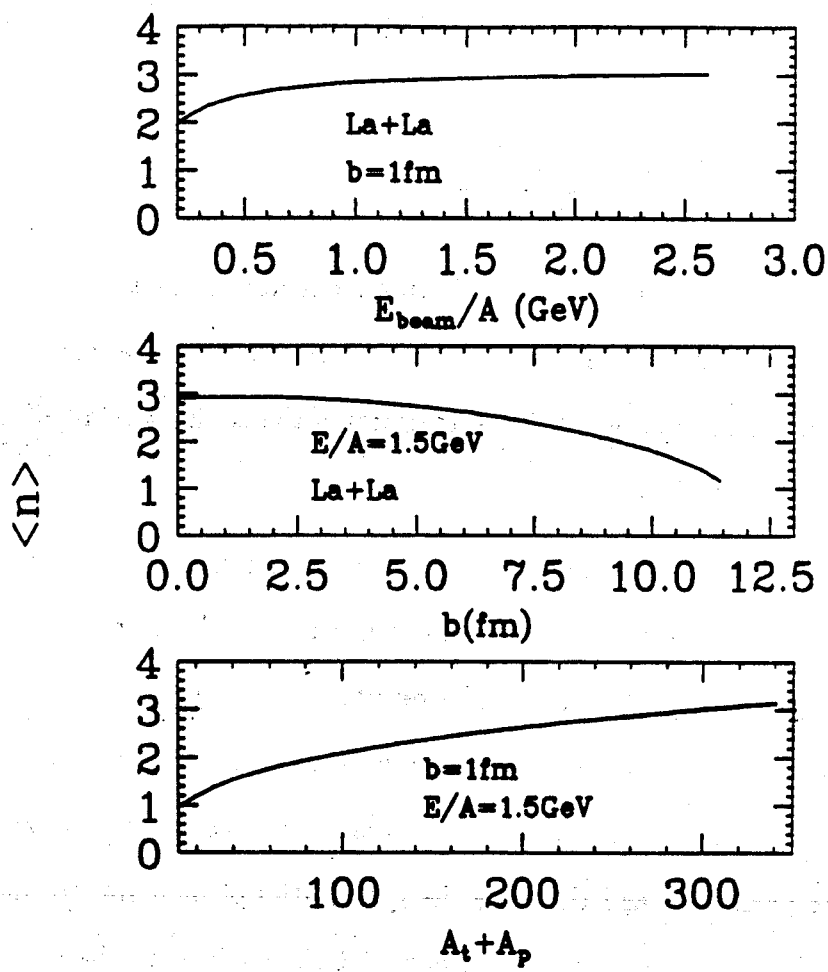

Figure 5.14: The systematics of the average number of nucleon-nucleon collisions suffered by each participant nucleon

lision. Here $\overline{n}$ is the average number of nucleon-nucleon collisions per nucleon[Baue88].

$$\overline{n} = \frac{\lambda_p \lambda_d \sigma_{nn}(E) \int_{\mathcal{O}} dxdy \int_{-\infty}^{\infty} dz_1 dz_2 \rho_t(x^2+y^2+z_1^2)^{1/2} \rho_p(x^2+y^2+z_2^2)^{1/2}}{\frac{1}{2}\int_{\mathcal{O}} dxdy \int_{-\infty}^{\infty} dz(\rho_p(x^2+y^2+z^2)^{1/2} + \rho_t(x^2+y^2+z^2)^{1/2})}. \quad (5.7)$$

Here $\sigma_{nn}(E)$ is the energy dependent total nucleon-nucleon cross section. The integrations over x and y are performed over the geometrical overlap area $\mathcal{O}$. λ_p is a correction factor resulting from the fact that the final-state phase space for the scattering nucleons is partially Pauli forbidden. With use of geometrical considerations, it can be approximated by

$$\lambda_p = \left(1 - \frac{2p_F^3 - \frac{1}{2}h^2(3p_F - h)}{(p_F + p_b)^3}\right)^2, \quad (5.8)$$

with $h = (p_F - p_b)\theta(p_F - p_b)$. λ_d is another correction factor used to include properly the effect of energy degradation and pion reabsorption. A constant of 0.6 has been used in our calculations. The systematics of the collision number calculated from eq. 5.7 have been displayed in Fig. 5.14.

Even though we expect the above scaling function for the shape parameter to be only an approximation, we can still compare it with the numerical values extracted from the calculated spectra. The results obtained from Eq. (5.6) are displayed by the solid lines in the lower parts in Figs. 9, 10 and 11. As can be seen, the qualitative features of the numerical calculations are reproduced, and the gross features of the shape parameter and therefore the systematics of pion spectra in relativistic heavy ion collisions at beam energies around 1 GeV/nucleon can be understood in terms of the simple scaling arguments presented here.

In summary of this chapter, an application of the hadronic model to the study of the pion spectrum shows that the shape of the pion spectrum reflects the effect of the reaction dynamics on pions, the mechanism for the concave shape of the pion spectra in central heavy ion collisions is found to be due to the different contributions of

the Delta resonances produced early and late during the course of the reaction. The available experimental pion spectra have been reproduced. The systematic study of the shape of the pion spectra indicates that the concavity of the pion spectra increases with both the beam energy and the mass of the colliding nuclei, and decrease with impact parameter.

An approximate scaling function for the shape parameter of the pion spectra has been derived from a Glauber-type multiple collision model to understand the systematics of the pion spectra. Upcoming experimental results from the KaoS collaboration on the systematics of the concave shape of the pion spectra are expected to further test our model predictions.

We conclude from our study in this chapter that in heavy ion collisions of beam energies around 1 GeV/nucleon it is necessary to treat mesonic degrees of freedom explicitly, without neglecting the nuclear mean field. This is important to the understanding of the observables sensitive to the dynamical degrees of freedom in relativistic heavy ion collisions and to reliably infer properties of hot and dense matter produced in these collisions.

Chapter 6

Preferential emission of pions

The existence of a collective flow signature among the final state baryons of relativistic heavy ion collisions at beam energies around 1 GeV/nucleon has been firmly established by the sphericity analysis[Gyul82, Dani83] and the in-plane transverse momentum analysis[Dani85] of the rich harvest of data from the Berkeley plastic ball detector. These methods have revealed the collective motion following the decompression of the hot and dense nuclear matter in both the reaction plane and perpendicular to the reaction plane. In the reaction plane a sideward deflection of spectator particles, the so called "bounce-off", and an azimuthally asymmetric emission of participant particles, the so called "side-splash" have been observed[Stöc80, Buch83, Gust84]. A collective flow of nucleons perpendicular to the reaction plane, the so called "squeeze-out", has also been found[Gutb89].

For ease of the following discussions, we discuss the basic idea of the transverse momentum analysis here in more detailed. The idea is to investigate whether a single particle of the event knows something about the whole event, i.e. the question whether the particles are collectively correlated. Danielewicz and Odyniec proposed to construct the reaction plane form the beam direction and the vector

$$\vec{Q}_j = \sum_{i \neq j} w_i \vec{p}_{\perp i} \tag{6.1}$$

determined from the detected particles in each event of mass symmetric nucleus-nucleus collisions. $\vec{p}_{\perp i}$ is the momentum component of the particle i perpendicular to the beam direction. The weight w_i is taken as 1 for $y_i > y_{cm}$ and -1 for $y_i < y_{cm}$, where y_{cm} is the center of mass rapidity of the nucleus-nucleus collision and y_i is the rapidity of the particle i defined as

$$y = \ln \frac{E + P_z}{E - p_z}. \tag{6.2}$$

The transverse momentum of the particle j in each event is defined as

$$p_{xj} = \left\{ \vec{Q}_j \cdot \vec{p}_{\perp j} / |\vec{Q}_j| \right\}. \tag{6.3}$$

The average transverse momentum $\langle p_x \rangle$ is obtained by averaging over all events. The average transverse momentum analysis, namely plotting the average transverse momentum $\langle p_x \rangle$ v.s. the rapidity y, can now be performed. A positive (negative) average transverse momentum for positive (negative) rapidity indicates that particles flow collectively. Fig. 6.1 shows as an example the average transverse momentum in the reaction plane, $\langle p_x \rangle$, as a function of the rapidity in the laboratory frame for La + La collisions at a beam energy of 800 MeV per nucleon. The characteristic S-shape of the resulting curves, is a clear signature of collective nuclear matter flow.

Due to the small mass of pions compared to that of baryons, it has been pointed out that the pions might serve as a good probe of any hydrodynamical flow[Goss89]. Moreover, as pions are mainly coming from the decay of Δ resonances in the relativistic heavy ion collisions, the remnant of the collective flow carried by Δ resonances might be seen in the final state pions.

Looking for flow signatures among the final state pions, several groups[Kean86, Dani88, Goss89] have studied the transverse momentum distribution in the reaction plane for pions. One of the most striking results from the DIOGENE collaboration[Goss89]

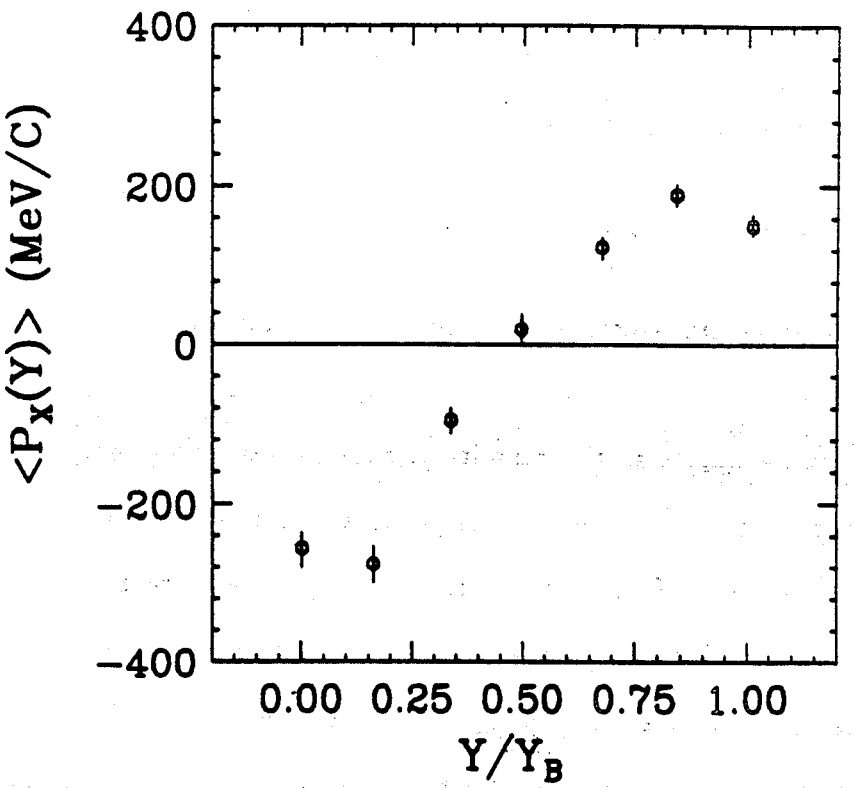

Figure 6.1: Transverse momentum analysis for La + La collisions at a beam energy of 800 MeV per nucleon. The data are from ref.[Dani88]

is that the in-plane transverse momentum of pions is always positive even for backward rapidities, for the asymmetric (Ne or Ar) + (Nb or Pb) systems.

However, the Intra-Nuclear-Cascade model predicts values compatible with zero over the whole range of rapidity[Goss89]. The Quantum-Molecular-Dynamics model calculation of the pion transverse momentum distribution[Hart88] indicates that the introduction of the mean field describes some of the experimental effect. but the model predicts less asymmetry than observed experimentally. Therefore, the question whether the experimentally observed preferential emission of pions away from the interaction zone towards the projectile side in the asymmetric nucleus-nucleus collisions is due to the collective flow of pions or due to the shadowing effect of the heavier target spectator has not been resolved.

In this chapter, we report on the results of a study about the pion transverse momentum distribution in the reaction plane by using of our hadronic transport model. The preferential emission of pions towards the projectile side in the transverse direction in the reaction Ne + Pb at a beam energy of 800 MeV/nucleon is found to be due to the stronger absorption of pions by the heavier target spectator. The calculated transverse momentum distribution of pions in the reaction plane agrees with that of the experimental data.

6.1 The mechanism for the preferential emission of pions

In our model calculation, the reaction plane is known *a priori* and we refer this plane as the true reaction plane in the following discussions. The reaction plane estimated from the observed charged particles will be referred to as the estimated reaction plane. To study the mechanism for the preferential emission of pions in the

transverse direction, we first study the pion transverse momentum distribution in the true reaction plane without using the experimental detector filter.

In Fig. 6.2, the rapidity distribution and the transverse momentum distribution (scaled with the mass of the pion) in the true reaction plane for π^+ from the reaction Ne + Pb at a beam energy of 800 MeV/nucleon are shown with the solid histograms. The calculation was done at an impact parameter of 3 fm which coincides with the condition of the experimental data[Goss89]. It is seen that the rapidity distribution peaks near the center of mass rapidity of 0.1 unit and is asymmetric about the center of mass rapidity. The transverse momentum of pions in the true reaction plane is positive even for negative rapidities, which reflects the fact that the pions are preferentially emitted towards one side of the participant region in the transverse direction.

As discussed earlier, in the baryon transverse momentum analysis, the S shaped distribution in the reaction plane with the average in-plane transverse momentum $\langle p_x \rangle$ positive (negative) for positive (negative) rapidities in the C.M. system for repulsive interactions has been taken as a signature of the collective baryon flow[Dani85], and S-shaped distributions of opposite sign are also found in the beam energy region below 100 MeV/nucleon where attractive interactions dominate[Krof89]. Both the flow parameter and the average in-plane transverse momentum have been found to be sensitive to the nuclear equation of state[Moli85, Gale87a, Bert88b].

Is the nonzero in-plane transverse momentum of pions a remnant of the baryon collective flow carried by Δ resonances ? To answer this question we have studied the dependence of the pion transverse momentum distribution on the nuclear equation of state. Within statistical fluctuations results from the calculations done with a stiff equation of state corresponding to a nuclear matter compressibility of K = 380 MeV and with a soft equation of state corresponding to K = 210 MeV are the same. This indicates that the effect of baryon collective flow on the pion transverse momentum

distribution is negligible and the origin of the positive in-plane transverse momentum of pions is not predominantly the remnant of the Δ flow.

It has been speculated that the mechanism that causes the positive pion transverse momentum in the reaction plane might be due to the target shadowing effect[Kean86, Goss89], and this idea has been demonstrated in a phenomenological model assuming that pions have a constant mean free path in nuclear matter[Goss89].

In the present dynamical model calculation, pions are reabsorbed through a two-step mechanism, namely,

$$\pi + N \rightarrow \Delta,$$
$$N + \Delta \rightarrow N + N. \tag{6.4}$$

The cross section for these processes in each isospin channel have been discussed in detail in Chapter 3.

To study the effect of the pion reabsorption and rescattering and therefore check the shadowing effect in forming the positive in-plane transverse momentum of pions, we calculated the pion transverse momentum distribution and the rapidity distribution by turning off the pion reabsorption channels (6.4) and the Δ rescattering channel $N + \Delta \rightarrow N + \Delta$. Results of this calculation are shown with the dashed histograms in Fig. 6.2. (For ease of comparison, we have normalized the total production cross section of these primordial pions to the one for the pions produced including the reabsorption and rescattering channels.) In this case the in-plane transverse momentum is zero within statistical error bars and the rapidity distribution is symmetric about half-beam rapidity of 0.6 unit, which reflects the fact that the pions are emitted isotropically in the center of mass frame of two colliding nucleons.

Comparing the rapidity distributions obtained with and without the reabsorption and rescattering channels (solid histogram and dashed histogram), we first

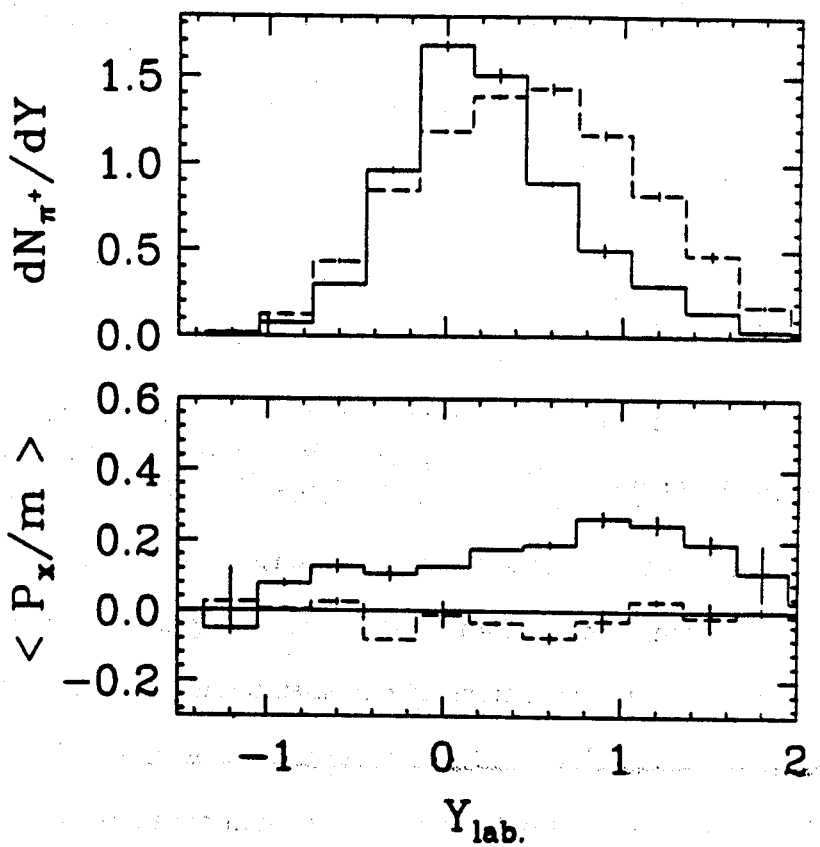

Figure 6.2: Upper figure: π^+ rapidity distribution calculated with (solid histogram) and without (dashed histogram) the pion reabsorption channels for the reaction of Ne + Pb. Lower figure: Calculated π^+ transverse momentum distributions in the true reaction plane with (solid histogram) and without (dashed histogram) the pion reabsorption channels.

notice that pions with positive rapidities emitted towards the target side are more reabsorbed compared to pions with negative rapidities emitted towards the projectile side. This reflects the preferential emission of pions in the longitudinal direction, as one would expect for the highly mass-asymmetric system. Second, the reabsorption and reemission of pions as well as the rescattering of Δ's help to thermalize the system. This effect appears as the change of the peak of the rapidity distribution from the mid-rapidity to the center of mass rapidity as the reabsorption, reemission and the rescattering channels are turned on.

From the results of these calculations, it is clear that the positive in-plane transverse momentum of pions in the asymmetric nucleus-nucleus collisions is due to the stronger reabsorption of pions by the heavier target and therefore the speculation about the shadowing effect of the target is confirmed.

In symmetric nucleus-nucleus collisions the spectators are the same on both sides of the interaction zone. It is interesting to study the pion transverse momentum distribution and the rapidity distribution in symmetric systems to test the sensitivity of the model to the geometry of the pion absorbing matter. In Fig. 6.3, the rapidity distribution and the transverse momentum distribution are shown for pions from central collisions of La + La at a beam energy of 800 MeV/nucleon. It is seen that both the rapidity and the in-plane transverse momentum distributions are symmetric about the center of mass rapidity of 0.6 unit and the transverse momentum distribution has a typical S shape.

6.2 Comparison to the experimental data

In order to compare the model predictions and the experimental data of the pion transverse momentum distribution, we have made a full simulation of the central

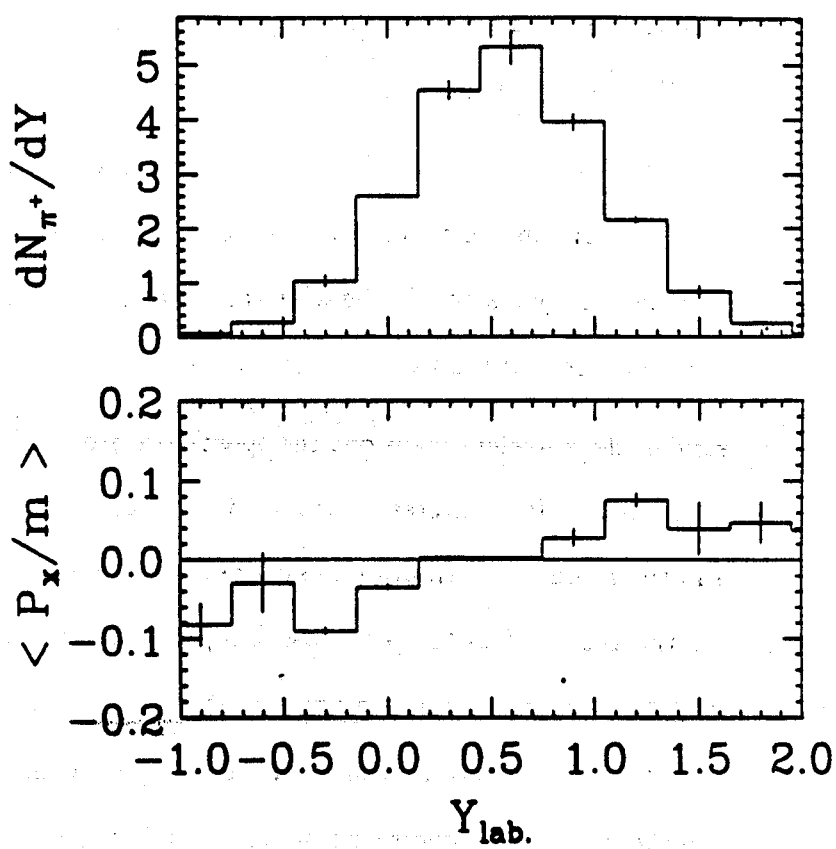

Figure 6.3: Rapidity distribution and transverse momentum distribution calculated for La + La reaction at E/A = 800 MeV and the impact parameter of 1 fm.

Pictorial Drift Chamber (PDC) acceptance of the DIOGENE collaboration[Goss89]. The PDC detector covers the polar angle θ from 20 to 132 degrees. Due to the low energy limit of the detector, only particles satisfying the following relations are accounted. For pions

$$p_\perp/m > 0.66 + 0.77y \ , \ y < 0; \tag{6.5}$$

$$p_\perp/m > 0.66 - 0.63y \ , \ y > 0. \tag{6.6}$$

For baryons

$$p_\perp/m > 0.36 + 0.72y \ , \ y < 0; \tag{6.7}$$

$$p_\perp/m > 0.36 - 0.8y \ , \ y > 0. \tag{6.8}$$

In the same way as in the experimental data analysis[Goss89], we estimate the reaction plane for each event from the beam direction and the vector

$$\vec{Q}_j = \sum_{i \neq j} w_i \vec{p}_{\perp i} \tag{6.9}$$

determined from the detected protons. Here the weight are $w_i = y_i - \bar{y}$, and $\bar{y}$ is the average rapidity of the detected protons. This weight is different from the one that was originally proposed for symmetric systems since the center of mass rapidity of the participant system is not known *a priori* in each event for asymmetric nucleus-nucleus collisions.

In Fig. 6.4, we perform a comparison between the experimental data and the model calculations for the Ne + Pb reaction. The experimental data are represented by the round plot symbols. The solid histograms are the model calculations, the error bars in the model calculations are statistical in nature, since we solve the coupled transport

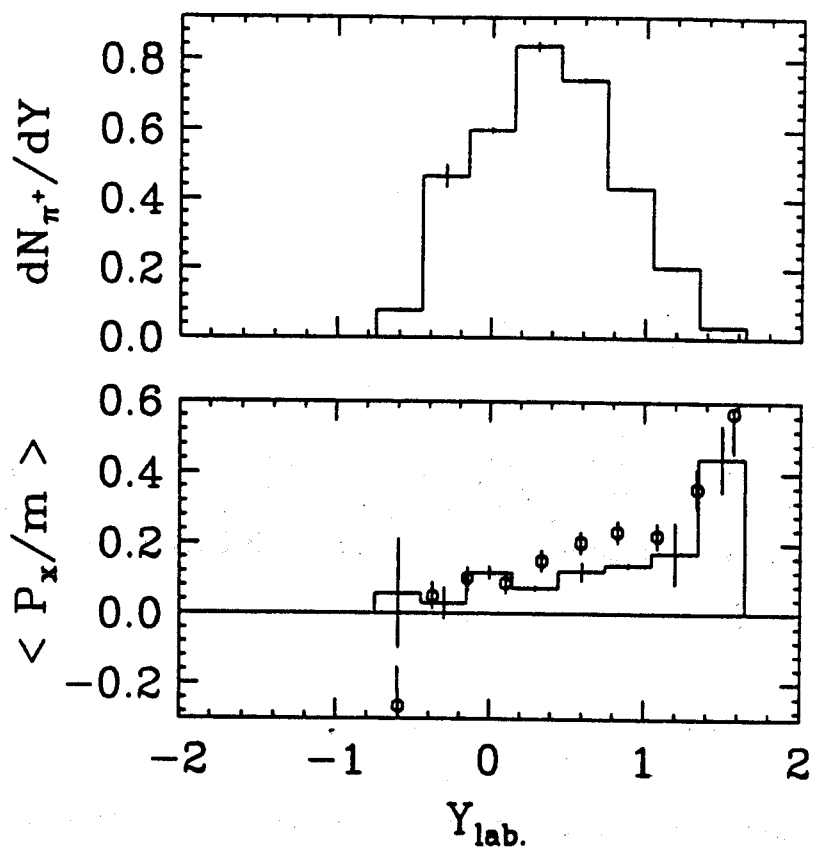

Figure 6.4: Upper figure: calculated π^+ rapidity distribution after using the detector filter cut for the Ne + Pb reaction at E/A = 800 MeV. Lower figure: Comparison between the experimental pion transverse momentum distribution (round plot symbols)and the model calculation (histogram) for the same reaction.

equations for the hadronic matter with a Monte Carlo integration technique. The experimental data are in reasonable agreement with our model predictions. To show the effect of the detector filter cut, the rapidity distribution of the detected π^+'s in the model calculation has been shown in the upper part of Fig. 6.4. Since the cascade model did not reproduce the preferential emission of pions, it has been conjectured that in-medium effects and pion production channels involving more than two nucleons could be important in the energy range studied here[Goss89]. However, our calculations indicates that it is not necessary to introduce additional medium effects and many-particle processes beyond the nuclear mean field and the Pauli exclusion principle for final state nucleons to understand the phenomenon of the preferential emission of pions.

In summary of this chapter, we performed hadronic transport model calculations of the pion rapidity distribution and the in-plane transverse momentum distribution. We discussed the effects of the target shadowing and the Δ flow in forming the positive in-plane transverse momentum of pions in asymmetric nucleus-nucleus collisions. We found that the mechanism for the preferential emission of pions from the interaction zone towards the projectile side in the transverse direction is due to the stronger reabsorption of pions by the heavier target. The model prediction of the pion in-plane transverse momentum distribution agrees with the experimental data.

Chapter 7

Summary and Outlook

In this work we have developed a new hadronic transport model for relativistic heavy ion collisions at beam energies around 1 GeV/nucleon by deriving and solving numerically a coupled set of transport equations for the phase space distribution functions of nucleons, Delta resonances and pions.

Starting from an effective hadronic Lagrangian density with minimal couplings between baryons and mesons, we first derived coupled equations of motion for the density matrices of nucleons, Delta resonances, and pion mesons as well as for the pion-baryon interaction vertex function. By truncating at the level of two-body correlations a closed set of equations of motion for the one body density matrix is obtained. A subsequent Wigner transformation then leads to a tractable set of relativistic transport equations for interacting nucleons, Delta resonances and pions. The transport equations are then solved numerically with the test particle method.

The model aims at formulating a framework for the theoretical understanding of the nuclear physics phenomena in relativistic heavy ion collisions. We first applied our model to study the dynamics of pion production and the pion multiplicity. The experimental excitation function of pion multiplicity was reproduced. The application of the model to the study of pion spectra reveals that the mechanism that causes the

concave shape of the pion spectra is due to the different contributions of the delta resonance produced during the early and the late stages of the heavy ion collision and due to the energy dependence of the pion and delta absorption cross sections. The dependence of the shape of the pion spectra on the beam energy, the target and projectile mass, and the impact parameter has also been studied. An approximate scaling function for the shape parameter of the pion spectra is predicted. Another new phenomenon that the model is able to explain is the preferential emission of pions in asymmetric nucleus-nucleus collisions. We have found that the preferential emission of pions away from the interaction zone towards the projectile side in the transverse direction and longitudinal direction is due to the stronger pion absorption by the heavier target spectator.

The success of the model in reproducing different experimental data sets for total pion excitation functions, pion kinetic energy spectra, the two-temperature appearance of pion spectra, and preferential emission of pions in asymmetric nucleus-nucleus collisions indicates that our model is able to describe most features of pion production physics in relativistic heavy ion collisions. This supports the conclusion that the approximations entering our model should be approximately valid.

Our transport equations for baryons contain a vector field and a scalar field, which are momentum dependent. As a first step of the model, only the zeroth component of the vector field has been taken into account, which has been parameterized by a density dependent functional. Further improvement of the model should incorporate the momentum dependent vector and scalar potentials.

Our transport equations include in principle the possibility for a changed dispersion relation for pions in nuclear matter. It was first pointed out by J. Kapusta and C. Gale that the pion dispersion in hot and dense nuclear matter can be studied by looking at the dilepton spectra in relativistic heavy ion collisions[Gale87b], since

$\pi^+\pi^-$ annihilation is the main source for the production of dileptons with large invariant masses. Interesting phenomena have been found in the dilepton spectra[Roch88] in BEVALAC heavy ion collisions. Conventional transport models[Xion90a, Wolf90] with the free space dispersion relation for pions seems unable to completely understand the observed features of the dilepton spectra. Extension of our hadronic transport model to include the in-medium dispersion relation for pions would be useful for the study of dilepton physics.

Further extensions to the study of two-pion correlations and kaon production are presently in the planning stages.

Appendix A

Derivation of $I^b_{b\pi}$ and $I^\pi_{b\pi}$

To calculate $I^b_{b\pi}$ and $I^\pi_{b\pi}$, we need to use the explicit expressions for $\hat{U}^\pi(x)$, $\hat{U}_\pi(x)$, and $\hat{u}(x)$, *i.e.* eqs. (2.24), (2.25) and (2.64). The explicit expressions for $\hat{\rho}(xx')$ is

$$\hat{\rho}(xx') = \psi^\dagger(x')\psi(x) \ , \tag{A.1}$$

where

$$\psi^\dagger(x) = \sum_{\alpha p}\left(\frac{M^*_\alpha}{E^*_\alpha(p)}\right)^{1/2} a^\dagger_{\alpha p}u^\dagger_{\alpha p}e^{ip\cdot x} \ , \tag{A.2}$$

and

$$\psi(x) = \sum_{\alpha p}\left(\frac{M^*_\alpha}{E^*_\alpha(p)}\right)^{1/2} a_{\alpha p}u_{\alpha p}e^{-ip\cdot x} \ . \tag{A.3}$$

The explicit expression for $\rho_\pi(xx')$ is

$$\rho_\pi(xx') = \boldsymbol{\pi}(x')\cdot\boldsymbol{\pi}(x) \tag{A.4}$$

where

$$\boldsymbol{\pi}(x) = \sum_{\pi k}\left(\frac{1}{2E_\pi(k)}\right)^{1/2}\left[b_{\pi k}e^{i\boldsymbol{k}\cdot\boldsymbol{x}-iE_\pi(k)t} + b^\dagger_{\pi k}e^{-i\boldsymbol{k}\cdot\boldsymbol{x}+iE_\pi(k)t}\right] , \tag{A.5}$$

where the creation and annihilation operators $b^\dagger_{\pi k}$ and $b_{\pi k}$ are isovectors. In the above expansions, only the positive energy components are included.

Before proceeding to calculate the collision terms due to pion-baryon collisions, we list the approximations to be used in the following

$$\begin{aligned}\langle a^\dagger_{\alpha' p'} a_{\alpha p} a^\dagger_{\alpha_1' p_1'} a_{\alpha_1 p_1}\rangle &\approx f_\alpha(p) f_{\alpha_1}(p_1)\delta_{\alpha\alpha'}\delta_{pp'}\delta_{\alpha_1\alpha_1'}\delta_{p_1 p_1'} \\ &+ f_{\alpha'}(p')(1-f_\alpha(p))\delta_{\alpha\alpha_1'}\delta_{pp_1'}\delta_{\alpha'\alpha_1}\delta_{p'p_1}\ ,\end{aligned} \tag{A.6}$$

$$\langle b^\dagger_{\pi k} b_{\pi' k'}\rangle \approx f_\pi(k)\delta_{\pi\pi'}\delta_{kk'}\ , \tag{A.7}$$

$$\langle b_{\pi k} b^\dagger_{\pi' k'}\rangle \approx (1+f_\pi(k))\delta_{\pi\pi'}\delta_{kk'}\ , \tag{A.8}$$

$$\langle b_{\pi k} b_{\pi' k'}\rangle = \langle b^\dagger_{\pi k} b^\dagger_{\pi' k'}\rangle = \langle b_{\pi k}\rangle = \langle b^\dagger_{\pi k}\rangle = 0\ . \tag{A.9}$$

Now we are ready to calculate the collision terms, first for $I^b_{b\pi}(xp)$. The collision operator can be written as

$$\hat{I}^b_{b\pi}(xx') = \hat{I}^L_{0\pi} + \hat{I}^L_{1\pi} + \hat{I}^L_{2\pi} - \hat{I}^R_{0\pi} - \hat{I}^R_{1\pi} - \hat{I}^R_{2\pi}\ , \tag{A.10}$$

where $\hat{I}^L$ and $\hat{I}^R$ are Hermitian conjugate of each other. The zero-order terms in $\pi(x)$ can be expressed as

$$\begin{aligned}&\hat{I}^L_{0\pi}(xx') \\ &= -\pi\hat{\rho}(xx')\delta(\bar{\hat{h}}\ (x) + \hat{E}_\pi(x) - \bar{\hat{h}}\ (x'))\hat{U}_\pi(\frac{\bar{\partial}}{\partial x})\frac{1}{\hat{E}_\pi(x)}\hat{u}(\frac{\bar{\partial}}{\partial x})\hat{\rho}(xx') \\ &= \pi\sum_{\alpha'p',\alpha p}\sum_{\alpha_1'p_1',\alpha_1 p_1}[u^\dagger_{\alpha' p'}\hat{u}(p_1'-p)u_{\alpha p}]\cdot[\hat{u}_{\alpha_1' p_1'}\hat{u}(p_1'-p)u_{\alpha_1 p_1}] \\ &\quad\cdot\frac{1}{E_\pi(p_1'-p_1)}[\frac{M^*_\alpha M^*_{\alpha'} M^*_{\alpha_1} M^*_{\alpha_1'}}{E^*_\alpha(p)E^*_{\alpha'}(p')E^*_{\alpha_1}(p_1)E^*_{\alpha_1'}(p_1')}]^{1/2} \\ &\quad\cdot\delta(E^*_\alpha(p)+E_\pi(p_1'-p_1)-E^*_{\alpha'}(p')) \\ &\quad\cdot a^\dagger_{\alpha' p'}a_{\alpha p}a^\dagger_{\alpha_1' p_1'}a_{\alpha_1 p_1}e^{ip'x'-ipx+ip_1'x-ip_1x}\ .\end{aligned} \tag{A.11}$$

The expectation value of this quantity is

$$I^L_{0\pi}(xx') = \langle \hat{I}^L_{0\pi}(xx') \rangle = \pi \sum_{\alpha' p', \alpha p} \frac{M^*_\alpha M^*_{\alpha'}}{E^*_\alpha(p) E^*_\alpha(p')} (u^\dagger_{\alpha' p'} \underline{\hat{u}}(p-p') u_{\alpha p})$$

$$\cdot \; (u^\dagger_{\alpha p} \underline{\hat{u}}(p-p') u_{\alpha' p'}) \frac{1}{E_\pi(p-p')}$$

$$\cdot \; \delta(E^*_\alpha(p) + E_\pi(p-p') - E^*_{\alpha'}(p'))$$

$$\cdot \; f_{\alpha'}(p')(1 - f_\alpha(p)) e^{ip'(x'-x)} \qquad \text{(A.12)}$$

In phase space it has the form

$$I^L_{0\pi}(xp) = \pi \sum_{\alpha' p'} \frac{M^*_\alpha M^*_{\alpha'}}{E^*_\alpha(p) E^*_{\alpha'}(p')} \langle u_{\alpha' p'} | \underline{\hat{u}}(p-p') | u_{\alpha p} \rangle \cdot \langle u_{\alpha p} | \underline{\hat{u}}(p-p') | u_{\alpha' p'} \rangle$$

$$\cdot \; \frac{1}{E_\pi(p-p')} \delta(E^*_\alpha(p) + E_\pi(p-p') - E^*_{\alpha'}(p'))$$

$$\cdot \; \delta(\boldsymbol{p} - \boldsymbol{p}') f_{\alpha'}(p')(1 - f_\alpha(p)) \; . \qquad \text{(A.13)}$$

To go further, we notice that the interaction matrix $\hat{u}$ (eq.2.64) contains differential operator ∂_μ in it's off-diagonal elements, namely the $N \leftrightarrow \Delta$ transition matrix elements. Correspondingly, it has terms linear in p and terms independent of p in momentum space. For terms linear in p, $\underline{\hat{u}}(p-p')$ and therefore $I^L_{0\pi}$ must be vanish in accordance with $\delta(\boldsymbol{p} - \boldsymbol{p}')$. Since $E^*_\alpha(p) + E_\pi(0) - E^*_{\alpha'}(p) \neq 0$ with $\alpha = N$ orΔ, terms independent of p, namely $\langle u_{\Delta' p'} | \underline{\hat{u}}(1) | u_{\Delta p} \rangle$ and $\langle u_{N' p'} | \underline{\hat{u}}(1) | u_{N p} \rangle$ also vanish in accordance with $\delta(E^*_\alpha(p) + E_\pi(0) - E^*_{\alpha'}(p))$. We then have $I^L_{0\pi}(xp) = 0$, and $I^R_{0\pi}(xp) = 0$. Because of $\langle b_{\pi k} \rangle$ and $\langle b^\dagger_{\pi k} \rangle$ are zero, the linear terms in π-field vanish identically, $I^L_{1\pi}(xp) = I^R_{1\pi}(xp) = 0$. Therefore, only bilinear terms in $\pi(x)$ contribute to $I^b_{b\pi}$. Formally

$$\hat{I}^b_{b\pi} = \hat{I}^L_{2\pi} - \hat{I}^R_{2\pi} \; , \qquad \text{(A.14)}$$

where

$$\hat{I}^L_{2\pi}(xx')$$

$$= -\frac{\pi}{8}[\hat{U}^{\pi}(x) - \hat{U}^{\pi}(x')]^2 \delta(\hat{h}(x) + \hat{E}_{\pi}(x) - \hat{h}(x'))$$

$$\cdot \quad \hat{U}_{\pi}(\frac{\overleftarrow{\partial}}{\partial x})\hat{\rho}(xx')\,(\hat{E}_{\pi}(\overrightarrow{x}))^{-3}\,\hat{u}(\frac{\overrightarrow{\partial}}{\partial x})\hat{\rho}(xx)$$

$$= -\frac{\pi}{8}[\hat{U}^{\pi}(x) - \hat{U}^{\pi}(x')]^2 \delta(\hat{h}(x) + \hat{E}_{\pi}(x) - \hat{h}(x'))$$

$$\cdot \quad \underline{\hat{u}}(\frac{\overleftarrow{\partial}}{\partial x})\hat{\rho}(xx')\,(\hat{E}_{\pi}(\overrightarrow{x}))^{-3}\,\underline{\hat{u}}(\frac{\overrightarrow{\partial}}{\partial x})\hat{\rho}(xx)$$

$$= \frac{\pi}{8}\sum_{\pi k,\pi' k'}\sum_{\alpha p,\alpha' p'}\sum_{\alpha_1 p_1,\alpha_1' p_1'}\left(\frac{M_{\pi}^{*}M_{\alpha'}^{*}M_{\alpha_1}^{*}M_{\alpha_1'}^{*}}{4E_{\pi}(k)E_{\pi'}(k')E_{\alpha}^{*}(p)E_{\alpha'}^{*}(p')E_{\alpha_1}^{*}(p_1)E_{\alpha_1'}^{*}(p_1')}\right)^{1/2}$$

$$\cdot \quad \delta(E_{\alpha}^{*}(p) + E_{\pi}(k) - E_{\alpha'}^{*}(p'))a_{\alpha' p'}^{\dagger}a_{\alpha p}a_{\alpha_1' p_1'}^{\dagger}a_{\alpha_1 p_1}$$

$$\cdot \quad e^{ip'x' - ipx + i(p_1' - p_1)x}(u_{\alpha_1' p_1'}^{\dagger}\underline{\hat{u}}(p_1' - p_1)u_{\alpha_1 p_1})\frac{1}{E_{\pi}^{3}(p_1' - p_1)}$$

$$\cdot \quad [(b_{\pi k}e^{ikx - iE_{\pi}(k)t} + b_{\pi k}^{\dagger}e^{-ikx + iE_{\pi}(k)t})$$

$$\cdot \quad (b_{\pi' k'}e^{ik'x - iE_{\pi'}(k')t} + b_{\pi' k'}^{\dagger}e^{-ik'x + iE_{\pi'}(k')t}) \cdot (u_{\alpha' p'}^{\dagger}\underline{\hat{u}}(k - k')\hat{u}(p)^2 u_{\alpha p})$$

$$+ \quad (u_{\alpha' p'}^{\dagger}\hat{u}(p')^2\underline{\hat{u}}(0)u_{\alpha p})(b_{\pi k}e^{ikx' - iE_{\pi}(k)t} + b_{\pi k}^{\dagger}e^{-ikx' + iE_{\pi}(k)t})$$

$$\cdot \quad (b_{\pi' k'}e^{ik'x' - iE_{\pi'}(k')t} + b_{\pi' k'}^{\dagger}e^{-ik'x' + iE_{\pi'}(k')t})$$

$$+ \quad 2(b_{\pi k}e^{ikx - iE_{\pi}(k)t} + b_{\pi k}^{\dagger}e^{-ikx + iE_{\pi}(k)t})$$

$$\cdot \quad (b_{\pi' k'}e^{ik'x' - iE_{\pi'}(k')t} + b_{\pi' k'}^{\dagger}e^{-ik'x' - iE_{\pi'}(k')t})(u_{\alpha' p'}^{\dagger}\hat{u}(p')\underline{\hat{u}}(k)\hat{u}(p)u_{\alpha p})]\,, \qquad \text{(A.15)}$$

and analogously for $\hat{I}_{2\pi}^{R}$. The expectation value of $\hat{I}_{2\pi}^{L}$ is then

$$I_{2\pi}^{L}(xx') = \langle \hat{I}_{2\pi}^{L}(xx') \rangle \qquad \text{(A.16)}$$

$$= \frac{\pi}{8}\sum_{\pi k}\sum_{\alpha p,\alpha' p'}\frac{M_{\alpha}^{*}M_{\alpha'}^{*}}{2E_{\pi}(k)E_{\alpha}^{*}(p)E_{\alpha'}^{*}(p')}\frac{1}{E_{\pi}^{3}[(p' - p)}(u_{\alpha p}^{\dagger}\underline{\hat{u}}(p' - p)u_{\alpha' p'})$$

$$\cdot \quad \delta(E_{\alpha}^{*}(p) + E_{\pi}(k) - E_{\alpha'}^{*}(p'))f_{\alpha'}(p')(1 - f_{\alpha}(p))e^{ip'(x' - x)}$$

$$\cdot \quad \Big([f_{\pi}(k) + (1 + f_{\pi}(k))][u_{\alpha' p'}^{\dagger}(\hat{u}(p')^2\underline{\hat{u}}(0) + \underline{\hat{u}}(0)\hat{u}(p)^2)u_{\alpha p}]$$

$$+ 2[f_{\pi}(k)e^{-ik(x - x')} + (1 + f_{\pi}(k))e^{ik(x - x')}](u_{\alpha' p'}^{\dagger}\hat{u}(p')\underline{\hat{u}}(k)\hat{u}(p)u_{\alpha p})\Big)\,.$$

The baryon component of the Wigner transformation of $I^L_{2\pi}(xx')$ is therefore

$$I^L_{2\pi}(xp) = \frac{1}{(2\pi)^3}\int \mathrm{Tr}_{(b)} I^L_{2\pi}(xx')e^{-i\boldsymbol{p}\cdot\boldsymbol{r}}d\boldsymbol{r} \tag{A.17}$$

$$\begin{aligned}
= \; & \frac{\pi}{8}\sum_{\pi k}\sum_{\alpha' p' p''}\frac{M^*_b M^*_{\alpha'}}{2E_\pi(k)E^*_b(p'')E^*_{\alpha'}(p')}\frac{1}{E^3_\pi(p''-p')}\langle u_{\alpha p''}|\underline{\hat{u}}(p''-p)|u_{\alpha' p'}\rangle \\
& ([f_\pi(k)+(1+f_\pi(k))]f_{\alpha'}(p')(1-f_b(p'')) \\
& \cdot\delta(E^*_b(p'')+E_\pi(k)-E^*_{\alpha'}(p'))\delta(\boldsymbol{p}'-\boldsymbol{p})\cdot\langle u_{\alpha' p'}|\hat{u}(p')^2\underline{\hat{u}}(0)+\underline{\hat{u}}(0)\hat{u}(p)^2|u_{\alpha p}\rangle \\
& +2[f_\pi(k)f_{\alpha'}(p')(1-f_b(p''))\delta(\boldsymbol{p}'+\boldsymbol{k}-\boldsymbol{p})\delta(E^*_b(p'')-E_\pi(k)-E^*_{\alpha'}(p')) \\
& +(1+f_\pi(k))f_{\alpha'}(p')(1-f_b(p''))\delta(\boldsymbol{p}'-\boldsymbol{k}-\boldsymbol{p})\delta(E^*_b(p'')+E_\pi(k)-E^*_{\alpha'}(p'))] \\
& \cdot\langle u_{\alpha' p'}|\hat{u}(p')\underline{\hat{u}}(k)\hat{u}(p)|u_{\alpha p}\rangle) \; .
\end{aligned}$$

This expression for the collision terms can be simplified, as we shall show. As discussed previously in the calculation of $I^L_{0\pi}(xp)$, the terms containing $\langle u_{\alpha' p'}|\underline{\hat{u}}(0)|u_{\alpha p}\rangle$ vanish. Moreover, $\underline{\hat{u}}(k)$ consists of terms linear in k and terms independent of k. For the first kind, $\underline{\hat{u}}(k=0)=0$. For the second kind, $\underline{\hat{u}}(k)=\underline{\hat{u}}(1)$. We also have $\langle u_{Np'}|\hat{u}(p')^2\underline{\hat{u}}(1)+\underline{\hat{u}}(1)\hat{u}(p)^2|u_{\Delta p}\rangle = 0$. Therefore only the "diagonal" terms survive, $\langle u_{\alpha p'}|\hat{u}(p')^2\underline{\hat{u}}(1)+\underline{\hat{u}}(1)\hat{u}(p)^2|u_{\alpha p}\rangle \neq 0$, with α=N or Δ. With the on-shell approximation, we also have $p''=p$, and $\delta(E^*_b(p)+E_\pi(k)-E^*_{\alpha'}(p'))\delta(\boldsymbol{p}'-\boldsymbol{p})=0$. Therefore the terms containing $\underline{\hat{u}}(0)$ vanish. With the above conditions and approximations, the collision terms for baryons due to pion-baryon interactions can be simplified and, furthermore, they can be separated into gain terms and loss terms,

$$I^{\mathrm{gain}}_{B\pi}(xp) \tag{A.18}$$

$$\begin{aligned}
= \; & \frac{\pi}{8}\sum_{\pi k}\sum_{\alpha' p' m^*_j}\frac{M^*_b M^*_{\alpha'}}{E^*_b(p)E^*_{\alpha'}(p')}\frac{\langle u_{\alpha' p'}|\hat{u}(p')\underline{\hat{u}}(k)\hat{u}(p)|u_{\alpha p}\rangle\cdot\langle u_{\alpha p}|\underline{\hat{u}}(k)|u_{\alpha' p'}\rangle}{E^4_\pi(k)} \\
\cdot \; & [f_\pi(k)f_{\alpha'}(p')(1-f_b(p))\delta(E^*_b(p)-E_\pi(k)-E^*_{\alpha'}(p'))\delta(\boldsymbol{p}'+\boldsymbol{k}-\boldsymbol{p}) \\
+ \; & (1+f_\pi(k))f_{\alpha'}(p')(1-f_b(p))\delta(E^*_b(p)+E_\pi(k)-E^*_{\alpha'}(p'))\delta(\boldsymbol{p}'-\boldsymbol{k}-\boldsymbol{p})]
\end{aligned}$$

and

$$
\begin{aligned}
& I^{\rm loss}_{B\pi}(xp) \qquad\qquad (A.19)\\
= \; & \frac{\pi}{8}\sum_{\pi k}\sum_{\alpha' p' m^b_j}\frac{M^*_b M^*_{\alpha'}}{E^*_b(p)E^*_{\alpha'}(p')}\frac{\langle u_{\alpha' p'}|\hat{u}(p')\underline{\hat{u}}(k)\hat{u}(p)|u_{\alpha p}\rangle\cdot\langle u_{\alpha p}|\underline{\hat{u}}(k)|u_{\alpha' p'}\rangle}{E^4_\pi(k)}\\
\cdot \; & [f_\pi(k)(1-f_{\alpha'}(p'))f_b(p)\delta(E^*_b(p)+E_\pi(k)-E^*_{\alpha'}(p'))\delta(\boldsymbol{p}'-\boldsymbol{k}-\boldsymbol{p})\\
+ \; & (1+f_\pi(k))(1-f_{\alpha'}(p'))f_b(p)\delta(E^*_b(p)-E_\pi(k)-E^*_{\alpha'}(p'))\delta(\boldsymbol{p}'+\boldsymbol{k}-\boldsymbol{p})] \; .
\end{aligned}
$$

Finally, let us calculate $I^\pi_{b\pi}$. Its operator form is

$$\hat{I}^\pi_{b\pi}(xx') = \hat{I}^\pi_{\rm gain}(xx') - \hat{I}^\pi_{\rm loss}(xx') \; , \qquad (A.20)$$

where

$$\hat{I}^\pi_{\rm gain}(xx') = \frac{1}{2\hat{E}_\pi(x)}\underline{\hat{u}}(x)\hat{\Gamma}(x,x',x) \; , \qquad (A.21)$$

and

$$\hat{I}^\pi_{\rm loss}(xx') = \hat{\Gamma}(x',x,x')\underline{\hat{u}}(x')\frac{1}{2\hat{E}_\pi(x')} \; . \qquad (A.22)$$

In more detail

$$
\begin{aligned}
\hat{I}^\pi_{\rm gain}(xx') \; = \; & -\frac{\pi}{16}\frac{1}{\hat{E}_\pi(x)}\underline{\hat{u}}(x)\delta(\hat{h}(x_-)+\hat{E}_\pi(x')-\hat{h}(x_+)) \qquad (A.23)\\
\cdot \; & [\hat{U}^\pi(x_-)-\hat{U}^\pi(x_+)]^2\hat{\rho}(x_-x_+)\frac{1}{\hat{E}_\pi(x')^3}\cdot\underline{\hat{u}}(x')\hat{\rho}(xx') \; ,
\end{aligned}
$$

where $x_\pm = x\pm\epsilon(\epsilon\to 0)$ means that $\hat{h}(x_-), \hat{h}(x_+), \hat{U}^\pi(x_-)$ and $\hat{U}^\pi(x_+)$ should operate on $\hat{\rho}(x_-x_+)$. After having operated, $x_\pm$ should assume the value x. Since $\hat{U}^\pi(x)$ contains the pion field $\boldsymbol{\pi}(x)$, we encounter the difficulty of calculating the expectation value $\langle\boldsymbol{\pi}(x)\cdot\boldsymbol{\pi}(x)\rangle$ for the gain term and $\langle\boldsymbol{\pi}(x')\cdot\boldsymbol{\pi}(x')\rangle$ for the loss term. Since we know that

$$\rho_\pi(xx') = \langle\boldsymbol{\pi}(x')\cdot\boldsymbol{\pi}(x)\rangle$$

$$\rightarrow \int \frac{1}{E_\pi(k)} f_\pi(k) d^3k$$

$$\rightarrow \sum_k \frac{1}{2E_\pi(k)} \langle (b_k(x') + b_k^\dagger(x'))(b_k(x) + b_k^\dagger(x)) \rangle$$

$$\rightarrow \sum_k \frac{1}{2E_\pi(k)} \langle b_k^\dagger(x') b_k(x) + b_k^\dagger(x) b_k(x') + b_k(x') b_k(x) + b_k^\dagger(x') b_k^\dagger(x) \rangle$$

$$\rightarrow \sum_k \frac{1}{E_\pi(k)} f_\pi(k) \ , \tag{A.24}$$

as $x' \rightarrow x$, there is an uncertainty for the order of operators $b_k(x)$ and $b_k^\dagger(x)$. Since the gain term for the pion due to pion-baryon interactions is related to the pion production process and the loss term is related to the pion reabsorption process, to eliminate the above uncertainty one should use

$$\langle \pi(x) \cdot \pi(x) \rangle$$

$$\rightarrow \sum_k \frac{1}{2E_\pi(k)} \langle (b_k(x) b_k^\dagger(x) + b_k(x) b_k^\dagger(x) + b_k(x) b_k(x) + b_k^\dagger(x) b_k^\dagger(x) \rangle$$

$$= \sum_k \frac{1}{E_\pi(k)} (1 + f_\pi(k)) \ , \tag{A.25}$$

and

$$\langle \pi(x') \cdot \pi(x') \rangle$$

$$\rightarrow \sum_k \frac{1}{2E_\pi(k)} \langle b_k^\dagger(x) b_k(x) + b_k^\dagger(x) b_k(x) + b_k(x) b_k(x) + b_k^\dagger(x) b_k^\dagger(x) \rangle$$

$$= \sum_k \frac{1}{E_\pi(k)} f_\pi(k) \ . \tag{A.26}$$

Apart from the above exceptions, the calculation of $I^\pi_{B\pi}$ is similar to that of $\hat{I}^b_{b\pi}$. The expectation value of the gain term $I^\pi_{\rm gain}$ is

$$I^\pi_{\rm gain}(xx') = \langle \hat{I}^\pi_{\rm gain} \rangle$$

$$= \frac{\pi}{16} \sum_{\pi k} \sum_{\alpha p \alpha' p'} \sum_{\alpha_1 p_1 \alpha_1' p_1'} \frac{1}{E_\pi(k)} \frac{M^*_\alpha M^*_{\alpha'}}{E^*_\alpha(p) E^*_{\alpha'}(p')}$$

$$\cdot \int dq dy \frac{e^{iq(x-y)+i(p'-p)y}}{(2\pi)^3 E_\pi(q)} \delta(E_{\alpha'}(p') - E_\pi(p'_1 - p_1) - E_\alpha(p))$$

$$\cdot (u^\dagger_{\alpha' p'} \hat{\underline{u}}(q) \hat{u}(p'+p)^2 u_{\alpha p}) \int dq' dy' \frac{e^{iq'(x'-y')+i(p'_1-p_1)y'}}{(2\pi)^3 E^3_\pi(q')}$$

$$\cdot (u^\dagger_{\alpha'_1 p'_1} \hat{\underline{u}}(q') u_{\alpha_1 p_1})(1 + f_\pi(k)) f_{\alpha'}(p')(1 - f_\alpha(p)) \delta_{\alpha'\alpha_1} \delta_{\alpha\alpha'_1} \delta_{p'p_1} \delta_{pp'_1}$$

$$= \frac{\pi}{16} \sum_{\pi k} \sum_{\alpha p \alpha' p'} \frac{1}{E_\pi(k)} \frac{M^*_{\alpha'}}{E^*_{\alpha'}(p') E^*_\alpha(p)} \delta(E_{\alpha'}(p') - E_\pi(p-p') - E_\alpha(p))$$

$$\cdot e^{i(p'-p)(x-x')} \frac{1}{E^4_\pi(p-p')} (1 + f_\pi(k)) f_{\alpha'}(p')(1 - f_\alpha(p))$$

$$\cdot (u^\dagger_{\alpha' p'} \hat{\underline{u}}(p-p') \hat{u}(p+p')^2 u_{\alpha p}) \cdot (u^\dagger_{\alpha p} \hat{\underline{u}}(p-p') u_{\alpha' p'}). \tag{A.27}$$

The gain term in phase space is then

$$I^\pi_{\text{gain}}(xk) = \int \mathrm{Tr} I^\pi_{\text{gain}}(xx') e^{-ip\cdot r} dr E_\pi(k)$$

$$= \frac{\pi}{16} \sum_{\alpha p \alpha' p'} \frac{M^*_\alpha M^*_{\alpha'}}{E^*_\alpha(p) E^*_{\alpha'}(p')}$$

$$\cdot \frac{\langle u_{\alpha' p'} | \hat{\underline{u}}(k) \hat{u}(p+p')^2 | u_{\alpha p} \rangle \cdot \langle u_{\alpha p} | \hat{\underline{u}}(k) | u_{\alpha' p'} \rangle}{E^4_\pi(k)}$$

$$\cdot \delta(E^*_{\alpha'}(p') - E_\pi(k) - E_\alpha(p)) \delta(\boldsymbol{p}' - \boldsymbol{p} - \boldsymbol{k})$$

$$\cdot (1 + f_\pi(k)) f_{\alpha'}(p')(1 - f_\alpha(p)) \,. \tag{A.28}$$

The loss term can be found analogously to be

$$I^\pi_{\text{loss}}(xk)$$

$$= \int \mathrm{Tr} I^\pi_{\text{loss}}(xx') e^{-ip\cdot r} dr E_\pi(k)$$

$$= \frac{\pi}{16} \sum_{\alpha p \alpha' p'} \frac{M^*_\alpha M^*_{\alpha'}}{E^*_\alpha(p) E^*_{\alpha'}(p')}$$

$$\cdot \frac{\langle u_{\alpha' p'} | \hat{\underline{u}}(k) \hat{u}(p+p')^2 | u_{\alpha p} \rangle \cdot \langle u_{\alpha p} | \hat{\underline{u}}(k) | u_{\alpha' p'} \rangle}{E^4_\pi(k)}$$

$$\cdot \delta(E^*_{\alpha'}(p') - E_\pi(k) - E_\alpha(p)) \delta(\boldsymbol{p}' - \boldsymbol{p} - \boldsymbol{k})$$

$$\cdot f_\pi(k) f_\alpha(p)(1 - f_{\alpha'}(p')) \,. \tag{A.29}$$

In the continuous limit, changing the summation over momentum into integrations, we obtain the expressions for I^{π}_{gain} and I^{π}_{loss} as in eqs. (2.101) and (2.102).

Bibliography

[Aich85] J. Aichelin, Phys. Lett. **164B**, 261 (1985).

[Aich91] J. Aichelin, Phys. Rep. **202**, 233 (1991).

[Barz81] H.W. Barz, B. Lukács, J. Zimányi, G. Fái and B. Jakobsson Z. Phys. **A302**, 73 (1981).

[Baue86] W. Bauer, G.F. Bertsch, W. Cassing and U. Mosel, Phys. Rev. **C34**, 2127 (1986).

[Baue88] W. Bauer, Phys. Rev. Lett. **61**, 2534 (1988).

[Baue89] W. Bauer, Phys. Rev. **C40** (1989) 715.

[Baue90] W. Bauer, MSUCL preprint-699.

[Baue91a] W. Bauer, B.A. Li, S.J. Wang and J. Randrup, in Proceedings of the Seventh Winter Workshop on Nuclear Dynamics,*Eds.* W. Bauer and J. Kapusta (1991). p210. (World Scientific, Signapore).

[Baue91b] W. Bauer and B.A. Li, in Proceedings of the Workshop on Relativistic Aspects of Nuclear Physics, Rio de Janeiro, 28-30 August 1991, to be published by World Scientific, Signapore.

[Baym62] L.P. Kadanoff and G. Baym, "Quantum Statistical Mechanics", Benjamin, New York (1962).

[Bert84] G.F. Bertsch, H. Kruse and S. Das Gupta, Phys. Rev. **C29** (1984) 673.

[Bert88a] G.F. Bertsch and S. Das Gupta, Phys. Rep. **160**, 189 (1988).

[Bert88b] G.F. Bertsch, G.E. Brown, V. Koch, and B.A. Li Nucl. Phys. **A490**, 745 (1988).

[Blaiz80] J.P. Blaizot, Phys. Rep. **64**, 171 (1980).

[Bloc56] M.M. Block Phys. Rev. **101**, 796 (1956).

[Brow75] G.E. Brown and W. Weise, Phys. Rep. **22**, 279 (1975).

[Brow89a] G.E. Brown, Proc. Int. Nuclear Physics Conference, Sao Paulo, Brazil. 1989, P.3, *Ed.* M.S. Hussein, Singapore: World Scientific (1990).

[Brow89b] G.E. Brown, E. Oset, M. Vicente Vacas, and W. Weise, Nucl. Phys. **A505**, 823 (1989).

[Brow91] G.E. Brown, J. Stachel, and G.M. Welke, Phys. Lett. **253B**, 19 (1991).

[Blät88] B. Blättel, V. Koch, W. Cassing, and U. Mosel, Phys. Rev. C**38**, 1767 (1988); B. Blättel, V. Koch, K. Webber, W. Cassing and U. Mossel, Nucl. Phys. **A495**, 381c (1989).

[Blät90] B. Blättel, V. Koch, A. Lang, K. Weber, W. Cassing, and U. Mosel, NATO ASI Series A216,321 (1990).

[Bote90] W. Botermans and R. Malfliet, Phys. Rep. **198**, 115 (1990).

[Broc84] R. Brockmann, J.W. Harris, A. Sandoval, R. Stock, H. Ströbele, G. Odyniec, H.G. Paugh, L.S. Schroeder, R.E. Renfordt, D. Schall, D. Bangert, W. Rauch and K.L. Wolf, Phys. Rev. Lett. **53**, 2012 (1984).

[Buch83] G. Buchwald, G. Graebner, J. Theis, J. Maruhn, W. Greiner and H. Stöcker, Phys. Rev. C**28**, 2349 (1983); Phys. Rev. Lett. **52**, 1594 (1984).

[Cass88] W. Cassing, K. Niita, and S.J. Wang, Z. Phys. A331, 439 (1988).

[Cass90a] W. Cassing, V. Metag, U. Mosel and K. Niita, Phys. Rep. **6**, 363 (1990).

[Cass90b] W. Cassing and U. Mosel, Prog. Part. Nucl. Phys. 25, 235 (1990).

[Cass90c] W. Cassing and S.J. Wang, Z. Phys. A337, 1 (1990).

[Cava90] C. Cavata, Ph.D. thesis 1990, Saclay, Frence.

[Cugn81] J. Cugnon, T. Mizutani, and J. Vandermeulen, Nucl. Phys. A352, 505 (1981).

[Cugn82] J. Cugnon, D. Kinet, and J. Vandermeulen, Nucl. Phys. A379, 553 (1982).

[Cugn88] J. Cugnon and M.C. Lemaire, Nucl. Phys. A489, 781 (1988).

[Chas90] S.I. Chase *et al.*, in: Proceedings of the Workshop on Nuclear Dynamics VI, LBL-28709, *Ed.* J. Randrup, p.67 (1990).

[Cube90] M. Cubero, Ph.D. thesis, TH Darmstadt, GSI report GSI-90-17 (1990).

[Dani83] P. Danielewicz and M. Gyulassy, Phys. Lett. **129B**, 283 (1983).

[Dani85] P. Danielewicz and G. Odyniec, Phys. Lett. **157B**, 146 (1985).

[Dani88] P. Danielewicz, H. Stroebele, G. Odyniec, D. Bangert, R. Bock, R. Brockmann, J.W. Harris, H.G. Pugh, W. Rauch, R.E. Renfordt, A. Sandoval, D. Schall, L.S. Schroeder and R. Stock, Phys. Rev. C**38**, 120 (1988).

[Dani90] P. Danielewicz, Phys. Rev. C**42**, 1564 (1990).

[Dani91] P. Danielewicz and G.F. Bertsch, Nucl. Phys. **A533**, 712 (1991).

[Davi91] J.E. Davis and R.J. Perry, Phys. Rev. C**43**,1893 (1991).

[Ferm54] E. Fermi, Phys. Rev. **92**, 452 (1953); Phys. Rev. **93**, 1434 (1954).

[Gino78] J.N. Ginocchio, Phys. Rev. C**17**, 195 (1978).

[Groo80] S.R. de Groot, W.A. van Leeuwen, and Ch.G. van Weert, "Relativistic Kinetic Theory", North Holland (1980).

[Gale87a] C. Gale, G.F. Bertsch and S. Das Gupta, Phys. ReV. C**35**, 1666 (1987).

[Gale87b] C. Gale and J. Kapusta, Phys. Rev. C**35**, 2107 (1987).

[Gale87c] C. Gale, Phys. Rev. C**36**, 2152 (1987).

[Glen88] N.K. Glendenning, Phys. Rev. C**37**, 2733 (1988).

[Goss89] J. Gosset, O. Valette, J.P. Alard, J. Augerat, R. Babinet, N. Bastid, F. Brochard, N. De Marco, P. Dupieux, Z. Fodor, L. Fraysse, P. Gorodetzky, M.C. Lemaire, D. L'Hôte, B. Lucas, J. Marroncle, G. Montarou, M.J. Parizet, J. Poitou, C. Racca, A. Rahmani, W. Schimmerling, and Y. Terrien, Phys. Rev. Lett. **62**, 1251 (1989).

[Gutb89] H. Gutbrod, K.H. Kampert, B.W. Kolb, A.M. Poskanzer, H.G. Ritter and H.R. Schmidt, Phys. Lett. **216B**, 267 (1989); Phys. Rev. Cbf 42, 640 (1990).

[Gong90] M. Gong and M. Tohyama, Z. Physik **A335**, 153 (1990); M. Gong, M. Tohyama, and J. Randrup Z. Physik **A335**, 331 (1990).

[Gong91] W.G. Gong, W. Bauer, C.K. Gelbke, and S. Pratt, Phys. Rev. C**43**, 781 (1991);

[Gyul82] M. Gyulassy, K.A. Fraenkel and H. Stöcker, Phys. Lett. **110B**, 185 (1982).

[Gust84] H.A. Gustafsson, H.H. Gutbrod, B. Kolb, H. Löhner, B. Ludewigt, A.M. Poskanzer, T. Renner, H. Riedesel, H.G. Ritter, A. Warwick, F. Weik and H. Wieman, Phys. Rev. Lett. **52**, 1590 (1984).

[Hart88] C. Hartnack, H. Stöcker and W. Greiner, in Proceedings of the International Workshop on Gross Properties of Nuclei and Nuclear Excitation XVI, Hirschegg, Austria, 1988, ed. H. Feldmeier p.138.

[Harw87] 8^{th} High-Energy Heavy-Ion Study, Berkeley, 16-20 November 1987. *Eds.* J.W. Harris and G.J. Wozniak (LBL-24580, Conf-8711116, UC-34C), and references therein.

[Harr87] J.W. Harris, R. Bock, R. Brockmann, A. Sandoval, R. Stock, H. Ströbele, G. Odyniec, H.G. Pugh, L.S. Schroeder, R.E. Renfordt, D. Schall, D. Bangert, W. Rauch and K.L. Wolf, Phys. Rev. Lett. **58**, 463 (1987).

[Hart88] C. Hartnack, H. Stöcker and W. Greiner in: Proceedings of the International Workshop on Gross Properties of Nuclei and Nuclear Excitations XVI, Hirschegg, Austria, ed. H. Feldmeier, GSI report, ISSN 0720-8715, p. 138 (1988).

[Hahn88] D. Hahn and N.K. Glendenning, Phys. Rev. C**37**, 1053 (1988).

[Harr89] J.W. Harris, NA35 collaboration, Nucl. Phys. **A498**, 133 (1989); J. Schukraft, Helios collaboration, Nucl. Phys. **A498**, 79 (1989); T.W. Atwater, P.S. Freier and J.I. Kapusta, Phys. Lett. **199B**, 30 (1987).

[Kapu91] J. Kapusta, P. Lichard and D. Seibert, High energy photons from quark-gluon plasma versus hot hadronic gas, University of Minnesota preprint, 1991.

[Koli87] C.M. Ko, Q. Li, and R. Wang, Phys. Rev. Lett. **59**, 1084 (1987). C.M. Ko and Q. Li, Phys. Rev. C**37**, 2270 (1988). Q. Li and C.M. Ko, Mod. Phys. Lett. **A3** (1988) 465. Q. Li, J.Q. Wu, and C.M. Ko, Phys. Rev. C**39**, 849 (1989).

[Kita86] Y. Kitazoe, M. Sano, H. Toki, and S. Nagamiya, Phys. Lett. **166B**, 35 (1986).

[Krus85] H. Kruse, B.V. Jacak, and H. Stöcker, Phys. Rev. Lett. **54**, 289 (1985). Phys Rev C**35**, 1666 (1987); C. Gale, Phys. Rev. C**36**, 2152 (1987); J. Aichelin, A. Rosenhauer, G. Peilert, H. Stöcker, and W. Greiner, Phys. Rev. Lett. **58**, 1926 (1987).

[Kusn89] D. Kusnezov and G.F. Bertsch, Phys. Rev. C**40**, 2075 (1989).

[Kata90] M. Kataja and P. V. Ruuskanen, Phys. Lett. **243B**, 181 (1990).

[Krof89] D. Krofcheck, W. Bauer, G.M. Crawley, C. Djalali, S. Howden, C.A. Ogilvie, A. Vander Molen, G.D. Westfall, W.K. Wilson, R.S. Tickle and C. Gale, Phys. Rev. Lett. **63**, 2028 (1989).

[Kean86] D. Keane, D. Beavis, S.Y. Chu, S.Y. Fung, W. Gorn, Y.M. Liu, G. VanDalen and M. Vient, in Proceedings of the 4^{th} Nuclear Dynamics Workshop, Copper Mountain, Colorado, p.151 (1986).

[Liba91a] B. A. Li and W. Bauer, Phys. Lett. **254B**, 335(1991).

[Liba91b] B.A. Li and W. Bauer, Phys. Rev. C**44**, 450 (1991).

[Liba91c] B.A. Li, W. Bauer and G. F. Bertsch, Phys. Rev. C**44**, 2095 (1991).

[Leeh89] K.S. Lee and U. Heinz, Z. Phys. C**43**, 425 (1989).

[Moli85] J.J. Molitoris and H. Stöcker, Phys. Lett. **162B**, 47 (1985).

[Moli87] J.J. Molitoris, H. Söcker, and B.L. Winer, Phys. Rev. C**36**, 220 (1987).

[Mose91] U. Mosel, Ann. Rev. of Nucl. Part. Science, **V41** (1991).

[Mart59] P. C. Martin and J. Schwinger, Phys. Rev. **115**, 1342 (1959); J. Schwinger, J. Math. Phys. **2**, 407 (1961); L.V. Keldysh, Sov. Phys.-JETP 20 (1965) 108.

[Migd78] A.B. Migdal, Rev. Mod. Phys. **50**, 107 (1978); B. Friedman, V.R. Pandharipande, and O.N. Usmani, Nucl. Phys. **A372**, 483 (1981).

[Oesc89] H. Oeschler et al., KAOS proposal to the Program Advisory Committee of the Gesellschaft für Schwerionenforschung (1989).

[Odyn88] G. Odyniec, J. Bartke, S.I. Chase, J.W. Harris, H.G. Pugh, G. Rai, W. Rauch, L.S. Schroeder, L. Teitelbaum, M. Tincknell, R. Stock, R. Renfordt, R. Brockmann, A. Sandoval, H. Ströbele, K.L. Wolf and J.P. Sullivan in: Proceedings of the 8th High Energy Heavy Ion Study, Berkeley, eds. J. Harris and G. Wozniak, LBL Report 24580, p.215 (1988).

[Oset82] E. Oset, H. Toki and W. Weise, Phys. Rep. **83**, 281 (1982).

[Pirn79] H.J. Pirner and B. Schurmann, Nucl. Phys. **A316**, 461 (1979).

[Part88] Particle Data Group, Phys. Lett. **B204**, 1 (1988).

[Pori91] N. Porile et al., in: Proceedings of the Seventh Winter Workshop on Nuclear Dynamics, eds. J. Kapusta and W. Bauer, World Scientific, to be published (1991).

[Qmat87] Proc. Sixth Int. Conference on Ultra-Relativistic Nucleus-Nucleus collisions-Quark Matter 1987, Nordkirchen, FRG,24-28 Aug. 1987, *Eds.* H. Satz, H.J. Specht, and R. Stock, and reference therein.

[Qmat90] Quark Matter 90's, Nucl. Phys. A525, (1991).

[Rari41] W. Rarita and J. Schwinger, Phys. Rev. **60**, 41(1941).

[Rand79] J. Randrup, Nucl. Phys. A314, 429 (1979).

[Rand90] Workshop on Nuclear Dynamics VI, 17-24 February 1990, Jackson Hole, Wyoming, *Ed.* J. Randrup (LBL-28709, Conf-900295, UC-413), and references therein.

[Roch88] G. Roche *et al.*, Phys. Lett. 226B, 228 (1989); Rhys. Rev. Lett. **61** (1988) 1069; C. Naudet *et al.*, Phys. Rev. Lett. **62**, 2652 (1989).

[Schö89] M. Schönhofen, M. Cubero, M. Gering, M. Sambataro, H. Feldmeier, and W. Nörenberg, Nucl. Phys. A504, 875 (1989); M. Cubero, M. Schönhofen, B.L. Friman, and W. Nörenberg, GSI preprint GSI-90-30, Proc. of the Int. Workshop on Nuclear Dynamics, Elba, Italy, April 2-7, 1990.

[Stöc86] H. Stöcker and W. Greiner, Phys. Rep. **137**, 277 (1986).

[Shar88] M.M. Sharma, W.T.A. Borghols, S. Brandenburg, S.Crona, A. van der Woude and M.N. Harakeh, Phys. Rev. C**38**, 2562 (1988).

[Siem88] P.J. Siemens, in Proceedings of 8^{th} High-Energy Heavy-Ion Study, Berkeley, eds. J. Harris and G. Wozniak LBL Report 24580, p. 511 (1988).

[Siem89] P.J. Siemens, M. Soyeur, G.D. White, L.J. Lantto, and K.T.R. Davies, Phys. Rev. C**40**, 2641 (1989).

[Schö90a] M. Schönhofen, Ph.D. thesis, TH Darmstadt, GSI report GSI-90-16 (1990).

[Schö90b] M. Schönhofen, M. Cubero, B.L. Friman, W. Nörenberg, in: Proceedings of the International Workshop on Gross Properties of Nuclei and Nuclear Excitations XVIII, Hirschegg, Austria, *Ed.* H. Feldmeier, p.15 (1990).

[Stoc82] R. Stock, R. Bock, R. Brockmann, J.W. Harris, A. Sandoval, H. Ströbele, K.L. Wolf, H.G. Pugh, L.S. Schroeder, M. Maier, R.E. Renfordt, A. Dacal and M.E. Ortiz, Phys. Rev. Lett. **49**, 1236 (1982).

[Stöc80] H. Stöcker, J.A. Maruhn and W. Greiner, Phys. Rev. Lett. **44**, 725 (1980).

[Shur88] E.V. Shuryak, Phys. Lett. **207B**, 345 (1988); E.V. Shuryak, Phys. Rev. D**42**, 1764 (1990).

[Verw82] B.J. VerWest and R.A. Arndt, Phys. Rev. C**25**, 1979 (1982).

[Welk91] G. Welke and G.F. Bertsch, MSU preprint MSUCL-772 (1991).

[Wolf90] Gy. Wolf, G. Batko, W. Cassing, U. Mosel, K. Niita, and M. Schäfer, Proc. Corinnes (Nantes, 1990), ed. D. Ardouin (World Scientific, Singapore, 1990); Gy. Wolf, G. Batko, W. Cassing, and U. Mosel, Nucl. Phys. **A517**, 615 (1990).

[wolf91] Gy. Wolf, W. Cassing, U. Mossel, and M. Schäfer, Phys. Rev. **C43**, R1501 (1991).

[Wlbr91a] S.J. Wang, B.A. Li, W. Bauer and J. Randrup, Ann. Phys. (N.Y.) **209**, 251 (1991).

[Wlbr91b] S.J. Wang, B.A. Li, W.Bauer and J. Randrup, In Proceedings of the Lanzhou International Symposium on Heavy Ion Physics and Applications, (1991). (World Scientific, Signapore in press).

[Wang85] S.J. Wang and W. Cassing, Ann. Phys. (N.Y.) **159**, 328 (1985).

[Wang89] S.J. Wang and W. Cassing, Nucl. Phys. **A495**, 371c (1989).

[Webe90] K. Weber, B. Blättel, V. Koch, A. Lang, W. Cassing, and U. Mosel, Nucl. Phys. **A515**, 747 (1990).

[Wong82] C.Y. Wong, Phys. Rev. C**25**, 1460 (1982).

[Xion90a] L. Xiong, J.Q. Wu, Z.G. Wu, C.M. Ko and J.H. Shi, Phys. Rev. C**41**, R1355 (1990).

[Xion90b] L. Xiong, Z.G. Wu, C.M. Ko and J.Q. Wu, Nucl. Phys. **A512**, 772 (1990).